

STUDIES OF
HIGH ISOSPIN STATES IN LIGHT EVEN-EVEN NUCLEI
AND OF LOW-LYING COLLECTIVE STATES IN MEDIUM WEIGHT
ODD-MASS NUCLEI

by

William J. Caelli

A Thesis submitted to
The Australian National University
for the Degree of
Doctor of Philosophy

Canberra, A.C.T.

April, 1971

To Edward and Betty

TABLE OF CONTENTS

	Page
PREFACE AND ACKNOWLEDGEMENTS	v
ABSTRACT	vii

CHAPTER 1

ISOBARIC ANALOGUE STATES IN LOW MASS NUCLEI

1.1	ISOSPIN IN NUCLEAR STRUCTURE PHYSICS	1
1.1.1	Isospin - The Formalism and Semantics	1
1.1.2	Isospin for a Given Nucleus - Isospin Multiplets	3
1.1.3	Charge Independence and Isospin Mixing	4
1.2	ISOBARIC ANALOGUE STATES	7
1.2.1	Isobaric Analogue States in Heavy Nuclei	7
1.2.2	Isobaric Analogue Resonances	9
1.3	ISOSPIN ALLOWED AND FORBIDDEN REACTIONS	11
1.3.1	Isospin Allowed Reactions	11
1.3.2	Isospin Forbidden Reactions and Widths of High T States	12
1.3	ISOSPIN MULTIPLY MASS EQUATIONS	14

CHAPTER 2

T = 3/2 STATES IN $T_z = \pm 1/2$ NUCLEI AND
T = 2 STATES IN $T_z = 0$ NUCLEI - A SURVEY

2.1	T = 3/2 STATES IN $T_z = \pm 1/2$ NUCLEI	18
2.2	DIRECT REACTION EXPERIMENTS	19
2.2.1	Two-Nucleon Transfer Reactions	19
2.2.2	Single-Nucleon Transfer Reactions	21
2.3	COMPOUND NUCLEUS REACTIONS	21
2.3.1	T = 3/2 States in $4n + 1$ Nuclei	22
2.3.2	T = 3/2 States in $4n - 1$ Nuclei	23

TABLE OF CONTENTS (continued)

	Page
2.3.3 General Discussion	23
2.4 T = 2 STATES IN $T_z = 0$ NUCLEI	24
2.5 ^{40}Ca : SUMMARY	25
2.5.1 ^{40}Ca : Allowed Reactions	26
2.5.2 ^{40}Ca : Forbidden Reactions	26
2.5.3 Experimental Search for the Lowest T = 2 State in ^{40}Ca via $^{39}\text{K}(p,p_0)$	27
2.5.4 Conclusions	29
2.5.5 Gamma Decay of the Lowest T = 2 State in ^{40}Ca	30
2.6 ^{36}Ar : SUMMARY	32
2.7 ^{32}S : SUMMARY	32
2.7.1 ^{32}S : Allowed Reactions	33
2.7.2 ^{32}S : Forbidden Reactions	33
2.8 ^{28}Si : SUMMARY	34
2.8.1 ^{28}Si : Allowed Reactions	34
2.8.2 ^{28}Si : Forbidden Reactions	34
2.9 ^{24}Mg : SUMMARY	36
2.9.1 ^{24}Mg : Allowed Reactions	36
2.9.2 ^{24}Mg : Forbidden Reactions	37
2.9.3 ^{24}Mg : Discussion	38
2.10 ^{20}Ne : SUMMARY	39
2.10.1 ^{20}Ne : Allowed Reactions	40
2.10.2 ^{20}Ne : Forbidden Reactions	41
2.11 ^{16}O : SUMMARY	42
2.12 ^{12}C : SUMMARY	43
2.13 ^8Be : SUMMARY	43
2.14 SUMMARY OF T = 2 STATES IN LOW MASS EVEN-EVEN NUCLEI	43
2.15 GAMMA DECAY OF HIGH ISOSPIN STATES	45

TABLE OF CONTENTS (continued)

	Page
CHAPTER 3	
SEARCH FOR THE LOWEST $T = 2$ STATE OF ^8Be VIA ISOSPIN-FORBIDDEN REACTIONS	
3.1	PREVIOUS WORK 48
3.2	THEORETICAL WORK 48
3.3	EXPERIMENTAL SEARCH FOR THE LOWEST $T = 2$ STATE IN ^8Be 49
3.3.1	Experimental Details 50
3.3.2	Excitation Functions 52
3.3.3	Observed Resonance 53
3.3.4	Basis for Using Ratios 53
3.4	CALCULATIONS AND DISCUSSION 54
3.5	SUMMARY 55
CHAPTER 4	
SEARCH FOR THE LOWEST $T = 2$ STATE OF ^{12}C VIA ISOSPIN-FORBIDDEN REACTIONS	
4.1	PREVIOUS WORK 57
4.2	THEORETICAL CALCULATIONS 57
4.3	EXPERIMENTAL WORK - $^{10}\text{B}(d,p)$; (d,α) 58
4.4	THE $^{10}\text{B}(d,\gamma\gamma)$ REACTION 60
4.5	THE $^9\text{Be}(^3\text{He},\gamma\gamma)$ REACTION 62
4.6	ESTIMATES OF PARTIAL WIDTHS 63
4.7	SUMMARIES AND CONCLUSIONS 64
CHAPTER 5	
INELASTIC PROTON SCATTERING FROM ^{103}Rh , ^{107}Ag AND ^{109}Ag	
5.1	INTRODUCTION - CORE EXCITATION MODEL 66

TABLE OF CONTENTS (continued)

	Page
5.2 USE OF THE BUECHNER BROAD-RANGE SPECTROGRAPH	68
5.3 THE REACTION $^{103}\text{Rh}(p,p')^{103}\text{Rh}^*$	69
5.4 THE REACTIONS $^{107}\text{Ag}(p,p')^{107}\text{Ag}^*$ AND $^{109}\text{Ag}(p,p')^{109}\text{Ag}^*$	71
5.4.1 $^{107}\text{Ag}(p,p')^{107}\text{Ag}^*$	71
5.4.2 $^{109}\text{Ag}(p,p')^{109}\text{Ag}^*$	72
CHAPTER 6	
COULOMB EXCITATION OF ^{103}Rh	
6.1 INTRODUCTION	74
6.2 EXPERIMENTAL DETAILS - CALIBRATION OF Ge(Li) γ -RAY SPECTROMETER	75
6.3 COULOMB EXCITATION USING OXYGEN IONS	78
CHAPTER 7	
STATES OF ^{103}Rh , ^{107}Ag AND ^{109}Ag	
7.1 ^{103}Rh STATES	81
7.2 STATES OF ^{103}Rh AND DECAY SCHEMES - EXPERIMENT	82
7.3 INTENSITIES OF γ -DECAYS IN ^{103}Rh AND B(E2) VALUES	84
7.3.1 γ -Ray Intensities	84
7.3.2 B(E2) Values	86
7.4 STATES OF ^{103}Rh - DISCUSSION	89
7.5 STATES OF ^{107}Ag AND ^{109}Ag	94
7.5.1 ^{107}Ag	94
7.5.2 ^{109}Ag	96
7.6 INTERPRETATION OF ^{103}Rh DATA	98
7.6.1 Positive Parity States	98
7.6.2 Negative Parity States	99
7.7 INTERPRETATION OF ^{107}Ag AND ^{109}Ag DATA	102
REFERENCES	105

PREFACE

This thesis describes a series of experiments carried out within the Department of Nuclear Physics at the Australian National University. Use was made of both the 12 MeV tandem Van de Graaff and 2 MeV model AK Van de Graaff accelerators in the department.

The thesis is divided into two sections. The first section covers work done on searches for the lowest $T = 2$ states of the low mass even-even nuclei ^{40}Ca , ^{12}C and ^8Be . The experimental work was performed equally, in the cases of ^{40}Ca and ^8Be , by Dr. J.L. Black, Professor D.L. Livesey, Mr. R.B. Watson and myself. Data analysis was shared among the members of the participating group. The experimental work on the ^{12}C $T = 2$ state was performed equally by Dr. J.L. Black, Mr. R.B. Watson and myself. Extensive use was made of both the IBM 1800 data acquisition and control system in the Department of Nuclear Physics, and the IBM System/360 Model 50 at the Computer Centre of the A.N.U. Data analysis programs for these machines were written by myself involving the use of both high and low level languages.

The second section covers work done on an examination of the low-lying states of the medium weight, odd-mass nuclei ^{103}Rh , ^{107}Ag and ^{109}Ag . In these cases the experimental work was carried out by Dr. J.L. Black, Mr. R.B. Watson and myself. The major part of data analysis was performed by Dr. J.L. Black and myself. All work in this thesis was carried out under the supervision of Dr. J.L. Black.

References are made in the thesis to work carried out by myself on the IBM 1800 data acquisition system. This work is not submitted as part of the thesis although it is referred to and

included in the list of references.

The work described in the first section of this thesis has appeared in the following publications:

"Search for the Lowest $T = 2$ State of ${}^8\text{Be}$: Experimental"
J.L. Black, W.J. Caelli, D.L. Livesey and R.B. Watson
Physics Letters 30B (1969) 100.

"Systematic Search for the Lowest $T = 2$ State of ${}^{12}\text{C}$ using
Deuteron and ${}^3\text{He}$ -Induced Reactions"
J.L. Black, W.J. Caelli and R.B. Watson
Physical Review Letters 25 (1970) 877.

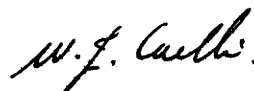
Similarly, the work performed on the low-lying collective states of odd-mass nuclei has been reported in the following publication:

"The Low-Lying Excited States of ${}^{103}\text{Rh}$ "
J.L. Black, W.J. Caelli and R.B. Watson
Nuclear Physics A125 (1969) 545.

It is difficult to be concise in my acknowledgements to the many members, past and present, of the Department of Nuclear Physics who have offered me help and consideration. My special thanks go to Dr. J.L. Black for his completely unselfish supervision and to my co-worker Mr. R.B. Watson for his help and encouragement. I would also like to thank Professor D.L. Livesey for his kind help and advice during his stay at the laboratory.

I would like to thank all the technical staff of the department for their help in experimental problems and in the development of the 10" crystal system. I am very grateful to Miss Norma Chin for her typing of this thesis. I thank Professors J.O. Newton and E.W. Titterton for the opportunity to work in the laboratories and for their helpful advice on many occasions. Finally, I thank the Australian National University for the award of a Post-graduate Research Scholarship.

No part of this thesis has been submitted for a degree at any other University.



W.J. Caelli

ABSTRACT

The thesis is divided into two sections. The first section deals with searches for the lowest $T = 2$ states in ^{40}Ca , ^{12}C and ^8Be . Studies of the reaction $^{39}\text{K}(p,p_0)$ were made in an attempt to locate the lowest $T = 2$ state in ^{40}Ca . No resonance in the cross section for this isospin-forbidden reaction was observed. The lowest $T = 2$ state in ^{12}C was interpreted as having been found as a peak in the γ - γ coincidence experiment $^9\text{Be}(^3\text{He},\gamma\gamma)$. This was observed at an excitation energy of $E_x = 27.585 \pm 0.005$ MeV in agreement with previous results. The state was not observed in particle reactions initiated by the $^{10}\text{B} + d$ channel. The lowest $T = 2$ state in ^8Be was found at an excitation energy of 27.483 ± 0.010 MeV in ^8Be using the $^6\text{Li} + d$ reaction. Proton and alpha particle excitation functions from this reaction were measured.

The second section deals with a study of low-lying collective states in the odd-mass nuclei ^{103}Rh , ^{107}Ag and ^{109}Ag . The ^{103}Rh nucleus was studied using the reaction $^{103}\text{Rh}(p,p')^{103}\text{Rh}^*$ as well as Coulomb excitation using oxygen ions. The states of ^{107}Ag and ^{109}Ag were also studied using the reactions $^{107}\text{Ag}(p,p')^{107}\text{Ag}^*$ and $^{109}\text{Ag}(p,p')^{109}\text{Ag}^*$. Many new levels were found in these nuclei. The states of these nuclei are discussed in relation to the weak coupling model of de-Shalit.

CHAPTER 1

ISOBARIC ANALOGUE STATES IN LOW MASS NUCLEI

1.1 ISOSPIN IN NUCLEAR STRUCTURE PHYSICS

Over the last few years, interest in isospin in low energy nuclear physics has increased markedly with the observation of high isospin states in nuclei covering almost the whole of the periodic table. Correspondingly, theoretical calculations on the properties of these states have also been performed with somewhat mixed results [Jo 70, Bl 70]. Following from these trends in research a number of review articles and books on isospin in nuclear physics have been published. In addition, a number of specialist conferences on the topic have been held. In this section of the thesis, it is hoped to examine the work done on isobaric analogue states, particularly in the low mass region (up to around mass 40). An outline of the basis for this work will also be given.

1.1.1 Isospin - The Formalism and Semantics

Wilkinson describes isospin as being "shorthand for the charge independence of the nuclear force". That this statement is true to within a few per cent has long been established. A discussion is provided by Wilkinson [Wi 70] in the book "Isospin in Nuclear Physics". The convention of using the term "isospin" rather than its full forms of "isotopic spin" or "isobaric spin" now seems well established and will thus be used.

The proposition that the neutron and proton should be considered as two states of a particle, the nucleon, followed soon after the discovery of the neutron by Chadwick [Ch 32]. The isospin formalism, with its charge independence nature, followed some time after [Wi 37]. This formalism is given in nearly all basic text-

books on nuclear physics. The above binary nature leads to a description of the two states analogous to that for particle spin developed by Pauli. Isospin (t) of $\frac{1}{2}$ is assigned to the nucleon. Two states are possible for the nucleon depending upon whether the isospin is "up" ($+\frac{1}{2}$, neutron) or "down" ($-\frac{1}{2}$, proton). (It is to be noted that this convention is the reverse to that sometimes used where the proton is taken as $+\frac{1}{2}$, (see De Benedetti, "Nuclear Interactions", pg. 58, [De 64]).) Using the formalism of normal spin, a description of the neutron and proton as two-dimensional column matrices is obtained as follows:

$$\xi(n) \equiv \begin{pmatrix} 1 \\ 0 \end{pmatrix} ; \quad \xi(p) \equiv \begin{pmatrix} 0 \\ 1 \end{pmatrix} \quad \dots \dots \quad (1)$$

Resolving an isospin operator (t) into three cartesian co-ordinates, the components of the isospin can be expressed as:

$$t_1 = \frac{1}{2} \begin{pmatrix} 0 & 1 \\ 1 & 0 \end{pmatrix}$$

$$t_2 = \frac{1}{2} \begin{pmatrix} 0 & -i \\ i & 0 \end{pmatrix} \quad \dots \dots \dots \quad (2)$$

and

$$t_3 = \frac{1}{2} \begin{pmatrix} 1 & 0 \\ 0 & -1 \end{pmatrix}$$

involving the usual Pauli spin matrices. The projection of the isospin vector onto the 3-axis produces the two possible values $+\frac{1}{2}$ and $-\frac{1}{2}$. The third component of the isospin operator operating on the two nucleon states produces:

$$t_3 \cdot \xi(n) = \frac{1}{2} \xi(n) \quad \dots \dots \dots (3)$$

and $t_3 \cdot \xi(p) = -\frac{1}{2} \xi(p)$

as expected. A charge operator "Q" can then be defined as:

$$Q \cdot \xi(N) = q \xi(N) \quad \dots \dots \dots (4)$$

where N stands for "nucleon" and the eigenvalues "q" have the values 0 or 1 for the neutron and proton respectively. From this it follows that:

$$Q = \frac{1}{2} - t_3 \quad \dots \dots \dots (5)$$

The "charge transfer" operators:

$$\underline{t}^{\pm} = \underline{t}_1 \pm i \underline{t}_2$$

can also be defined to perform this function, as follows:

$$\begin{aligned} \underline{t}^+ \cdot \xi(n) &= 0 \\ \underline{t}^- \cdot \xi(n) &= \xi(p) \\ \underline{t}^+ \cdot \xi(p) &= \xi(n) \\ \underline{t}^- \cdot \xi(p) &= 0 \end{aligned} \quad \dots \dots \dots (6)$$

Also the operator \underline{t}^2 satisfies the following equation to produce eigenvalues $t(t + 1)$:

$$\underline{t}^2 \cdot \xi(N) = t(t + 1) \xi(N) \quad \dots \dots \dots (7)$$

where, again, $\xi(N)$ is the nucleon wave function.

1.1.2 Isospin for a Given Nucleus - Isospin Multiplets

The total isospin, and its third component, for a nucleus

of "N" neutrons and "Z" protons may be obtained as the usual summations:

$$\tilde{T} = \sum_{i=1}^A \tilde{t}^i \quad \dots \dots \dots (8)$$

and

$$\tilde{T}_3 = \sum_{i=1}^A \tilde{t}_3^i$$

the eigenvalues of \tilde{T}^2 being $T(T + 1)$ and those of \tilde{T}_3 being $M_T = \frac{1}{2}(N - Z)$. This latter result can be seen from equations (3), for the case of a single particle. As is the case for normal spin there are $(2T + 1)$ values for each \tilde{T} . These can be integer or half-integer values in the range $-T \leq T_3 \leq T$. Thus nuclei of the same number of nucleons, A, corresponding to the same T value form an isospin "multiplet". There are $2T + 1$ members in each multiplet and their T_3 values lie in the above range specified. The charge-transfer operators:

$$\tilde{T}^{\pm} = \tilde{T}_1 \pm i \tilde{T}_2$$

can be used to go from one member of a multiplet to another. These operators, then, connect isospin states $\chi(T, M_T)$ and $\chi(T, M_T \pm 1)$, (see Robson, pg. 121, [Ro 66a]).

1.1.3 Charge Independence and Isospin Mixing

Use of the isospin formalism does not require the proposition that the neutron and proton are physically the same. The use of such a system depends upon how the neutron and proton may be treated in a nucleus. The differences necessary in the treatments of these particles provide the test of isospin formalism. Thus, in a charge dependent interaction, T and M_T may be used as good quantum numbers. In the case of a given nucleus, then, the isospin formalism

is good, i.e. T and M_T are good quantum numbers for nuclear states, if T^2 commutes with the nuclear Hamiltonian, i.e.:

$$(T^2, H) = 0 \quad \quad (9)$$

The specifically nuclear force does, as has been stated, appear to be charge independent to a very good approximation. However, in the case of a real nuclear Hamiltonian, Coulomb interaction, though small, cannot be ignored so that equation (9) does not hold. It does hold if all charge dependent terms in the nuclear Hamiltonian can be ignored. It is to be noted that the third component of the isospin operator, i.e. t_3 , always commutes with the nuclear Hamiltonian, H , from charge conservation. Thus, although a given state may not possess a definite $T(T + 1)$ eigenvalue, it must have a definite T_3 .

The Coulomb terms lead to "isospin mixing" in nuclear states. However, the isospin formalism is retained and the Coulomb effects in the nuclear Hamiltonian are treated using first order perturbation theory. This assumption is justified in that the Coulomb effects are usually small compared to the charge independent ones particularly for light nuclei where Z is fairly small. It can thus be assumed that isospin mixing between nuclear states only comes from Coulomb interactions. A Coulomb interaction, V^C , mixes into a state $\Psi_0(T)$ another state $\Psi_n(T')$ of the same spin and parity by an amplitude $a_n(T')$. Similarly, states of the same isospin and J^π values can also be mixed in by amplitudes $b_m(T)$. Equation (10) summarises this:

$$\begin{aligned}
 \Psi_0(T) &= \Psi_0(T) \\
 &+ \sum_{\mu \neq 0} b_{\mu}(T) \cdot \Psi_{\mu}(T) \quad \dots \dots \dots (10) \\
 &+ \sum_{\nu, T' \neq T} a_{\nu}(T') \cdot \Psi_{\nu}(T')
 \end{aligned}$$

where it can be shown from first order perturbation theory [Ro 66a] that:

$$a_n(T') = \frac{\langle \Psi_n | V^C | \Psi_0 \rangle}{E_0 - E_n} \quad \dots \dots \dots (11)$$

where E_0 and E_n are the energies of the respective states. Equation (11) is obtained as follows. The nuclear Hamiltonian, H , is written as:

$$H = H + V^C$$

where H = charge independent interaction Hamiltonian, and V^C = Coulomb interaction. Now:

$$H \cdot \Phi_{\lambda} = E_{\lambda} \Phi_{\lambda}$$

where:

$$\Phi_{\lambda} = \Psi_{\lambda} + \sum_{\mu} a_{\mu}^{\lambda} \Psi_{\mu} \quad \dots \dots \dots (12)$$

and:

$$a_{\lambda}^{\lambda} = 0$$

Also:

$$H \cdot \Psi_{\lambda} = E_{\lambda} \Psi_{\lambda}$$

Then:

$$\left(H + V^C - E_\lambda \right) \left(\Psi_\lambda + \sum_\mu a_\mu^\lambda \Psi_\mu \right) = 0$$

and:

$$\left(E_\lambda + V^C - E_\lambda \right) \Psi_\lambda + \sum_\mu a_\mu^\lambda \left(E_\mu + V^C - E_\lambda \right) \Psi_\mu = 0$$

Ignoring those terms of second order in V^C of a_μ^λ , multiplying by Ψ_ν^* and integrating:

$$\left(E_\lambda - E_\lambda \right) \delta_{\nu\lambda} + \langle \Psi_\nu | V^C | \Psi_\lambda \rangle + a_\nu^\lambda \left(E_\nu - E_\lambda \right) = 0 \quad (13)$$

For $\nu = \lambda$, from equation (14):

$$E_\lambda = E_\lambda + \langle \Psi_\lambda | V^C | \Psi_\lambda \rangle$$

and for $\nu \neq \lambda$:

$$a_\nu^\lambda = \frac{\langle \Psi_\nu | V^C | \Psi_\lambda \rangle}{E_\lambda - E_\nu} \dots \dots \dots (14)$$

In examining the decay of a $T = 2$ state, the admixtures due to other $T = 2$ states as well as $T = 3, 4$, etc. states can be ignored so that:

$$\Phi_2 = \Psi_2 + \sum_n \alpha_{1n} \Psi_{1n} + \sum_n \alpha_{0n} \Psi_{0n}$$

where α_{1n} and α_{0n} are the admixtures of a state n of the same spin and parity and isospins 0 and 1 respectively into the $T = 2$ state and Ψ_{1n} and Ψ_{0n} are their corresponding wave functions.

1.2 ISOBARIC ANALOGUE STATES

1.2.1 Isobaric Analogue States in Heavy Nuclei

Before 1961, the light nuclei had already been extensively examined experimentally and the states of known isobars compared. As already stated, isospin is expected to be a good quantum number

for the description of nuclear states. This is true as long as, in a given real nuclear Hamiltonian, the Coulomb interaction terms are less than the specifically nuclear terms. It thus seems obvious to examine the concept of isospin in relation to the low mass nuclei. If T is a good quantum number the states of "mirror" nuclei, (for the odd A case, two nuclei with $N = Z - 1$ and $N = Z + 1$), should be identical once Coulomb energy corrections are made, etc. That this is so is demonstrated well in the textbooks where many mirror nuclei and isospin multiplet examples are given for low mass cases (see figure 1.2.1, references [Bu 63, La 66]).

The first observation of isobaric analogue states in heavy nuclei was made by Anderson et al. in 1961 [An 62] when they bombarded various targets with 14.8 MeV protons. Neutrons produced were measured using time-of-flight techniques with an 8.7 metre flight path. A prominent neutron group at high excitation was observed in each of the spectra taken. The groups appeared as narrow peaks superimposed on a continuous background due to the feeding of overlapping high energy states in the residual nucleus. The case for a ^{51}V target is shown in figure 1.2.2 which is taken from the review paper by Coker and Moore [Co 69]. These neutron groups were interpreted as arising from the population of an isobaric analogue state in the final nucleus.

In the case of the proton bombardment of a ^{51}V target, the narrow neutron group was found to have an equivalent Q value of 8.0 MeV (see table 1 in reference [An 62]). This Q value compared very well with the calculated Coulomb energy difference between the target and final nuclei. Thus, the analogue state was seen as the analogue of the ground state of the target nucleus. However, the $|T_z|$ value for the analogue state differs from that of the ground

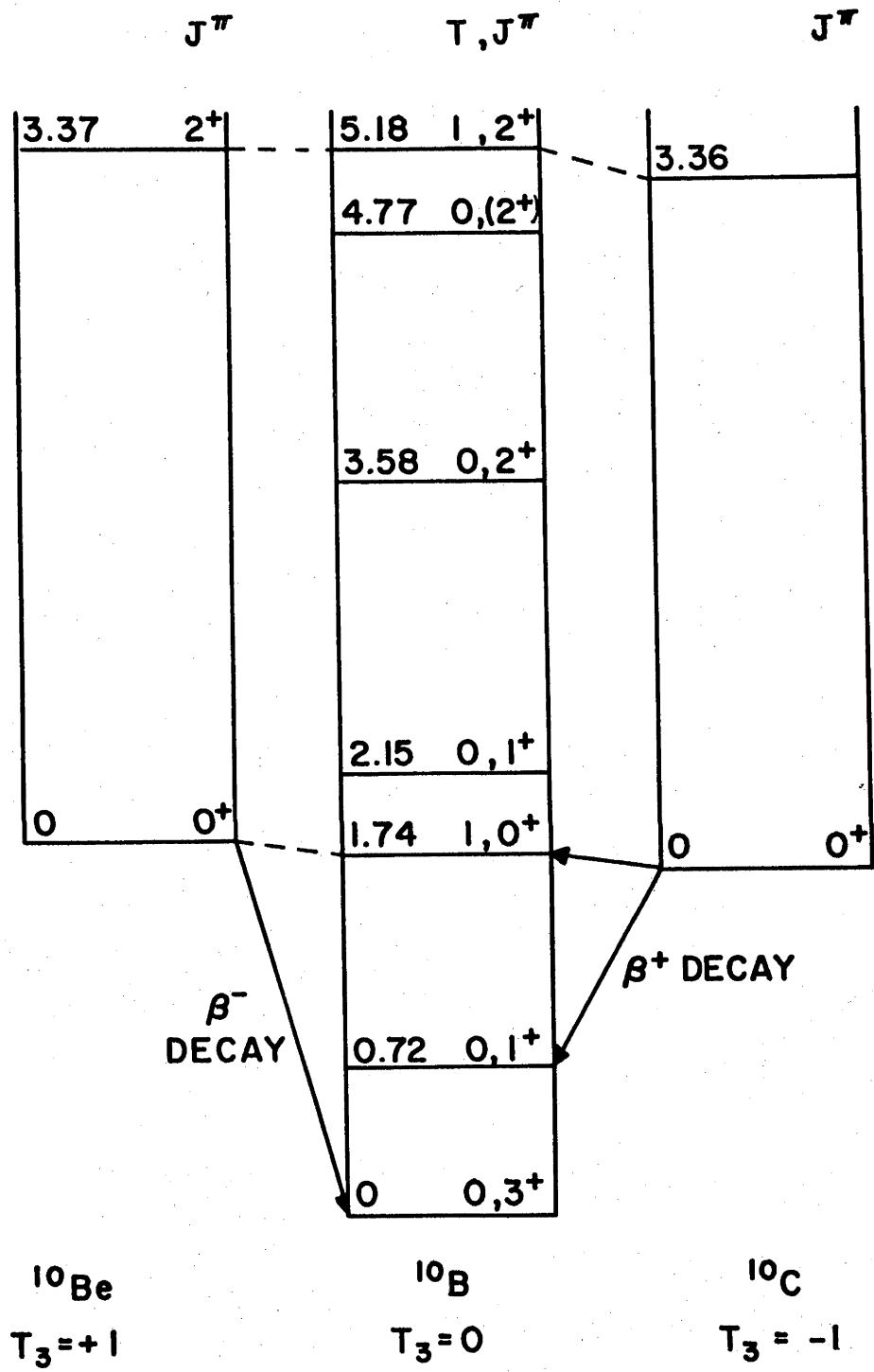


Figure 1.2.1: Low-lying levels of the isobars of mass 10 in an isobar diagram (references [Bu 63, La 66]).

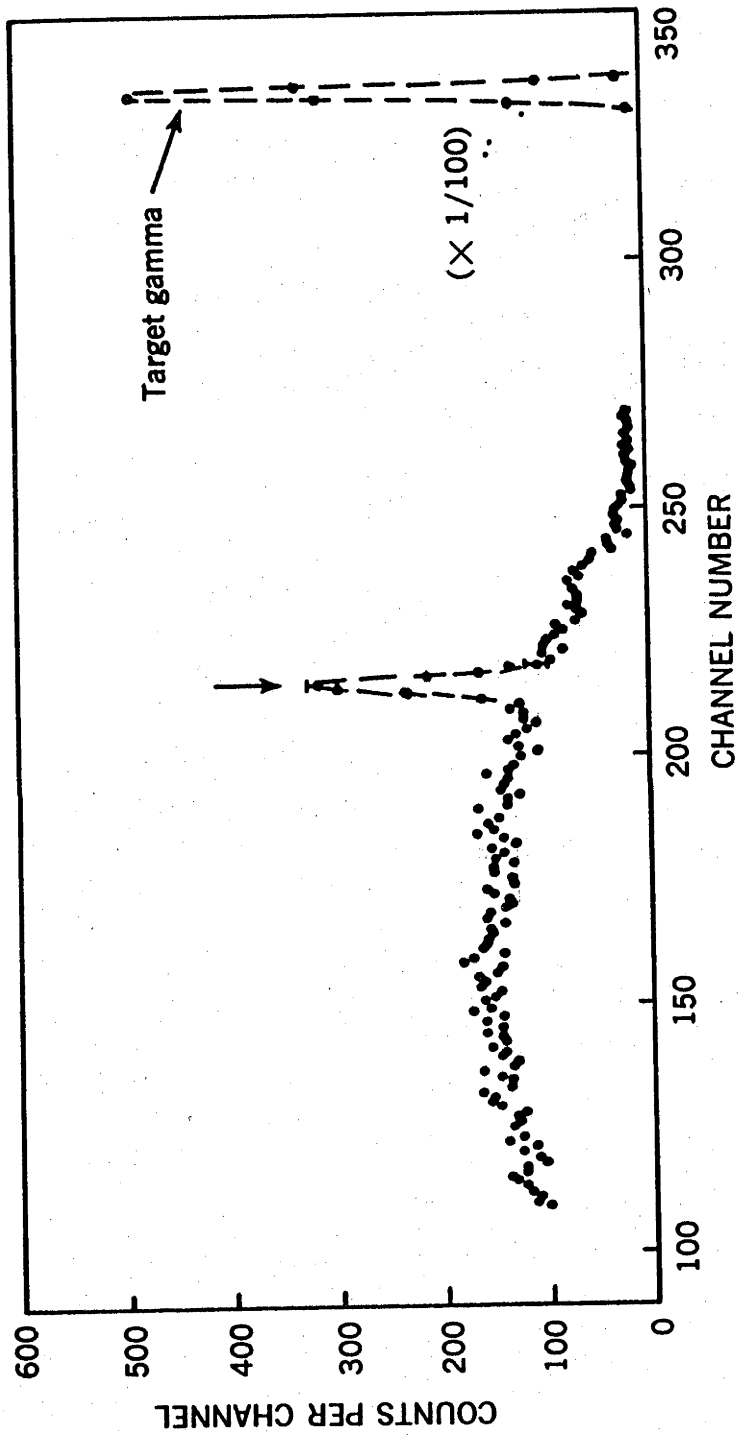


Figure 1.2.2: Time-of-flight neutron spectrum from proton bombardment of ^{51}V . Increasing time-of-flight is to the left. Analogue state is indicated with the arrow.

state of the target nucleus in that, (see footnote *):

$$T_z^{\text{analogue}} = T_z^{\text{target}} - 1.$$

In all other quantum numbers the states are the same. In this regard the ground state of ^{51}V , for example, is called the "parent" state of the $T = 5/2$ analogue state in the $T_z = 3/2$ nucleus ^{51}Cr .

Lane and Soper [La 62] in 1962 performed a theoretical study of the properties of isobaric analogue states in medium mass to high mass nuclei. The question of isospin purity for states in these nuclei was the main theme of the work. It was found that isospin is a relatively good quantum number in heavy nuclei. It also increases in purity with increasing mass for nuclei close to the stability line. In these cases, the neutron excess acts in such a way as to dilute the amount of isospin mixing due to Coulomb effects. Lane and Soper pointed out that the observed width of the analogue states is due purely to Coulomb mixing of the state with neighbouring states. They were able to predict that qualitatively the observed widths (Γ_c) of isobaric analogue states in nuclei of $A > 90$ would be around 0.2 MeV, showing some reduction at magic numbers.

1.2.2 Isobaric Analogue Resonances

Fox, Moore and Robson, in a paper published in 1964 [Fo 64], reported the observation of isobaric analogue states in ^{89}Y and ^{90}Zr as compound nucleus resonances in the proton bombardment of ^{88}Sr and ^{89}Y . These states were interpreted as analogues of the low lying states of ^{89}Sr and ^{90}Y . Excitation functions for the

* The symbol T_z is used synonymously with the term T_3 . In essence the second form is preferable in that no reference to x, y, z co-ordinates in real space is intended and, by using the number 3 rather than the letter z, no confusion can arise.

reactions $^{88}\text{Sr}(p,n)$ and $^{89}\text{Y}(p,n)$ were taken near threshold. Using the same targets, elastic scattering angular distributions for protons were also taken. These latter measurements permitted spin and parity assignments to be made for the anomalies seen in $^{89}\text{Y} + p$ (at proton bombarding energies of 4.82 and 5.02 MeV, 2^- and 3^- assigned) and in $^{88}\text{Sr} + p$ (at a proton bombarding energy of 5.08 MeV, $5/2^+$ assigned). These states were found to be the analogues of the ground and first excited states of ^{90}Y and the ground state of ^{89}Sr respectively. These analogue states are notable since they appear as sharp, isolated resonances at high excitation in the compound nucleus in this case around 14 MeV (see table 1.2.1). At such high excitation energies the ordinary, overlapping levels of the compound nucleus appear as a continuous background in the excitation function as can be seen in figure 1.2.3.

Table 1.2.1 (Reference [Fo 64])

Analogue Resonances in ^{89}Y and ^{90}Zr

Nucleus	Analogue State Excitation (MeV)	Parent	J^π
^{89}Y	12.47 ± 0.05	^{89}Sr , ground	$5/2^+$
^{90}Zr	13.12 ± 0.03	^{90}Y , ground	2^-
	13.32 ± 0.03	^{90}Y , 1st	3^-

Since this work was done, isobaric analogue resonances have been observed in compound nucleus reactions over much of the periodic table. The observation of such resonances permits the study of states of a given nucleus by bombarding the isotope of one less neutron, for example, with protons. Measurement of angular

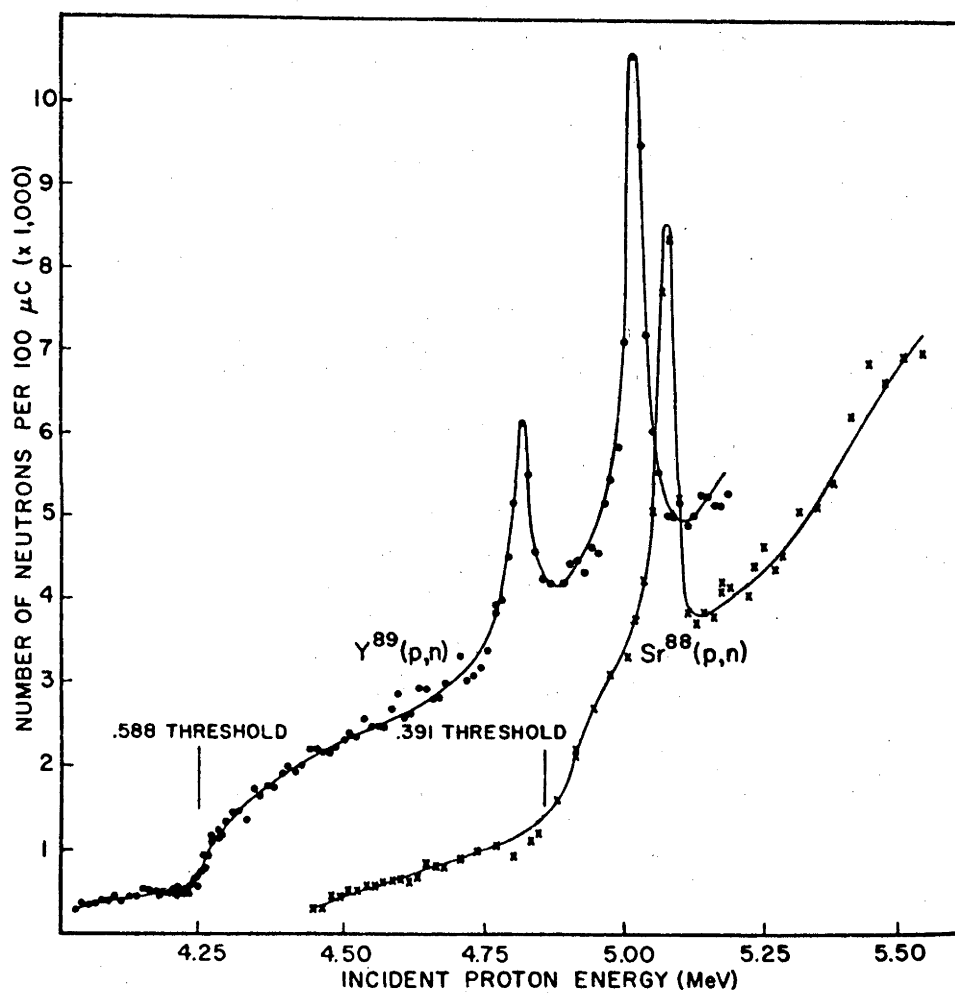


Figure 1.2.3: Neutron yields for $^{88}\text{Sr}(p,n)$ and $^{89}\text{Y}(p,n)$ near threshold. Long counter placed at 50° to beam direction.

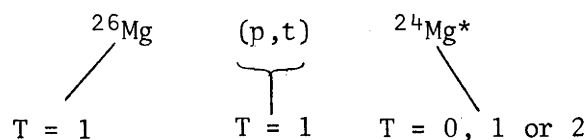
distributions for elastic proton scattering enables " ℓ " values to be assigned to the various resonances and thus to the parent states of these analogues.

1.3 ISOSPIN ALLOWED AND FORBIDDEN REACTIONS

As outlined in section 1.1.3, a given state of isospin T may have mixed into it states of isospin differing from it by integer values. For example, from the point of view of the decay of a lowest $T = 2$ state in a given $T_z = 0$ nucleus, the $T = 0$ and $T = 1$ admixtures in the state are of interest. As has also been stated, isospin appears to be a relatively good quantum number for nuclei over most of the periodic table. Thus a violation of its conservation in nuclear reactions must be reflected in a small overlap of channel and nuclear state wave functions. This leads to the definition of so-called isospin "allowed" and "forbidden", direct and resonance reactions.

1.3.1 Isospin Allowed Reactions

An isospin allowed direct or compound nucleus reaction is one which enables states of a given T in the residual or compound nucleus to be populated without violation of isospin conservation. In the direct reaction case, the isospin of the target nucleus and reaction channel must be able to vector couple to give the isospin of the residual nucleus state. For example, the following direct reaction is an isospin allowed reaction for the population of $T = 2$ states in ^{24}Mg :



In this case two neutrons are being transferred and from the Pauli principle they must have antiparallel spins, $S = 0$ and parallel isospins, $T = 1$. Thus $T = 0, 1$ or 2 states may be populated in the residual nucleus.

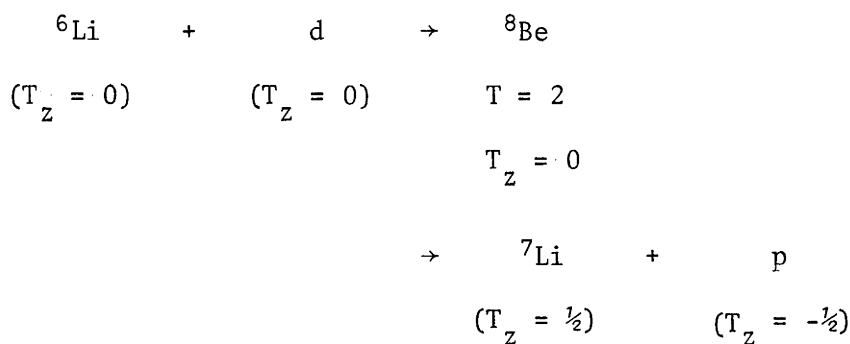
Isospin allowed compound nucleus reactions are quite common but do not allow the study of high T states in a nucleus of lower T_z value by two units. For example the reaction $^{12}\text{C}(\alpha, \alpha')^{12}\text{C}$ allows $T = 0$ states in the compound nucleus $^{16}\text{O}(T_z = 0)$ to be studied but this is a trivial case. Similarly, by bombarding a $T_z = 1$ target nucleus with a $T_z = 1$ beam, $T = 2$ states in a $T_z = 2$ nucleus can also be populated, e.g. $^{18}\text{O}(^{18}\text{O}, ^{18}\text{O})^{18}\text{O}$ would allow $T = 2$ states in the $T_z = 2$ nucleus ^{36}S to be populated.

1.3.2 Isospin Forbidden Reactions and Widths of High T States

If a given state in a compound or residual nucleus is populated via a reaction in which the isospin, T , of the state under investigation cannot be formed from isospin conservation of the reactants then we have an isospin forbidden reaction. Examples tend to clarify this situation. Consider the compound nucleus reaction $^7\text{Li} + d \rightarrow ^9\text{Be} \rightarrow ^8\text{Li} + p$ where we wish to populate the $T = 3/2$ states in the $T_z = 1/2$ nucleus ^9Be . The population of these states is forbidden by isospin conservation in the entrance channel ($^7\text{Li}, T_z = 1/2$ and $d, T_z = 0$), but the decay of a $T = 3/2$ state in ^9Be via the $^8\text{Li} + p$ channel is allowed ($^8\text{Li}, T_z = 1$ and $p, T_z = -1/2$). This condition also applies to radiative capture reactions, e.g. $^6\text{Li} + d \rightarrow ^8\text{Be} + \gamma$. The reaction is again forbidden in the entrance channel but allowed in the exit channel. Such reactions are referred to as "once forbidden" reactions. Similarly a reaction that is forbidden both in the entrance and exit channels is referred to as being "doubly forbidden". An example of this type of reaction is elastic

proton scattering by an even-even target nucleus. Here it is desired to populate $T = 3/2$ states in the compound $T_z = 1/2$ nucleus, i.e. $A(T_z = 0) + p \rightarrow B^*(T = 3/2, T_z = 1/2) \rightarrow A + p$.

The observation of such $T = 3/2$ states in $T_z = 1/2$ nuclei by elastic scattering of protons from even-even nuclei will be discussed later. A similar type of doubly-forbidden reaction is the compound nucleus reaction:



used for the population of the lowest $T = 2$ state in ${}^8\text{Be}$. This and similar reactions will again be discussed later.

In the case of these high isospin states observed as resonances in compound nucleus reactions, it is important to examine the reasons for their observation as very narrow resonances, despite their high excitation energy. This is discussed by Temmer in his article "Isobaric Analogue Resonances and Nuclear Spectroscopy" [Te 70]. The narrow width arises from the fact that particle decay channels are usually isospin forbidden for these states leaving only radiative decay as the decay mode. For $T = 3/2$ states in $T_z = \pm 1/2$ nuclei, the following diagram from Temmer's article [Te 70] is appropriate (figure 1.3.1). In the case of elastic proton scattering, say, from a $4n$ type nucleus, decay via the $T = 1$ states in the $T_z = 0$ nucleus is energetically not possible. In the $4n + 2$ type target nucleus case, the low excitation energies of the $T = 1$ states make such allowed particle decays energetically possible.

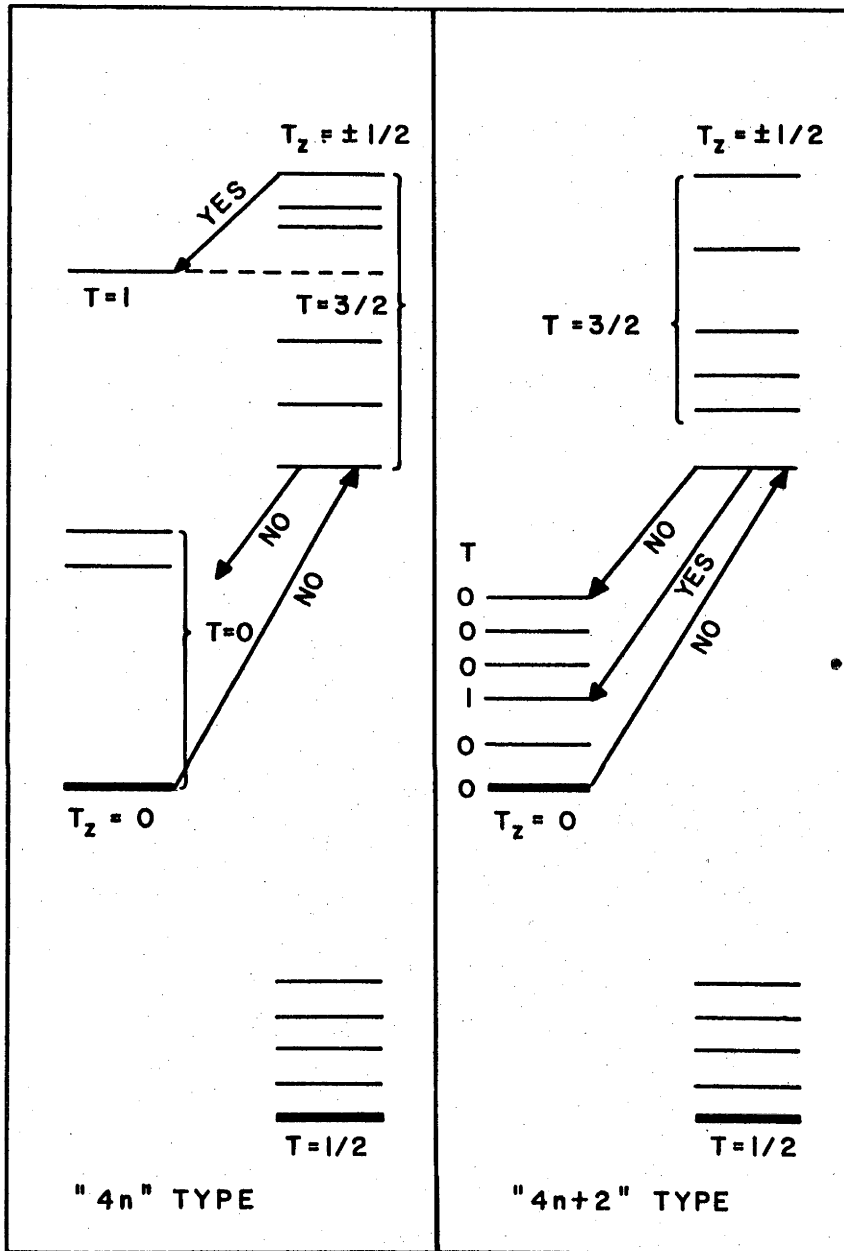


Figure 1.3.1: $T = 3/2$ states in $T_z = \pm 1/2$ nuclei. Energetics for isospin-forbidden analogue resonances by bombardment of "4n" and "4n + 2" type target nuclei [Te 70].

The study of such isospin forbidden reactions enables estimates to be made of the mixing parameters (α) for given high T states.

It is only through this mixing of lower T states into the higher T state that the high T state can be populated. The isospin mixing parameters are, in turn, predicted theoretically. Likewise theoretical estimates of the partial widths of a particular high T state can also be made. For the case of ^8Be , for example, shell model estimates of partial widths have been made by Barker and Kumar [Ba 69]. Their results and the corresponding experimental results will be discussed later.

1.4 ISOSPIN MULTIPLY MASS EQUATIONS

Isospin multiplet mass equations are equations that relate the masses of members of a given isospin multiplet. Of late, with the theoretical and experimental examination of high isospin states, investigation of these relations has increased [Sn 69a, Ce 68]. The familiar isobaric multiplet mass relation takes the form:

$$M(A, T, T_z) = a(A, T) + b(A, T)T_z + c(A, T)T_z^2 \quad \dots \quad (15)$$

i.e. the masses are related quadratically on the third component of isospin, T_z , and are related to the total mass number, A, and total isospin, T. Equation (15) is referred to as the isobaric-multiplet mass equation and has been derived by a number of authors [Ga 69a, Ga 69b] by treating the charge dependent section of the nuclear Hamiltonian by first order perturbation techniques. This equation has been successfully used for mass relations in a number of multiplets [Ce 68].

Since a quadratic relation applies, any isospin multiplet

of more than three members ($2T + 1$ members) enables a check of the equation to be made, i.e. an isospin multiplet with $T > 1$. Data for the odd A multiplets with $T = 3/2$ are presented by Garvey [Ga 69b] and are reproduced in table 1.4.1. The table contains the experimentally determined mass defects for the $T = 3/2$ isospin multiplets where all four members are known. If a cubic term of the form $d(A,T)T_z^3$ is added to the mass equation, possible values for this term can be extracted from the above data. The values of "d" are shown in the right hand side column of table 1.4.1. Garvey also shows a table of the values of the coefficients a , b and c in MeV as determined from a χ^2 fit to the masses shown in table 1.4.1. A χ^2 value of 4.05 for the accurately known mass 9 case illustrates limitations of the equation and leads to the inclusion of the cubic term. This term, as pointed out by Garvey, cannot be simply taken as indicating the presence of three-body charge dependent interactions since, by its nature, equation (15) is not exact because of isospin mixing due to the two-body Coulomb interaction.

Extensions to the quartic equation have been made to account for the mass 9 discrepancies [Ga 69b, Ja 70, Ja 69]. Here the charge dependent interaction is treated using second order perturbation theory. This treatment still maintains the constant, linear and quadratic terms but adds small cubic and quartic ones. The new equation is generally written in the form [Ja 69b]:

$$M(A,T,T_z) = \tilde{a}(A,T) + \tilde{b}(A,T)T_z + \tilde{c}(A,T)T_z^2 + \tilde{d}(A,T)T_z^3 + \tilde{e}(A,T)T_z^4 \dots \dots \dots (16)$$

It is to be noted that the constant, linear and quadratic terms have now changed, the corrections in these terms along with the cubic and quartic terms arising from off-diagonal reduced Coulomb matrix

Table 1.4.1 (Reference [Ga 69b], pg. 436)

Experimentally determined mass defects of the $T = 3/2$ multiplets in which all four members are known. The right hand side column indicates the value of a possible cubic term to be added to equation (15).

A	$T_z = 3/2$	$T_z = 1/2$	$T_z = -1/2$	$T_z = -3/2$	d (keV)
7	25.11 ± 0.030	26.19 ± 0.040	26.75 ± 0.030	27.94 ± 0.100	-25 ± 30
9	24.965 ± 0.005	25.743 ± 0.005	27.075 ± 0.005	28.916 ± 0.005	7.5 ± 2.3
13	16.562 ± 0.004	18.231 ± 0.003	20.411 ± 0.004	23.11 ± 0.040	1 ± 11
17	7.871 ± 0.015	10.267 ± 0.006	13.149 ± 0.004	16.47 ± 0.250	8 ± 42
21	-0.046 ± 0.007	3.126 ± 0.006	6.790 ± 0.005	10.95 ± 0.120	-1 ± 20
23	-5.148 ± 0.003	-1.628 ± 0.021	2.298 ± 0.040	6.766 ± 0.080	-23 ± 26
25	-9.356 ± 0.009	-5.395 ± 0.013	-1.017 ± 0.005	3.86 ± 0.120	-14 ± 21
37	-31.765 ± 0.001	-25.941 ± 0.030	-19.753 ± 0.005	-13.23 ± 0.050	5 ± 17

elements. The use of this equation in the mass 9, $T = 3/2$ multiplet is discussed by Garvey [Ga 69b].

The isobaric multiplet mass equation follows from a model independent discussion of the nuclear Hamiltonian. It is possible by using the various models to produce relations for the various coefficients in the mass equation. A detailed discussion of these relations lies outside the scope of the thesis.

CHAPTER 2

T = 3/2 STATES IN $T_z = \pm 1/2$ NUCLEI AND
T = 2 STATES IN $T_z = 0$ NUCLEI - A SURVEY

2.1 T = 3/2 STATES IN $T_z = \pm 1/2$ NUCLEI

Before dealing with the main topic of this section, viz. the search for the lowest T = 2 state of ^8Be , ^{12}C and ^{40}Ca , it is appropriate to examine the work done on the observation of T = 3/2 states in $T_z = \pm 1/2$ nuclei. This work has progressed at a rapid pace over the last few years so that the states have been seen via both isospin allowed and forbidden reactions. In order to clarify points to be outlined, examination of the four member T = 3/2, mass 13 isospin multiplet is helpful. Table 2.1.1 shows the situation.

Table 2.1.1

Mass 13 Isospin Multiplet, T = 3/2

Member	^{13}B	^{13}C	^{13}N	^{13}O
T_z	3/2	1/2	-1/2	-1/2
E_x of lowest T = 3/2 state (MeV)		15.107	15.066	

There are four ($2T + 1$) members in the multiplet. The analogues of the $T_z = \pm 3/2$ nuclei ground states have been found in the $T_z = \pm 1/2$ nuclei. A survey of the T = 3/2 states is found in an article by Temmer [Te 70]. It remains, then, to make some general points here.

2.2 DIRECT REACTION EXPERIMENTS

2.2.1 Two-Nucleon Transfer Reactions

Two-nucleon transfer reactions have been used to populate $T = 3/2$ states in $T_z = \pm 1/2$ nuclei. Such experiments involve usually the use of (p,t) , $(p,^3\text{He})$, $(^3\text{He},n)$ or $(^3\text{He},p)$ reactions. Simultaneous observation of the (p,t) and $(p,^3\text{He})$ reactions on $T_z = \pm 1/2$ target nuclei can be used to locate the $T = 3/2$ states in the $T_z = 1/2$ and $-1/2$ mirror residual nuclei. These reactions involve the pickup of the two nucleons in an $S = 0$, $T = 1$ configuration. If a $T_z = 3/2$ member of the multiplet is known then the approximate location of the lowest $T = 3/2$ states in the $T_z = \pm 1/2$ members of the multiplet can be calculated from the mass equation linking the isobars. The excitation energy is then obtained by using the appropriate Coulomb energy and correcting for the n-p mass difference. Vector coupling of the $T = 1$ transfer nucleons to the target $T_z = 1/2$ ground state permits the population of the $T = 3/2$ states in the final nucleus. This is an isospin-allowed reaction. Measurement of angular distributions for these states permits an assignment of an angular momentum transfer value. This leads to a spin and parity assignment for the analogue state which must be equivalent to the parent states in the $T_z = 3/2$ members of the multiplet. It is to be noted that transitions to at least the lower $T = 3/2$ states in a $T_z = \pm 1/2$ nucleus are, in general, enhanced over those to surrounding states of lower isospin. This arises since these latter states have more complex configurations at these high energies whereas the analogue states usually bear simple relations to the target nucleus.

An example of these two-nucleon transfer reactions is the mass 7 case as outlined by Cerny [Ce 68]. The $T = 3/2$ states in

${}^7\text{Be}$ and ${}^7\text{Li}$ were populated via the (p,t) and (p, ${}^3\text{He}$) reactions on a ${}^9\text{Be}$ target. Cerny also presents a survey of the data taken on $T = 3/2$ states seen in low mass $T_z = \pm 1/2$ nuclei. An updated version of this compilation for the lowest $T = 3/2$ states is given in table 2.2.1 for nuclei up to mass 40. The isospin allowed reactions (p,t) and (p, ${}^3\text{He}$) have been used to excite $T = 3/2$ states in nuclei of mass 7, 11, 13, 19, 23, 25, 29 and 37 while the (${}^3\text{He},n$) and (${}^3\text{He},p$) reactions have been used to search for analogue states in nuclei in masses 9, 13, 17 and 21.

Table 2.2.1

Lowest $T = 3/2$ States in $T_z = \pm 1/2$ Nuclei

A	$T_z = +1/2$		$T_z = -1/2$	
	Nucleus	Excitation (MeV)	Nucleus	Excitation (MeV)
7	${}^7\text{Li}$	11.28	${}^7\text{Be}$	11.006
9	${}^9\text{Be}$	14.392	${}^9\text{B}$	14.656
11	${}^{11}\text{B}$	-	${}^{11}\text{C}$	-
13	${}^{13}\text{C}$	15.107	${}^{13}\text{N}$	15.068
15	${}^{15}\text{N}$	11.61	${}^{15}\text{O}$	-
17	${}^{17}\text{O}$	11.075	${}^{17}\text{F}$	11.196
19	${}^{19}\text{F}$	7.432	${}^{19}\text{Ne}$	-
21	${}^{21}\text{Ne}$	8.856	${}^{21}\text{Na}$	8.973
23	${}^{23}\text{Na}$	7.900	${}^{23}\text{Mg}$	7.788
25	${}^{25}\text{Mg}$	7.796	${}^{25}\text{Al}$	7.916
27	${}^{27}\text{Al}$	6.815	${}^{27}\text{Si}$	-
29	${}^{29}\text{Si}$	8.294	${}^{29}\text{P}$	8.375
31	${}^{31}\text{P}$	6.380	${}^{31}\text{S}$	-
33	${}^{33}\text{S}$	5.483	${}^{33}\text{Cl}$	5.555
35	${}^{35}\text{Cl}$	-	${}^{35}\text{Ar}$	-
37	${}^{37}\text{Ar}$	5.010	${}^{37}\text{K}$	5.048
39	${}^{39}\text{K}$	-	${}^{39}\text{Ca}$	-

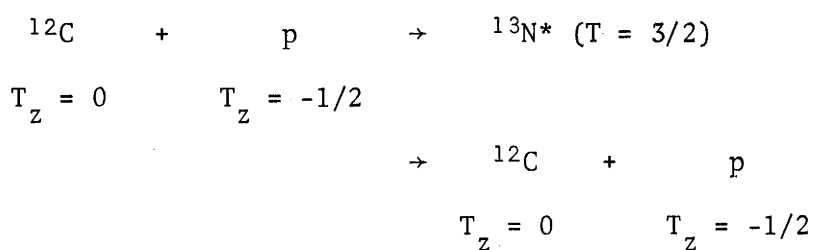
2.2.2 Single-Nucleon Transfer Reactions

Population of $T = 3/2$ states in residual nuclei by direct reactions has been performed via single nucleon transfer reactions on $T_z = 1$ target nuclei. As an example, the $^{22}\text{Ne}(^3\text{He},\alpha)^{21}\text{Ne}$ reaction has been used by Henley to populate $T = 3/2$ states in the ^{21}Ne final nucleus. Such other reactions as (d,t) , $(^3\text{He},\alpha)$ and (d,n) have also been used to populate $T = 3/2$ states in nuclei of masses 21, 23 and 27.

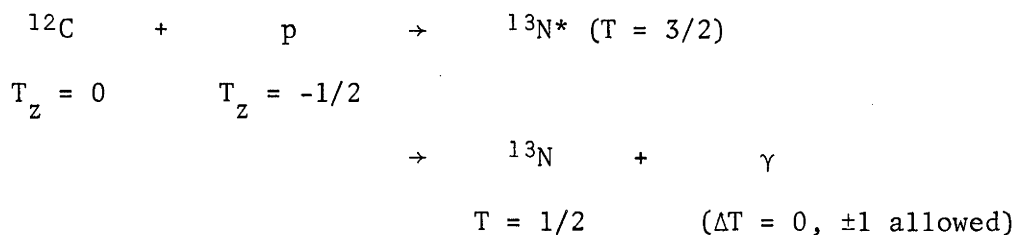
2.3 COMPOUND NUCLEUS REACTIONS

$T = 3/2$ states in both $4n + 1$ and $4n - 1$ nuclei have been studied using isospin forbidden resonance reactions. Nuclei of mass up to 40 have been examined. Such isospin forbidden reactions enable the locations, widths and decay modes of $T = 3/2$ states to be accurately measured. Since, as previously stated, the aim of this section is to look at $T = 2$ states, only a short summary of $T = 3/2$ work will be given. Cerny's review article [Ce 68] already provides a detailed account of $T = 3/2$ states although that survey was stopped in February 1968. Hanna's articles [Ha 70a, Ha 69] also cover the field of forbidden resonance reactions.

The reactions that can be used may be singly or doubly isospin forbidden. For example, proton scattering from a " $4n$ type" target nucleus is doubly forbidden, i.e. it is forbidden in the entrance and exit channels, as has been previously explained. An example of such a reaction is proton scattering from ^{12}C , i.e.



The proton capture reaction on this target nucleus is only once forbidden, in the entrance channel, as follows:



These reactions and others, e.g. elastic triton scattering, have all been used to successfully populate $T = 3/2$ states in $T_z = \pm 1/2$ nuclei. In examining the resonance reactions it is convenient [Ce 68] to group them into a number of classes.

2.3.1 $T = 3/2$ States in $4n + 1$ Nuclei

In this case n represents a positive integer up to around 9. A characteristic of these $4n + 1$ nuclei e.g. ${}^{17}\text{F}$, ${}^{21}\text{Ne}$, etc., is that all particle channels are isospin forbidden for the low-lying $T = 3/2$ states. Thus these states appear as sharp, strong resonances in say a (p, γ) capture reaction, provided that the proton width is not too small. Such reactions normally involve the bombardment of a $4n$ type nucleus. The situation that is current in these reactions is shown in figure 1.3.1 as previously discussed. The production of $T = 3/2$ states in $T_z = \pm 1/2$ nuclei by bombardment of $4n$ and $4n + 2$ nuclei is examined in this diagram. It illustrates (left hand side of diagram) the above reasons quoted for the narrowness of $T = 3/2$ states in $4n + 1$ type nuclei. It can be seen that in the $4n$ type ($T_z = 0$) target nucleus $T = 1$ states occur at high excitation energies, e.g. 15.1 MeV for the lowest $T = 1$ state in ${}^{12}\text{C}$. Allowed particle decays to these states from the $T = 3/2$ states are energetically impossible. Thus no isospin allowed decays can occur except for the inherently weak radiative decay.

2.3.2 $T = 3/2$ States in $4n - 1$ Nuclei

These states may be accessed via reactions on $4n + 2$ type target nuclei as illustrated on the right hand side of figure 1.3.1. Low-lying $T = 1$ states occur in these nuclei and are energetically available for allowed particle decay of the low $T = 3/2$ states. These states should be comparable to the usual $T = 1/2$, $T_z = 1/2$ states of a $4n - 1$ nucleus.

2.3.3 General Discussion

In the case of isospin forbidden reactions we are looking at states which have a finite width due to isospin impurities. The case of the lowest $T = 3/2$ state in ^{13}N is worth examining due to the fact that it has been the subject of much experimentation. The state has been observed as a resonance in both elastic and inelastic proton scattering from ^{12}C . It has also been seen in the (p, α) reaction to states in ^9B , this reaction also being isospin forbidden. The allowed gamma decay of the state to lower-lying $T = 1/2$ states has been investigated. The proton elastic scattering data produced a resonance at an excitation energy of 15.068 MeV in ^{13}N [Te 70]. This resonance was the only one observed over a 2 MeV range. In most of these isospin forbidden reactions, due to the very narrow widths of the resonances to be found, a uninformed search for the resonance would be doomed. However, in most cases, the state has been located previously in an isospin allowed reaction enabling the search area to be adequately limited. In the case of the lowest $T = 3/2$ state in ^{13}N the state had been seen previously via the $^{11}\text{B}(^3\text{He}, n)^{13}\text{N}$ and $^{15}\text{N}(p, t)^{13}\text{N}$ reactions. As Temmer [Te 70] points out, work on these allowed reactions has the disadvantage that the width of a $T = 3/2$ state populated in this way cannot be accurately obtained. This comes about due to the

limitations in resolution of particle detectors used to detect reactions products.

In the case of resonance reactions, the resonance width observed is a function of the accelerator's beam spread and the target thickness. Providing that a small beam spread is present and well known and that target thicknesses are known, the final results can be corrected for these to give far more accurate width measurements. These problems will be further discussed with the experimental work on $T = 2$ states. The table given by Temmer [Te 70] for $T = 3/2$ states in $T_z = -1/2$ nuclei, populated via bombardment of $2n$ type target nuclei, demonstrates the extremely narrow widths of these states, (see table 2.3.1). Particle proton widths are also given. Theoretical evaluation of these data in order to obtain isospin mixing parameters remains to be done. Such work would involve the calculation of matrix elements of the type:

$$\frac{\langle \psi_{3/2}^J | V^C | \psi_{1/2}^J \rangle}{E_{3/2} - E_{1/2}} \quad (\text{ref. [Te 70]}) \quad (17)$$

The calculations would then enable a systematic study of isospin mixing over the low mass region to be performed.

2.4 $T = 2$ STATES IN $T_z = 0$ NUCLEI

It is intended in this section to cover the survey of Cerny [Ce 68] in relation to $T = 2$ states and refer to new data published since then. Thus the present summary will treat only $T = 2$ states in $T_z = 0$ nuclei, i.e. those analogue states removed 2 units of isospin from the ground state of the nucleus. The study of these states in self-conjugate nuclei is important since the level properties provide sensitive tests of model predictions. Observa-

bidden particle decay observed. The state has not been seen in an isospin forbidden resonance reaction although these have been studied, e.g. $^{39}\text{K}(p,p_0)$, (p,γ_0) and $(p,\gamma\gamma)$. References for the work done on ^{40}Ca are contained in table 2.5.1 below.

Table 2.5.1

T = 2 State in ^{40}Ca : References

Allowed Reactions	Mc 69, Ce 68, Ha 70b, Mc 70
Forbidden Reactions	-

2.5.1 ^{40}Ca : Allowed Reactions

The lowest T = 2 state has been observed via the above (p,t) reaction by two groups, at energies of 11.978 ± 0.025 MeV [Ha 70b] and 11.970 ± 0.065 MeV [Ce 68] excitation energy respectively. In both cases angular distribution measurements on the state confirmed its J^π as 0^+ , as expected. Partial widths for decay of the state were determined by McGrath et al. [Mc 70] and are shown in table 2.5.2.

Table 2.5.2

Partial Widths from Allowed Reactions

$\Gamma_{\alpha_0}/\Gamma = 1.00 \pm 0.10$
$\Gamma_{\alpha_1}/\Gamma \sim 0.0$
$\Gamma_{p_1}/\Gamma \sim 0.0$

These conditions are illustrated in figure 2.5.1.

2.5.2 ^{40}Ca : Forbidden Reactions

A search for the lowest T = 2 state in ^{40}Ca via elastic

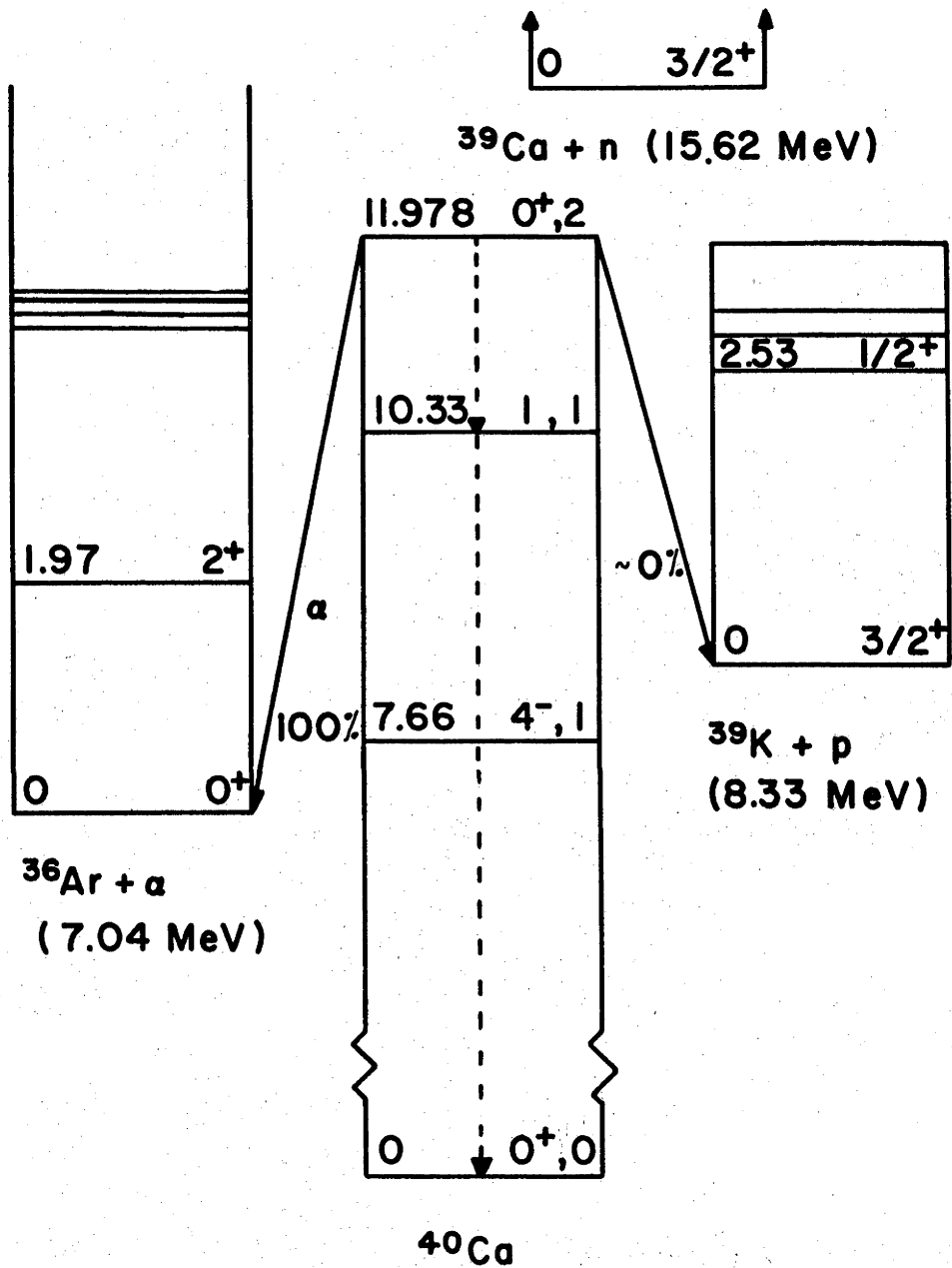


Figure 2.5.1: Excitation energy and decays of the lowest $T = 2$ state in ^{40}Ca [Mc 70]. Dotted decay indicates possible γ -decay of state as discussed in the text.

scattering of protons on ^{39}K has been performed at A.N.U. The search for the state via the isospin forbidden reaction was prompted by the successful search for the lowest $T = 2$ state in ^{24}Mg , at $E_x = 15.436 \pm 0.005$ MeV, via the $^{23}\text{Na}(p,\gamma\gamma)$ and $^{23}\text{Na}(p,p_0)$ reactions [Ri 67]. It is to be noted here that Γ_p/Γ for the lowest $T = 2$ state of ^{24}Mg (see section 2.9) is approximately 0.6. At the time of performing this experiment, the lowest $T = 2$ state in ^{40}Ca had been observed via the allowed $^{42}\text{Ca}(p,t)$ reaction (see "allowed reactions" section 2.5.1 above). The aims of the experiment were to attempt to measure the proton reduced width of the state and check on its isospin mixing. Figure 2.5.2(b) shows the energy levels of ^{40}Ca in relation to the $^{39}\text{K} + p$ threshold and the excited states of ^{40}K , the $|T_z| = 1$ nucleus. The ^{24}Mg case is also shown for comparison (see reference [Ri 67]).

2.5.3 Experimental Search for the Lowest $T = 2$ State in ^{40}Ca via $^{39}\text{K}(p,p_0)$

At the time of performing the above experiment, no elastic proton scattering data for ^{39}K were available within the desired energy range. The data taken consisted of two series of runs using protons supplied from the EN tandem accelerator at A.N.U. In order to excite the state protons of energy approximately 3.75 MeV were required.

In the first series of runs protons were elastically scattered from a natural potassium iodide target with a thickness of $20 \mu\text{g}/\text{cm}^2$ corresponding to an energy loss of approximately 1 keV for 2.75 MeV protons. The targets were made by vacuum evaporation and deposition of the material onto $15 \mu\text{g}/\text{cm}^2$ carbon foils. The scattered particles were detected using a 560μ silicon surface barrier detector at an angle of $\theta_{\text{LAB}} = 95^\circ$. The excitation func-

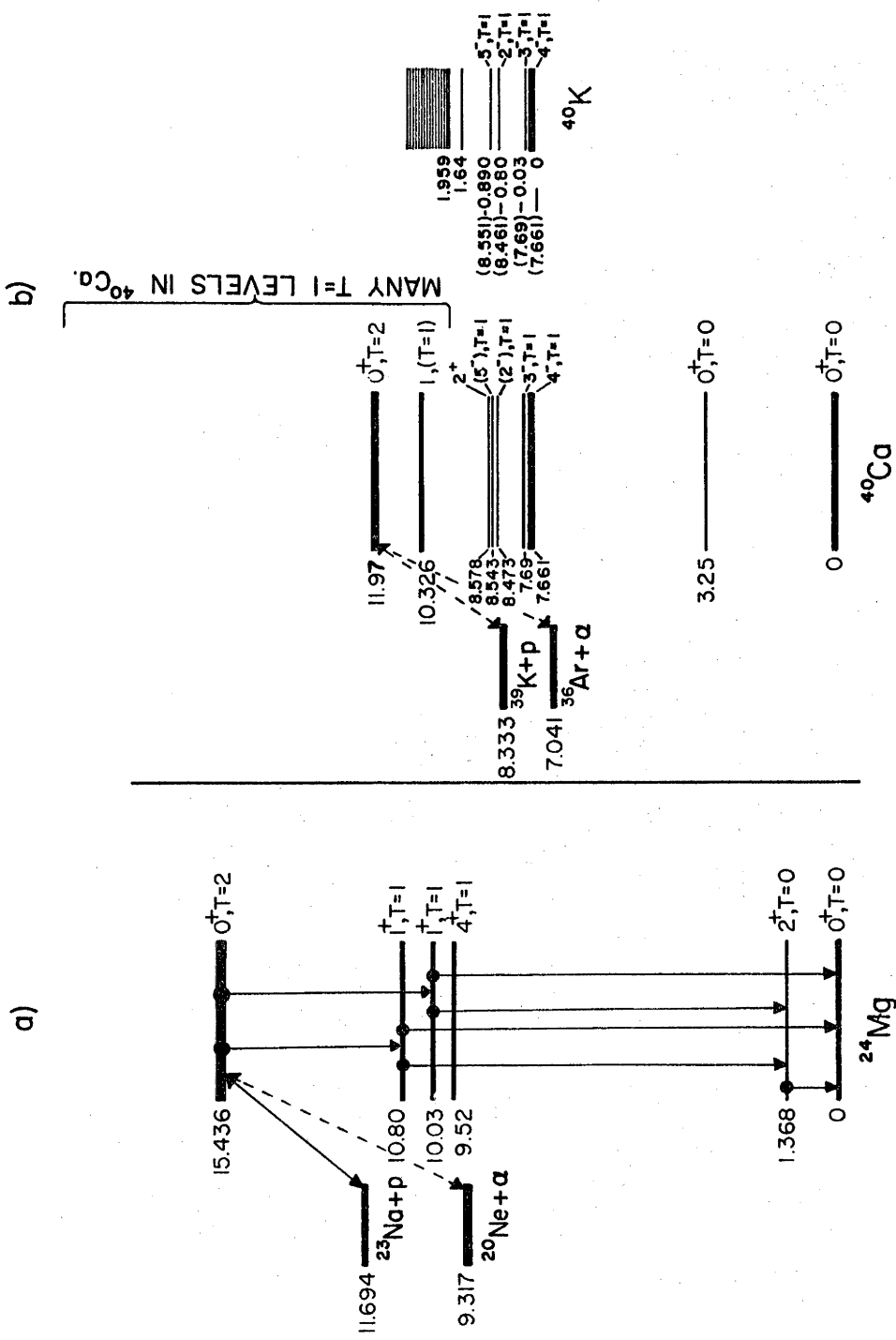


Figure 2.5.2: The lowest $T = 2$ states in ^{24}Mg and ^{40}Ca showing γ -decay of ^{24}Mg $T = 2$ state.

tion was measured in steps of approximately 2 keV proton bombarding energy from $E_p = 2.675$ MeV ($E_x = 11.916$ MeV) to $E_p = 3.788$ MeV ($E_x = 12.026$ MeV). A typical proton spectrum is shown at the top of figure 2.5.3. It can be seen from this figure that counts in the potassium peak had to be corrected for a small overlap of the iodine peak as well as for background. Figure 2.5.4 shows the excitation function measured, the errors in the data points mainly coming from background subtraction.

In the second series of runs, data were taken using a 40 $\mu\text{g}/\text{cm}^2$ natural potassium fluoride target. Since these targets rapidly absorb water when exposed to air, it was necessary to transfer them under vacuum from the evaporator to the scattering chamber. A special vacuum transfer target ladder assembly was used for the purpose. For this second series of runs an energy region of 65 keV was investigated spanning the $T = 2$ excitation energy reported by Garvey and Cerny [Ga 68]. Excitation functions were now taken at five angles simultaneously, namely $\theta_{\text{LAB}} = 95^\circ, 115^\circ, 135^\circ, 150^\circ$ and 155° . Surface barrier detectors of 1000 μ in thickness were used. A characteristic spectrum taken is shown in figure 2.5.3(b) for an observation angle of 155° and a proton bombarding energy of 3.76 MeV. This spectrum shows elastic scattering groups from carbon, oxygen, fluorine and potassium as well as inelastic scattering from fluorine. The data were recorded using the routing mode facility of the IBM 1800 on-line data acquisition system [Ca 69].

Figure 2.5.5 shows the excitation functions obtained at each angle for elastic scattering from ^{39}K . Due to the high natural abundance of ^{39}K (93%) the data are assumed to be unaffected by small amounts of ^{40}K and ^{41}K . The elastic scattering data for both ^{19}F and ^{12}C were also analyzed at each observation

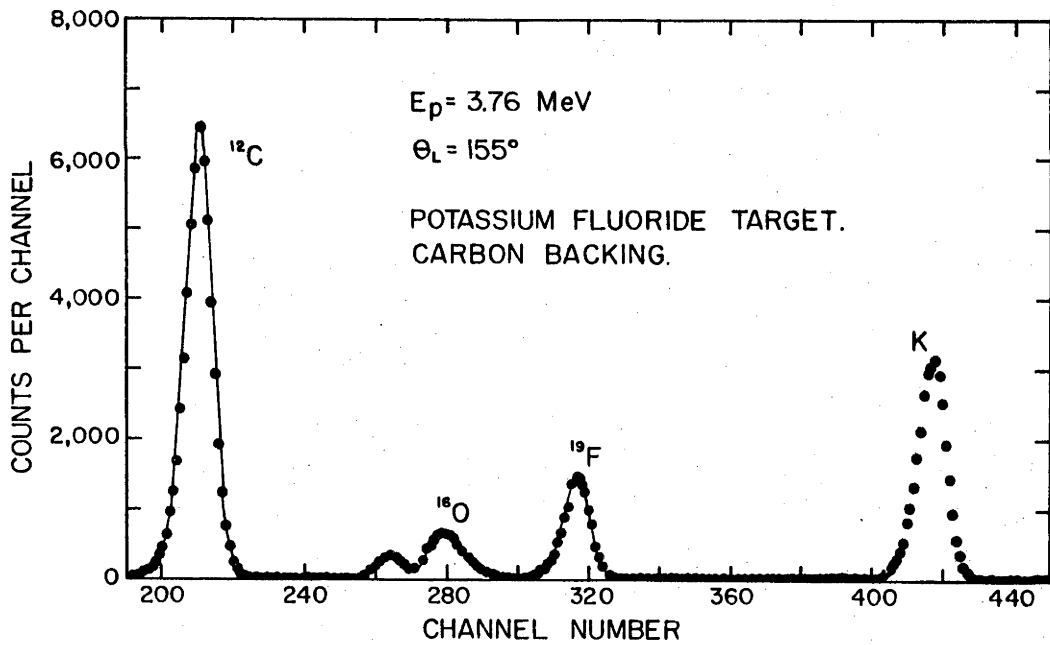
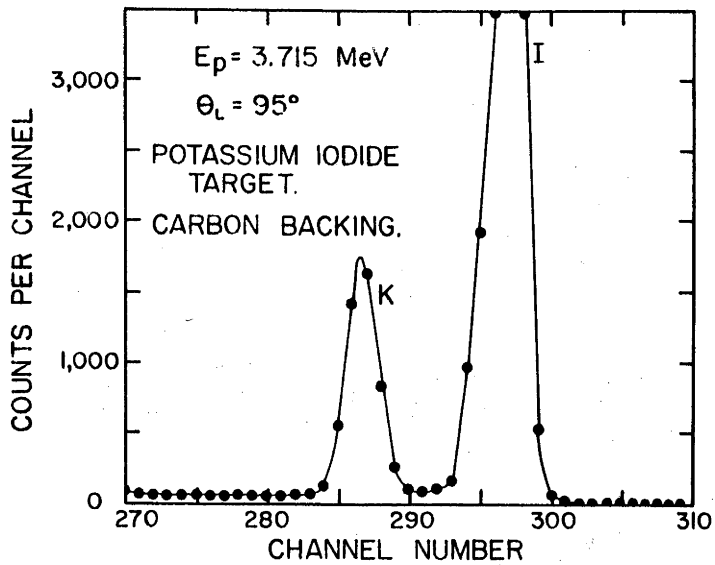


Figure 2.5.3: Typical proton spectra from $^{39}\text{K} + p$ experiments.

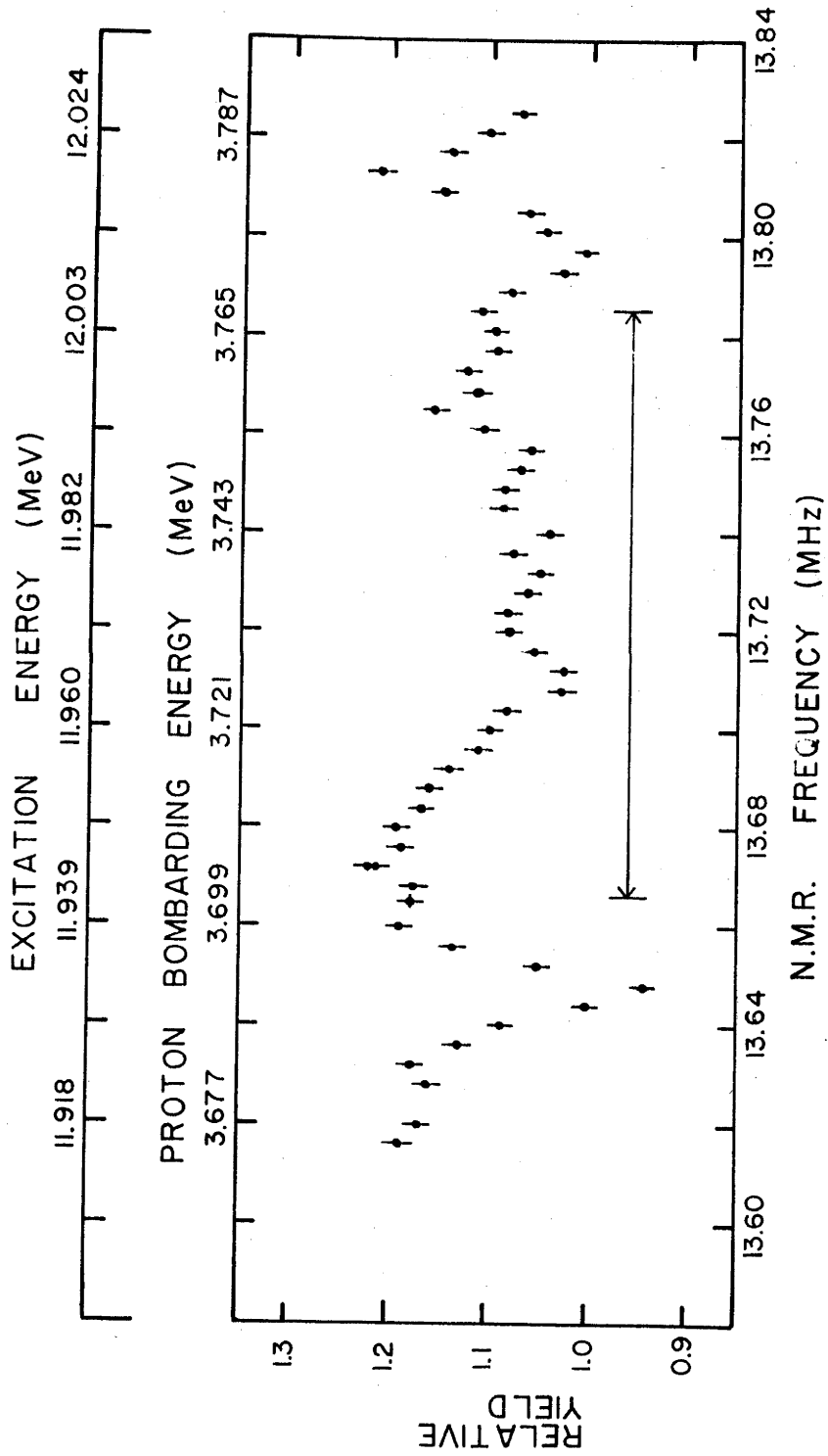


Figure 2.5.4: Excitation function for $^{39}\text{K} + p$ experiment, KI target.

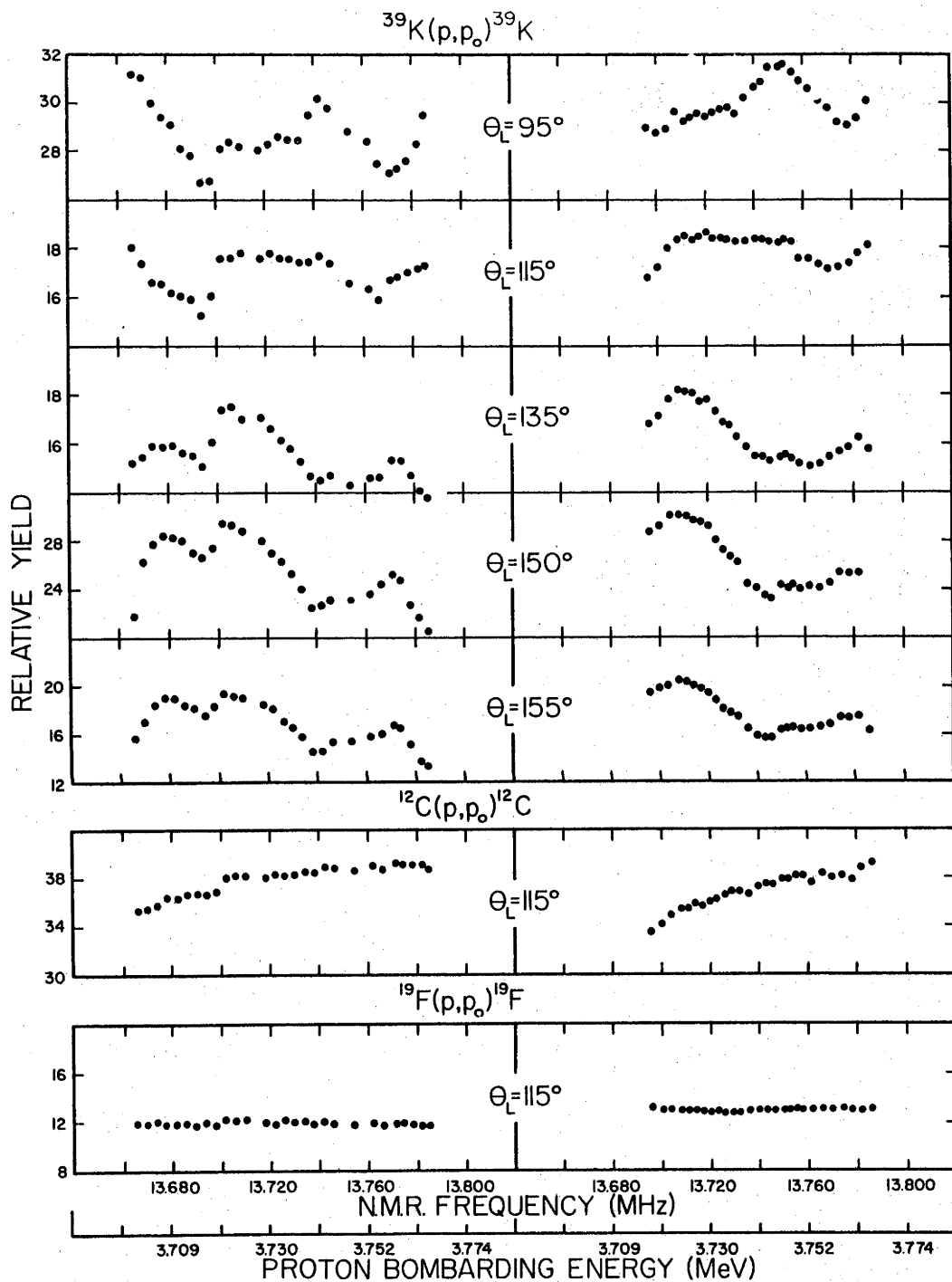


Figure 2.5.5: Excitation functions at 5 angles for $^{39}\text{K} + p$, KF target.

angle. Figure 2.5.5, however, only shows the data for one angle for each of these reactions ($\theta_{\text{LAB}} = 115^\circ$). This is done since the excitation functions are structureless at all angles in this region for these nuclei.

In contrast, the ^{39}K excitation functions show strong gross structure at all angles. Figure 2.5.5 also shows a repeat series of measurements which illustrates well the degree to which main features in the excitation functions could be reproduced. Both sets of data in this second series of runs had statistical errors of consistently less than 1% and generally $\pm\frac{1}{2}\%$. It is to be noted that the data from the second set of runs in the second series show a systematic energy shift upwards of around 3 keV compared to the first set of data, even though the 90° magnet of the EN tandem accelerator was recycled several times between these two sets of runs. Within each set of runs care was taken to change the 90° magnet current always in the same direction (increasing) in order to avoid any hysteresis effects that may occur in the magnet.

2.5.4 Conclusions

Since the ground state of ^{39}K has $J^\pi = 3/2^+$, the $J^\pi = 0^+$ lowest $T = 2$ state of ^{40}Ca could be formed by d-wave proton capture through channel spins $S = 1$ or 2 . Thus a $T = 2$ state proton scattering anomaly, if observed, would be expected to show a marked change in shape as the angle of observation moves from below $\theta_{\text{CM}} = 125^\circ$ to above 125° since $P_2(\cos \theta)$ goes through zero and changes sign. The data exhibit only one such anomaly which occurs at a proton bombarding energy of 3.742 MeV (E_x in $^{40}\text{Ca} = 11.981$ MeV) in good agreement with the energy range for the $T = 2$ state quoted earlier. To identify the resonance as a $T = 2$ state resonance is not possible without further supporting evidence. Such

evidence would possibly consist of the observation of the γ -decay of the state through the lower lying $T = 1$ states. This will be discussed in the next section. The small magnitude of the above resonance can be clearly seen from the excitation function shown in figure 2.5.4. Stronger broad resonances arising from excitation of overlapping $T = 1$ states surround the suspected $T = 2$ state. As a result determination of the ℓ -value for the resonance would require the fitting of resonance parameters for as many as five or six distinct resonances simultaneously. It is unlikely that sufficient accuracy for a unique assignment could be achieved.

2.5.5 Gamma Decay of the Lowest $T = 2$ state in ^{40}Ca

Figure 2.5.6 shows a simplified diagram of the energy levels near the lowest $T = 2$ state in ^{24}Mg and ^{40}Ca . As outlined by Hanna [Ha 70a] the $T = 2$ states are expected to decay through the lower $T = 1$ states. In the ^{24}Mg case, decay would occur through the $J^\pi = 1^+$, $T = 1$ state at 10.03 MeV, an M1 transition. The situation for ^{40}Ca is not as clear. A $J = 1$, $T = 1$ state at 1.033 MeV excitation is a likely candidate due to the high spins of the other surrounding states. Decay via these states would involve transitions of higher order multipolarity which are much less probable. However, the parity of the 10.33 MeV state is not known and cannot be assumed to be positive. Some preliminary calculations based on these facts are important.

For the ^{24}Mg decay the single particle M1 transition strength is:

$$\begin{aligned} \Gamma_{\text{M1}} &= 2.1 \cdot 10^{-2} \cdot E_\gamma^3 \\ &= 3.3 \text{ eV} \end{aligned} \quad [\text{Bu } 63]$$

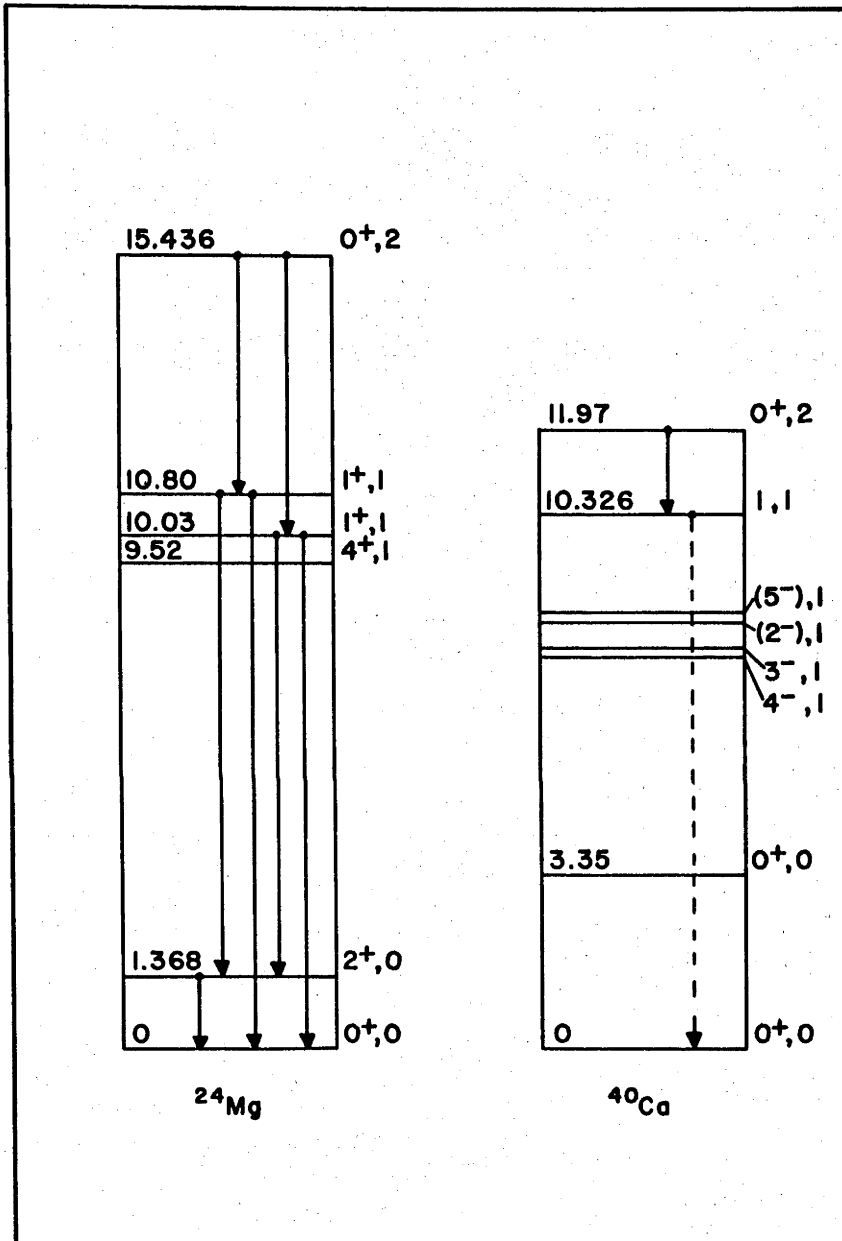


Figure 2.5.6: Simplified diagram of γ -decays of lowest $T = 2$ states in ^{24}Mg and ^{40}Ca .

for a γ -ray energy of 5.4 MeV. For the ^{40}Ca case, two calculations are needed. Assuming negative parity for the 10.33 MeV state, an E1 transition with $E_\gamma = 1.65$ MeV, would give:

$$\begin{aligned}\Gamma_{E1} &= 6.8 \cdot 10^{-2} \cdot A^{2/3} \cdot E_\gamma^3 \\ &= 3.57 \text{ eV}\end{aligned}\quad [\text{Bu } 63]$$

Assuming positive parity for the state an M1 transition has a strength of 0.094 eV. Now the 10.326 MeV $T = 1$ state we are considering is proton unbound and indeed has been populated via the $^{39}\text{K}(p,\gamma)^{40}\text{Ca}$ reaction [Le 66, Le 67]. These experiments by Leenhout and Endt showed a 90% branch to the ^{40}Ca ground state as well as an upper limit of 0.8 keV for the total width of the state.

Summarising the ^{40}Ca situation, the γ -decay of the lowest $T = 2$ state may proceed via a number of lower lying $T = 1$ states, in particular through the $T = 1, J = 1$ state at 10.326 MeV. This state is, however, proton unbound and so the cross section for a cascade γ -decay of the lowest $T = 2$ state through this state becomes very small. For this 10.33 MeV state we have that Γ_p/Γ is probably very much greater than Γ_γ/Γ . Coupling this with the now known small Γ_p/Γ value for the $T = 2$ state as well as possible decays through other $T = 1$ states makes a search for the lowest $T = 2$ state in ^{40}Ca via the $^{39}\text{K}(p,\gamma\gamma)^{40}\text{Ca}$ reaction hardly worthwhile. This argument would also apply, but to a lesser degree, to the reaction $^{36}\text{Ar}(\alpha,\gamma\gamma)^{40}\text{Ca}$. However, it does not apply to the $^{36}\text{Ar}(\alpha,\alpha)^{36}\text{Ar}$ reaction which appears to be the most favourable one to use for a search for the lowest $T = 2$ state in ^{40}Ca . Such an experiment would involve the use of an ^{36}Ar gas target. An approximate alpha-particle bombarding energy of 3 MeV would be needed, well within the capabilities of the A.N.U. EN tandem accelerator.

Surface barrier detectors could again be used and spectra collected simultaneously using the IBM 1800 data acquisition system.

2.6 ^{36}Ar : SUMMARY

The lowest $T = 2$ state in ^{36}Ar at 10.858 ± 0.035 MeV excitation energy has again only been observed via the allowed (p,t) reaction [Ha 70b], i.e. $^{38}\text{Ar}(p,t)^{36}\text{Ar}_{T=2}$. The 0^+ spin and parity of the state were confirmed via triton angular distribution measurements. Decay of the state into isospin-forbidden particle channels has not been studied. The allowed γ -decay of the state has also not been examined. The literature contains no reports of the use of isospin-forbidden resonance reactions to search for the state. Such forbidden reactions that could be studied are $^{35}\text{Cl}(p,\gamma)^{36}\text{Ar}$ and $^{35}\text{Cl}(p,p)^{35}\text{Cl}$ at proton bombarding energies of approximately 2.5 MeV. The alpha scattering reaction $^{32}\text{S}(\alpha,\alpha)^{32}\text{S}$ could also be used in an attempt to populate the lowest $T = 2$ state. Alphas of approximately 5 MeV bombarding energy would be needed.

Table 2.6.1

$T = 2$ States in ^{36}Ar , References

Allowed Reactions	Ha 70b
Forbidden Reactions	-

These results are illustrated in figure 2.6.1.

2.7 ^{32}S : SUMMARY

The lowest $T = 2$ state in ^{32}S has been observed both via the isospin-allowed reaction $^{34}\text{S}(p,t)^{32}\text{S}$ and the isospin-forbidden reactions $^{31}\text{P}(p,\gamma)^{32}\text{S}^*$ and $^{31}\text{P}(p,p_0)^{31}\text{P}$.

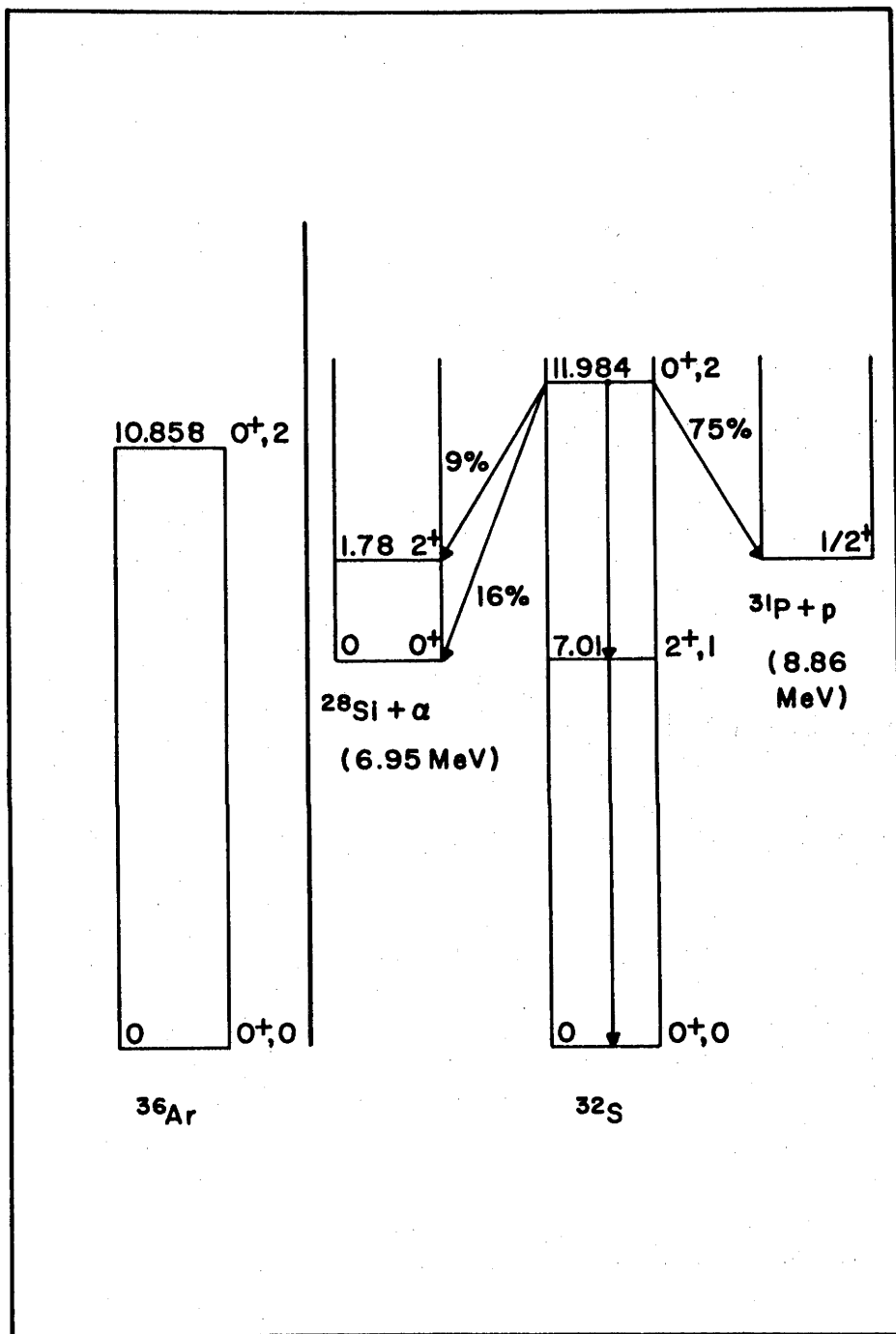


Figure 2.6.1: Lowest T = 2 states of ^{36}Ar and ^{32}S .

2.7.1 ^{32}S : Allowed Reactions

In the case of ^{32}S the lowest $T = 2$ state has been studied via both isospin-allowed and forbidden reactions. The allowed $^{34}\text{S}(p,t)$ reaction has been used by a number of groups to excite the lowest $T = 2$ state at $E_x = 12.034 \pm 0.040$ MeV [Ha 70b, Mc 69, Ce 68]. McGrath et al. [Mc 69] have also examined the isospin-forbidden particle decays of the state to obtain the partial widths given in table 2.7.1.

Table 2.7.1

Lowest $T = 2$ State in ^{32}S , Partial Widths

Γ_{p0}/Γ	0.75 ± 0.12
Γ_{α_0}/Γ	0.16 ± 0.06
Γ_{α_1}/Γ	0.09 ± 0.04
Normalised to 100% for all observed decays	

2.7.2 ^{32}S : Forbidden Reactions

The lowest $T = 2$ state in ^{32}S has also been populated at an excitation energy of $E_x = 11.984 \pm 0.004$ MeV using the isospin-forbidden reactions $^{31}\text{P}(p,p_0)^{31}\text{P}$ and $^{31}\text{P}(p,\gamma)^{32}\text{S}$ [He 68, Sn 69a]. The γ -decay of the state via a cascade through the $T = 1$ state around 7 MeV was observed by γ - γ coincidence measurements. An upper limit to the total width of the state of $\Gamma \leq 2.5$ keV was obtained. Measurements of the proton partial width give $\Gamma_p/\Gamma \approx 0.6$. The forbidden (p,α_0) and (p,α_1) reactions have also been studied but no evidence for the state was found from these reactions.

The above data are summarised in figure 2.6.1 and the references are given in table 2.7.2.

Table 2.7.2

Lowest $T = 2$ State in ^{32}S , References

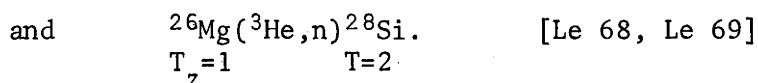
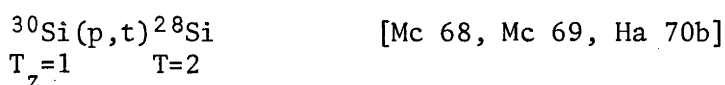
Allowed Reactions	Mc 69, Ha 70b, Ce 68, Mc 70
Forbidden Reactions	He 68, Sn 69a

2.8 ^{28}Si : SUMMARY

The lowest $T = 2$ state in ^{28}Si has been found using both isospin-allowed and forbidden reactions, as set out below.

2.8.1 ^{28}Si : Allowed Reactions

The lowest $T = 2$ state in ^{28}Si has been populated via the isospin-allowed, two-nucleon transfer reactions



Excitation energies for the state of 15.206 ± 0.025 MeV [Mc 68, Mc 69, Ha 70b] and 15.00 ± 0.05 MeV [Le 68, Le 69] respectively have been thus obtained. Decay of the state into forbidden particle channels has also been measured [Mc 70] and partial widths calculated as shown in table 2.8.1.

2.8.2 ^{28}Si : Forbidden Reactions

The following isospin-forbidden resonance reactions have been used to populate the state at an excitation energy in ^{28}Si of 15.221 ± 0.005 MeV [Sn 69b]:

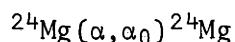
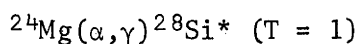


Table 2.8.1

Lowest $T = 2$ State in ^{28}Si , Partial Widths

Γ_{α_0}/Γ	0.81 ± 0.10	[Mc 70]
Γ_{α_1}/Γ	0.09 ± 0.04	
Γ_{p_0}/Γ	0.05 ± 0.09	
Γ_{p_1}/Γ	0.05 ± 0.06	

Special note should be made of the very small proton reduced widths for this state.

and $^{24}\text{Mg}(\alpha, \alpha_1)^{24}\text{Mg}^*$.

The gamma decay of the state via the 1^+ , $T = 1$ states in the region of 11 MeV in ^{28}Si has also been observed enabling an upper limit of 2 keV to be placed on the total width of the state. Using a "thick target" relative to resonance approximation [Fo 48], the resonance strength

$$\Gamma_{\alpha} \Gamma_{\gamma}/\Gamma = 1.25 \text{ eV}$$

was calculated. Combining this result with the previous alpha particle partial width measurements a radiative width of

$$\Gamma_{\gamma} \approx 1.7 \text{ eV}$$

is obtained for the state. This compares well with the Weisskopf estimate of 1.6 eV for the M1 decay of a $(0^+, T = 2)$ state to a $(1^+, T = 1)$ state. Searches for the state via the forbidden $^{27}\text{Al} + p$ channel have produced negative results [Ku 68, Sn 69b]. No evidence for the state was found in the $^{24}\text{Mg}(\alpha, p)$ work done at the same time as the $^{27}\text{Al} + p$ studies. These results placed an upper

limit for Γ_p/Γ_α of 0.08 on the state.

The above data are summarised in figure 2.8.1. References on the lowest $T = 2$ state in ^{28}Si are given in table 2.8.2.

Table 2.8.2

Lowest $T = 2$ State in ^{28}Si , References

Allowed Reactions	Mc 68, Ha 69, Mc 69, Mc 70, Le 68, Le 69, Th 69
Forbidden Reactions	Ku 68, Sn 69a, Sn 69b

2.9 ^{24}Mg : SUMMARY

A substantial amount of work has been done on the investigation of the lowest $T = 2$ state of ^{24}Mg using both isospin-allowed and forbidden reactions as outlined below.

2.9.1 ^{24}Mg : Allowed Reactions

Using the $^{22}\text{Ne}(^3\text{He},n)$ allowed reaction Adelberger et al. [Ad 67] observed the lowest $T = 2$ state in ^{24}Mg at 15.441 ± 0.015 MeV excitation energy and were able to assign an upper limit to the total width of the state of 35 keV ($\Gamma < 35$ keV). This value placed a much smaller error limit on the energy of the state compared to the value of 15.40 ± 0.12 MeV given by Garvey et al. in 1964 [Ga 64] using the allowed reaction $^{24}\text{Mg}(p,t)^{24}\text{Mg}$. McGrath et al. [Mc 67] also populated the state using the (p,t) allowed reaction, at an excitation energy of 15.43 ± 0.07 MeV and observed its decay into the isospin forbidden proton and alpha channels. The measurements were repeated by McGrath et al. [Mc 69] in 1969 and the results were in good agreement with the earlier work. Table 2.9.1 shows the data taken on the branching ratios for the proton and alpha

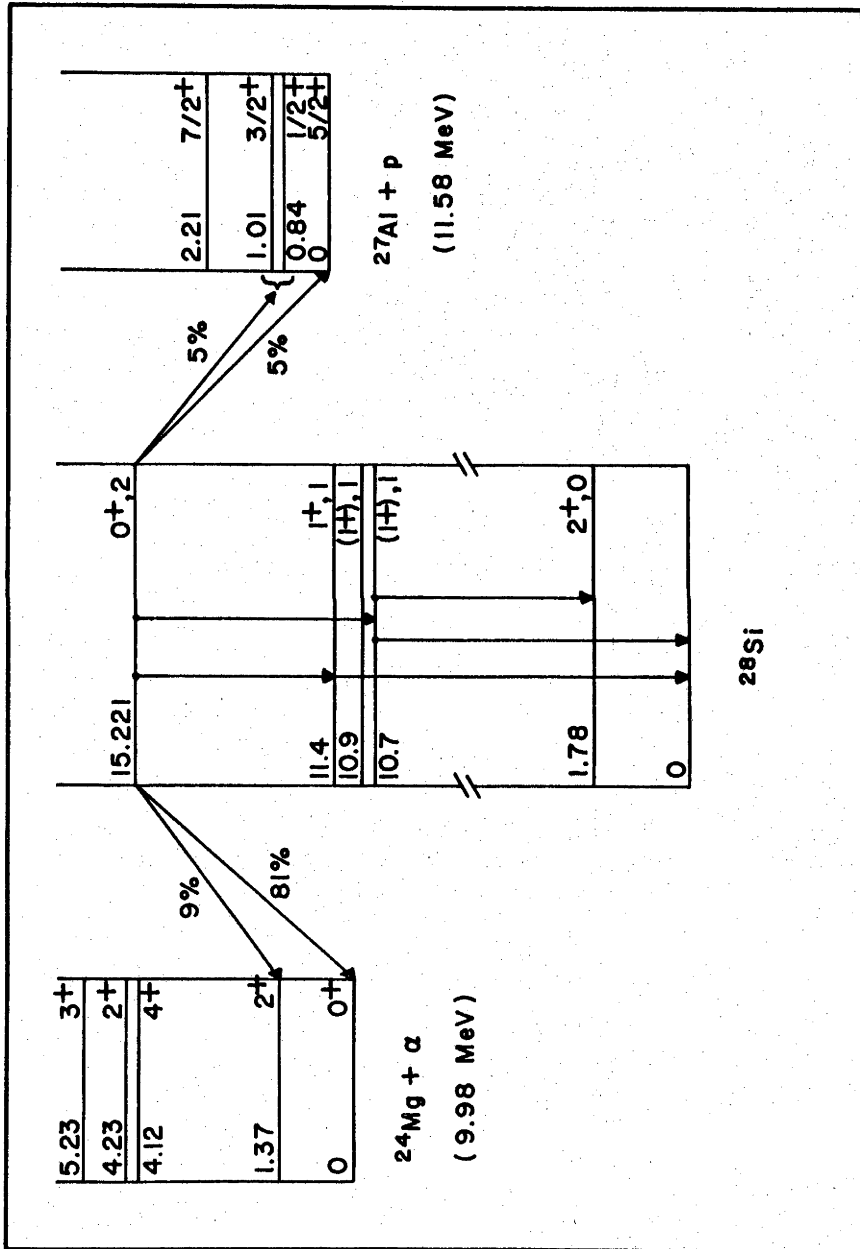


Figure 2.8.1: Lowest $T = 2$ state of ^{28}Si .

decay of the $T = 2$ state in both these experiments.

Table 2.9.1
Lowest $T = 2$ State in ^{24}Mg , Partial Widths

Decay	Value	
	Mc 67	Mc 69
Γ_{α_0}/Γ	0.08	0.03
Γ_{α_1}/Γ	0.17	0.22
Γ_{p_0}/Γ	0.59	0.74
Γ_{p_1}/Γ	0.05	0.01
Γ_{p_2}/Γ	0.01	-
$\Gamma_{p_3+p_4}/\Gamma$	0.10	-

2.9.2 ^{24}Mg : Forbidden Reactions.

Riess et al. [Ri 67] were able to populate the lowest $T = 2$ state in ^{24}Mg using the once- T -forbidden proton capture reaction $^{23}\text{Na}(p,\gamma)^{24}\text{Mg}_{T=1}^*$ and twice- T -forbidden elastic scattering reaction $^{23}\text{Na}(p,p)^{23}\text{Na}$. The γ -decay of this (0^+ , $T = 2$) state was found to proceed via two $T = 1$, $J^\pi = 1^+$ levels at 10.80 and 10.03 MeV. The state was found at an excitation energy of 15.436 ± 0.005 MeV which agreed well with the allowed reaction work. The capture reaction was relatively strong with $\Gamma_p/\Gamma \sim 1$ eV for the predominant decay to the 10.03 MeV level. An upper limit to the level width was assigned as 2 keV. The elastic scattering work indicated that Γ_p constitutes a major proportion of Γ in agreement with the results of McGrath et al. [Mc 67]. Figure 2.9.1 shows the observed γ -decays of the $T = 2$ state. Snover [Sn 69a] measured branching ratios for the allowed γ -decays of the $T = 2$ state and the $T = 1$

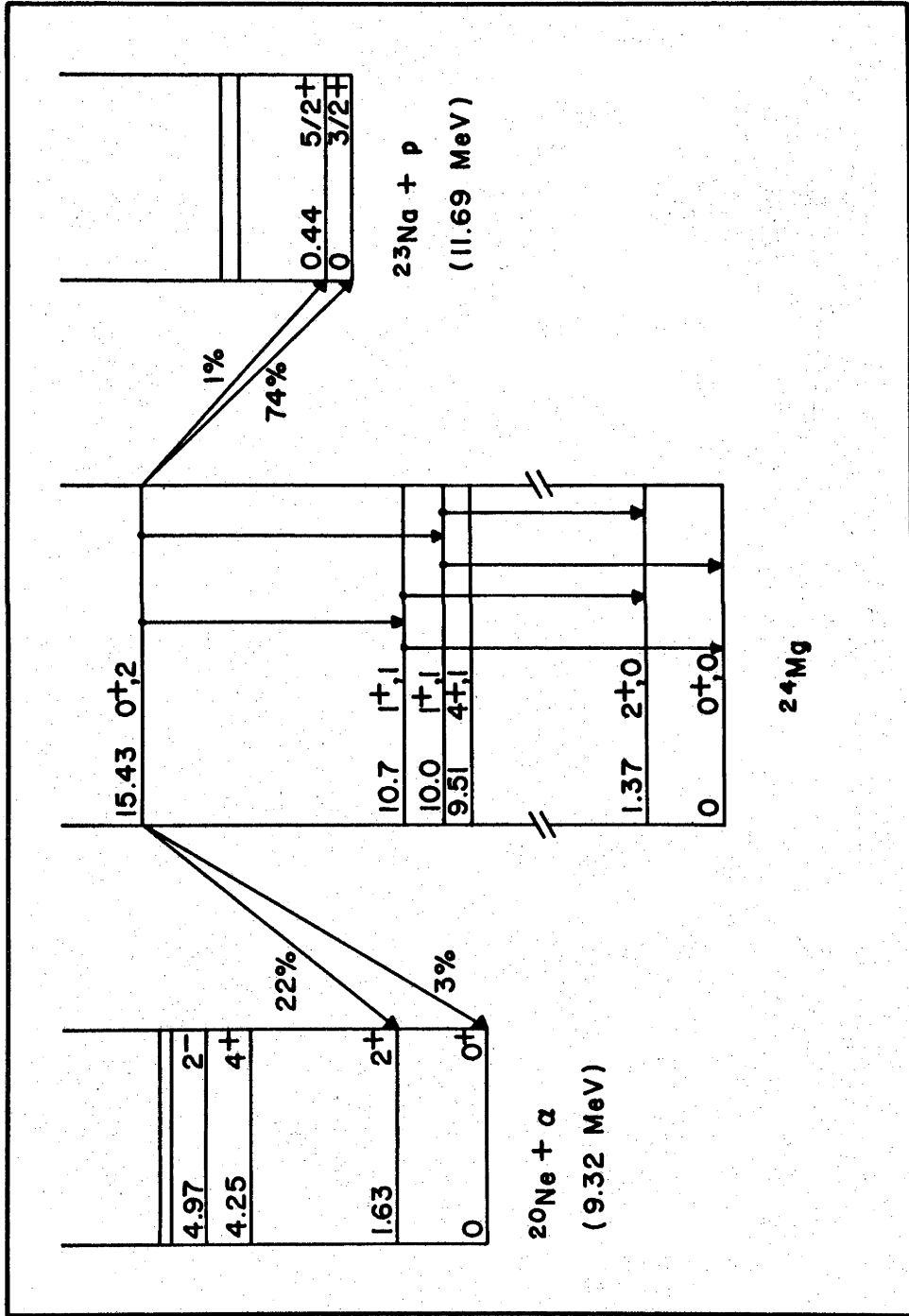


Figure 2.9.1: Lowest T = 2 state of ^{24}Mg .

states involved. The results, from his thesis, are shown in table 2.9.2.

Table 2.9.2

Lowest $T = 2$ State in ^{24}Mg , γ -Ray Branching Ratios

Transition	Relative Intensity
$(0^+, 2) \rightarrow (1^+, 1)$ 10.03 MeV	75%
$(0^+, 2) \rightarrow (1^+, 1)$ 10.80 MeV	25%
$(0^+, 2) \rightarrow (2^+, 0)$ 1.37 MeV	< 1.6%
$(1^+, 1)$ 10.03 MeV \rightarrow $(0^+, 0)$ 0.0 MeV	74%
$(1^+, 1)$ 10.03 MeV \rightarrow $(2^+, 0)$ 1.37 MeV	26%
$(1^+, 1)$ 10.80 MeV \rightarrow $(0^+, 0)$ 0.0 MeV	71%
$(1^+, 1)$ 10.80 MeV \rightarrow $(2^+, 0)$ 1.37 MeV	29%

From these results, Snover was able to assign a total decay strength upper limit of $\Gamma_{\gamma} \approx 2.3$ eV for the lowest $T = 2$ state.

2.9.3 ^{24}Mg : Discussion

Table 2.9.3 gives a summary of the measured excitation energies for the lowest $T = 2$ state in ^{24}Mg obtained from both allowed and forbidden reactions. Kingston et al. [Ki 66] present a discussion on a test of charge independence using the $T = 2$ multiplet of mass 24, of which three members are known, viz. ground state of ^{24}Ne , 5.9 MeV level of ^{24}Na and the 15.4 MeV level of ^{24}Mg . However, for a test of the mass equations, the analogue state in ^{24}Al is required. This can be calculated from the known ground state mass of ^{24}Al . Kingston's comparison of the $T = 2$

Table 2.9.3
Measured Excitation Energies and Total Widths
for the Lowest $T = 2$ State in ^{24}Mg

Reference	Ex (MeV)	Reaction Type	Total Width
Ad 67 } Ad 69 }	15.441 ± 0.015	Allowed	$< 35 \text{ keV}$
Ga 64	15.40 ± 0.12	Allowed	-
Mc 67	15.43 ± 0.07	Allowed	-
Ri 67	15.436 ± 0.005	Forbidden	$< 2 \text{ keV}$

multiplet and the $T = 1$ triplet shows that the charge independence assumption is justified. References for the work on ^{24}Mg are shown in table 2.9.4.

Table 2.9.4

^{24}Mg : References

Allowed Reactions	Ad 67, Ad 69, Ga 64, Mc 67, Mc 69, Mc 70
Forbidden Reactions	Ri 67, Sn 69a

2.10 ^{20}Ne : SUMMARY

The lowest $T = 2$ state in ^{20}Ne has been populated, as is the case for ^{24}Mg , by both isospin-allowed and forbidden reactions. Table 2.10.1 contains a summary of the measured excitation energies of the state.

Also, from this work, the state was found to have a small total width of approximately 2 keV. References for the work on ^{20}Ne are shown in table 2.10.2.

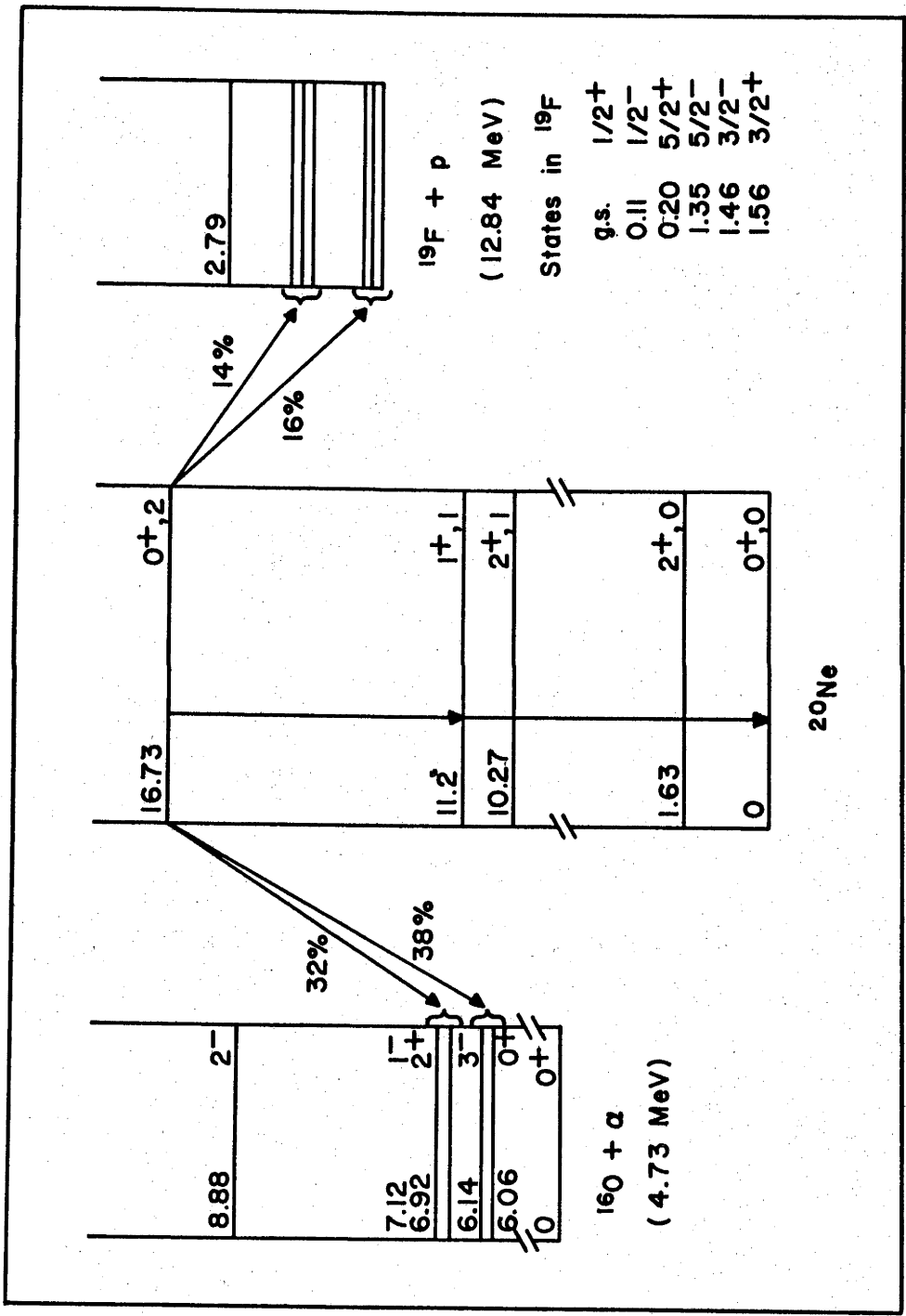


Figure 2.10.1: Lowest T = 2 state of ^{20}Ne .

Table 2.10.1
Measured Excitation Energies of the
Lowest $T = 2$ State in ^{20}Ne

Reference	Excitation Energy in MeV	Reaction
Ce 64	16.8 ± 0.1	$^{22}\text{Ne}(p,t)^{20}\text{Ne}_{T=2}^*$
Ad 67	16.730 ± 0.006	$^{18}\text{O}(^3\text{He},n)^{20}\text{Ne}_{T=2}^*$
B1 67a	16.734 ± 0.003	$^{19}\text{F}(p,p)^{19}\text{F}$
Ku 67 Sn 69a } }	16.729 ± 0.005	$^{19}\text{F}(p,\gamma)^{20}\text{Ne}$

Table 2.10.2
 ^{20}Ne References

Allowed Reactions	Ce 64, Ad 67, Mc 69, Mc 70
Forbidden Reactions	B1 67, Ku 67, Sn 69a

2.10.1 ^{20}Ne : Allowed Reactions

The lowest $T = 2$ state in ^{20}Ne has been populated using the isospin allowed reactions $^{22}\text{Ne}(p,t)^{20}\text{Ne}_{T=2}^*$ and $^{18}\text{O}(^3\text{He},n)^{20}\text{Ne}_{T=2}^*$ at excitation energies of 16.8 ± 0.1 MeV and 16.730 ± 0.006 MeV respectively [Ce 64, Ad 67]. Adelberger et al. were also able to assign an upper limit to the total width of the state of $\Gamma < 20$ keV. From angular distribution measurements they were able to assign 0^+ spin and parity to the state, as expected. Further work by McGrath et al. [Mc 69] on the population of the state via the allowed (p,t) reaction and its ensuing isospin-forbidden proton and alpha-particle decay provided estimates of the branching ratios for the decays of the $T = 2$ states, (table 2.10.3).

Table 2.10.3
 Measured Partial Widths of the Lowest
 $T = 2$ State in ^{20}Ne [Mc 69]

Decay Mode	Value
$\Gamma_{p_0+p_1+p_2}/\Gamma$	0.16 ± 0.10
$\Gamma_{p_3+p_4+p_5}/\Gamma$	0.14 ± 0.09
Γ_{α_0}/Γ	~ 0.0
$\Gamma_{\alpha_1+\alpha_2}/\Gamma$	0.38 ± 0.13
$\Gamma_{\alpha_3+\alpha_4}/\Gamma$	0.32 ± 0.13
These values normalised to 100% for all observed decay modes	

2.10.2 ^{20}Ne : Forbidden Reactions

The lowest $T = 2$ state in ^{20}Ne has been populated using the isospin forbidden reactions $^{19}\text{F}(p,p)^{19}\text{F}$ and $^{19}\text{F}(p,\gamma)^{20}\text{Ne}_{T=2}^*$. Bloch et al. [Bl 67a] populated the state using the reaction $^{19}\text{F}(p,p)^{19}\text{F}$ and measured an excitation energy of 16.734 ± 0.003 MeV, in good agreement with the values obtained from the allowed reaction work. They were also able to assign a total width of 2.1 ± 0.5 keV to the state, as well as a proton partial width of $\Gamma_p/\Gamma \sim 0.062$. The state was also observed by Kuan et al. [Ku 67] using the once-forbidden proton capture reaction $^{19}\text{F}(p,\gamma)^{20}\text{Ne}$ and again with the twice-forbidden elastic scattering of protons $^{19}\text{F}(p,p_0)^{19}\text{F}$. The state was seen, from the γ -ray work, as a resonance in the second γ -ray of the γ -cascade decay of the state through the 1^+ , $T = 1$ state at 11.2 MeV. The excitation energy of the $T = 2$ state from this experiment was found to be 16.729 ± 0.005 MeV as shown in figure 2.10.1. They were also able to assign an

upper limit to the total width of the state of $\Gamma \leq 2$ keV and to ascertain that $\Gamma_p/\Gamma \approx 0.1$. From the γ -ray yield they were able to estimate that $\Gamma_p \Gamma_\gamma/\Gamma \approx 0.5$ eV. Thus, from these values, $\Gamma_\gamma \approx 5$ eV, compared to the Weisskopf estimate for an M1 transition of 3.4 eV. Further work on these reactions by Snover et al. [Sn 69b] defined these values with more accuracy, as well as enabling estimates of relative widths for the α -decay of the state to be made (table 2.10.4).

Table 2.10.4

Results from Observation of Lowest
T = 2 State in ^{20}Ne [Sn 69a]

$$E_x = 16.729 \pm 0.005 \text{ MeV}$$

$$\Gamma = 2 \pm 1 \text{ keV}, \quad \Gamma_p \Gamma_\gamma/\Gamma = 0.92 \pm 0.23 \text{ eV}$$

$$\Gamma_\gamma (T = 2 \rightarrow T = 1) = 30 \pm 8 \text{ eV}$$

Another estimate derived from the α -decay of the state observed in this experiment and in that of McGrath et al.

[Mc 69] gives $\Gamma_\gamma \leq 8$ eV.

$$\Gamma_{\gamma_1}/\Gamma_\gamma (T = 2 \rightarrow T = 0)/(T = 2 \rightarrow T = 1) < 0.25$$

$$\Gamma_{\alpha_2}/\Gamma_{\alpha_3+\alpha_4} \leq 0.5$$

$$\Gamma_{\alpha_3+\alpha_4}/\Gamma_\gamma \leq 100$$

2.11 ^{16}O : SUMMARY

The lowest T = 2 state in ^{16}O has only been seen via the allowed reactions $^{18}\text{O}(p,t)^{16}\text{O}_{T=2}^*$ [Ce 64] and $^{14}\text{C}(^3\text{He},n)^{16}\text{O}_{T=2}^*$ [Ad 70] at excitation energies of 22.9 ± 0.1 MeV and 22.717 ± 0.008 MeV respectively. Angular distribution measurements on the reson-

ance indicated, in both cases, the $J^\pi = 0^+$ expected values for the state. It is notable that no measurements of the width of the state or of its partial widths for particle or gamma decay have yet been made.

The state has not been searched for using isospin forbidden reactions, according to the published literature. Proton bombardment on a ^{15}N target would require protons of approximate bombarding energy 11.5 MeV in order to observe the state via either scattering or capture (see figure 2.11.1). Similarly alpha particle bombardment of a ^{12}C target would require alpha particles of approximately 21 MeV energy to populate the state. References for work on ^{16}O are contained in table 2.11.1.

Table 2.11.1

^{16}O References

Allowed Reactions	Ce 64, Ad 70
Forbidden Reactions	-

2.12 ^{12}C : SUMMARY

See chapter 4 of the thesis.

2.13 ^8Be : SUMMARY

See chapter 3 of the thesis.

2.14 SUMMARY OF $T = 2$ STATES IN LOW MASS EVEN-EVEN NUCLEI

Table 2.14.1 contains a summary of the published information on the lowest $T = 2$ states in all even-even nuclei from mass 8 to mass 40. This table has been compiled from references up to November 1970 and reflects the volume of work that has been done on

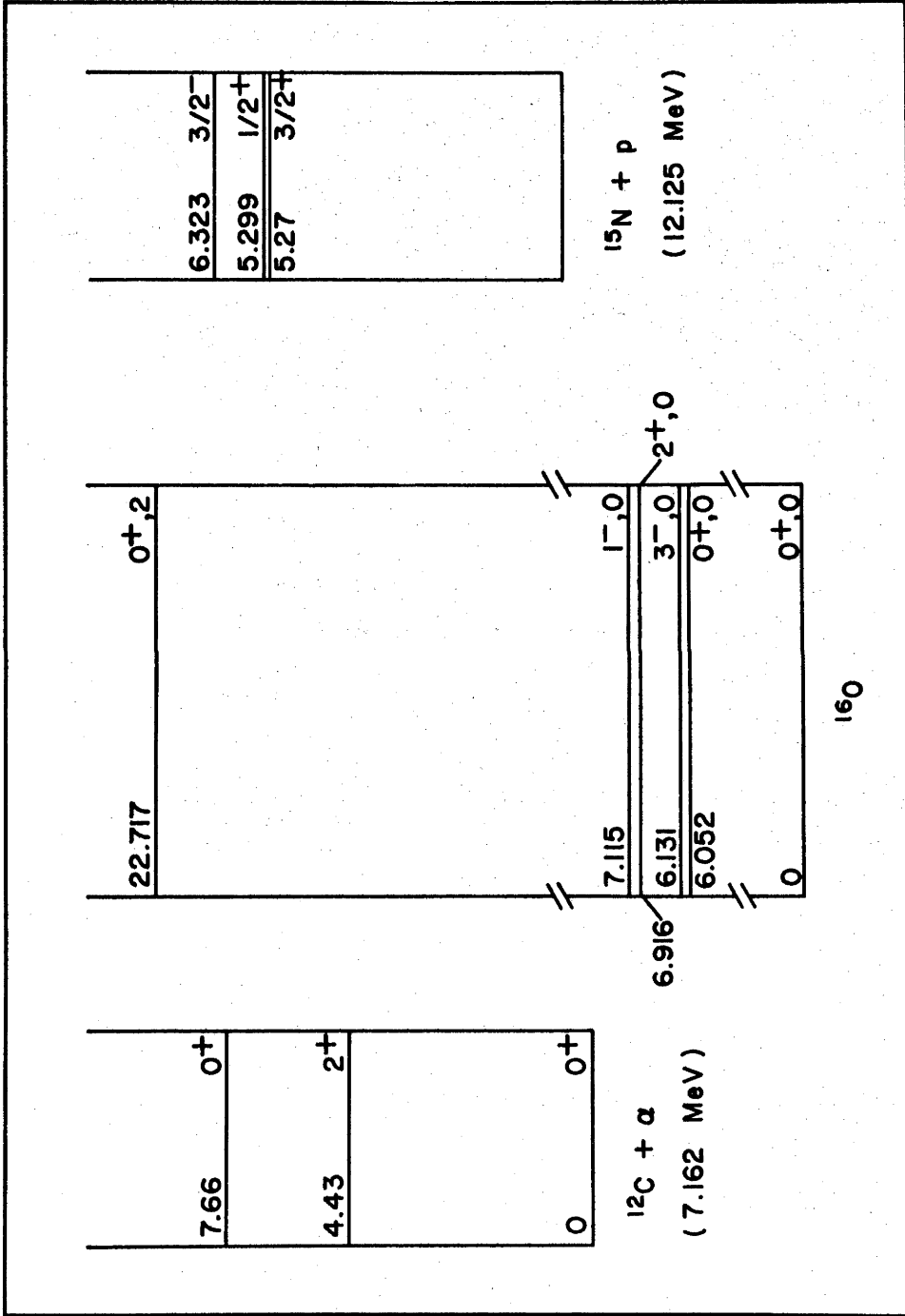


Figure 2.11.1: Lowest T = 2 state of ^{16}O .

Table 2.14.1

Lowest $T = 2$ States in Even-Even Nuclei, Masses 8 - 40

Nucleus	Ex (MeV)	Γ_{p_0}/Γ	Γ_{p_1}/Γ	Γ_{p_2}/Γ	Γ_{p_3}/Γ	Γ_{p_4}/Γ	Γ_{α_0}/Γ	Γ_{α_1}/Γ	Γ_{γ}
^8Be	27.483 ± 0.010	$p_0 < p_1$	-	-	-	-	-	-	$\Gamma \approx 10 \text{ keV}$
^{12}C	27.585 ± 0.020	$d_0 p_0 < 80 \text{ eV}$	$d_0 p_1 < 35 \text{ eV}$	$d_0 p_2 \leq 45 \text{ eV}$	$d_0 p_3 \leq 40 \text{ eV}$	-	$d_0 \alpha_0 \leq 100 \text{ eV}$	$d_0 \alpha_1 \leq 300 \text{ eV}$	-
^{16}O	22.717 ± 0.008	-	-	-	-	-	-	-	$\Gamma < 30 \text{ keV}$
^{20}Ne	16.729 ± 0.005	$p_0 + p_1 + p_2 - 0.16$	$p_3 + p_4 + p_5 - 0.14$	$p_3 + p_4 - 0.10$	$p_3 + p_4 + p_5 - 0.14$	$p_3 + p_4 + p_5 - 0.14$	0.0	$\alpha_1 + \alpha_2 - 0.38$	$\Gamma \leq 2 \text{ keV}$
^{24}Mg	15.436 ± 0.005	0.59	0.05	0.01	$p_3 + p_4 - 0.10$	$p_3 + p_4 - 0.10$	0.08	0.17	2.3 eV
^{28}Si	15.221 ± 0.005	0.05	0.05	-	-	-	0.81	0.09	1.7 eV $\Gamma_p/\Gamma_\alpha < 0.08$
^{32}S	11.984 ± 0.004	0.75	-	-	-	-	0.16	0.09	$\Gamma < 2.5 \text{ keV}$
^{36}Ar	10.858 ± 0.035	-	-	-	-	-	-	-	-
^{40}Ca	11.978 ± 0.025	0.0	-	-	-	-	1.00	0.0	-

$T = 2$ states over the last few years since Cerny's review [Ce 68]. Data on ^8Be and ^{12}C have been included in this table for completeness although these two cases are to be discussed in chapters 3 and 4. As can be seen from the table the excitation energies of the lowest $T = 2$ states are well known, in many cases to within a few kilovolts. However, there is a notable lack of data on the total width and partial widths for decay of these states. The table includes all data measured but does not include any theoretical calculations of excitation energies, total widths or partial widths. The gaps in measured widths are notable. It was intended in the above survey to point towards experiments that I feel can and should be done to clarify the systematics of these states over the mass range. Table 2.14.2 contains a summary of the references given in each appropriate section already, relating to observations of these lowest $T = 2$ states in low-mass, even-even nuclei.

2.15 GAMMA DECAY OF HIGH ISOSPIN STATES

There are two general rules that involve isospin in electromagnetic interactions. The proof of these rules can be found in the article by Warburton and Weneser [Wa 70]. These rules may be summarised as follows:

- a) Electromagnetic transitions between states are forbidden unless $\Delta T = 0$ or ± 1 , and
- b) Corresponding $\Delta T = \pm 1$ transitions in conjugate nuclei are identical in all properties.

An experimental search for a $\Delta T = 2$ radiative transition in violation of the first rule above, was reported by Snover in his thesis [Sn 69a]. Here a search was made for a γ -decay of the lowest $T = 2$ state in ^{24}Mg to the $J^\pi = 2^+$, $T = 0$ first excited state at 1.37 MeV.

Table 2.14.2

Lowest $T = 2$ States in $T_z = 0$
Even-Even Nuclei : References

Nucleus	Reaction Type	References
^{40}Ca	Allowed	Mc 69, Ce 68, Ha 70b, Mc 70
	Forbidden	This thesis - section 2.5.2
^{36}Ar	Allowed	Ha 70b
	Forbidden	-
^{32}S	Allowed	Mc 69, Ha 69b, Ce 68, Mc 70
	Forbidden	He 68, Sn 69a
^{28}Si	Allowed	Mc 68, Ha 69, Mc 69, Mc 70, Le 68, Le 69, Th 69
	Forbidden	Ku 68, Sn 69a, Sn 69b
^{24}Mg	Allowed	Ad 67, Ad 69, Ga 64, Mc 67, Mc 69, Mc 70
	Forbidden	Ri 67, Sn 69a
^{20}Ne	Allowed	Ce 64, Ad 67, Mc 69, Mc 70
	Forbidden	Bl 67a, Ku 67, Sn 69a
^{16}O	Allowed	Ce 64, Ad 70
	Forbidden	-
^{12}C	Allowed	Ce 68, Ba 70
	Forbidden	Bl 70, this thesis - chapter 4
^8Be	Allowed	-
	Forbidden	Ha 68, this thesis - chapter 3

Gamma decay to the ground state would involve a $0^+ \rightarrow 0^+$ transition which is forbidden by angular momentum conservation. A similar search for a $\Delta T = 2$ decay of the lowest $T = 2$ state in ^{28}Si to the 2^+ , $T = 0$ first excited state at 1.78 MeV was also reported by Snover. In both cases the $\Delta T = 2$ strength was found to be very small, less than 1.6% and less than 3% of the allowed strengths for the ^{24}Mg and ^{28}Si cases respectively. The implications of these upper limits on $\Delta T = 2$ transitions are discussed by Snover who concludes that, lacking a model for isospin mixing in these nuclei, a concise interpretation is at present impossible.

CHAPTER 3

SEARCH FOR THE LOWEST $T = 2$ STATE OF ${}^8\text{Be}$
VIA ISOSPIN-FORBIDDEN REACTIONS

3.1 PREVIOUS WORK

A search for the lowest $T = 2$ state in ${}^8\text{Be}$ was made by Harrison et al. [Ha 68] using the twice-forbidden reactions ${}^7\text{Li}(p,p_0){}^7\text{Li}$ and ${}^7\text{Li}(p,p_1){}^7\text{Li}^*$. This state is the analogue of the ground state of the $T_z = 2$ nucleus ${}^8\text{He}$. From the known mass of ${}^8\text{He}$ (31.65 ± 0.3 MeV), the lowest $T = 2$ state in ${}^8\text{Be}$ was anticipated to lie at an excitation energy of 27.3 ± 0.3 MeV, i.e. at a proton bombarding energy of 11.47 ± 0.3 MeV. The ${}^7\text{Li}(p,p)$ excitation function was then measured using a 1 keV thick LiOH target on a carbon backing. The excitation function was measured in small steps (1 and 2 keV proton bombarding energy steps) over an interval of 700 keV spanning the expected position of the $T = 2$ state. No structure was seen in either the p_0 or p_1 channel.

3.2 THEORETICAL WORK

As has been previously discussed, the decay of the lowest $T = 2$ state in ${}^8\text{Be}$ into particle channels is isospin forbidden and so its decay width can only come from isospin mixing into the state. A shell model calculation of the amount of mixing of $T = 0$ and $T = 1$ states into the $T = 2$ states has been performed by Barker and Kumar [Ba 69]. These calculations led to predictions for approximate values for various partial widths of the state (table 3.2.1).

Previous shell model calculations by Barger [Ba 66] had predicted the $T = 2, 0^+$ state at an energy of 27.1 MeV. Again, as has been mentioned already, calculations of the excitation energy

Table 3.2.1

Calculated Partial Widths for Decay of the
Lowest $T = 2$ State in ${}^8\text{Be}$ [Ba 69]

Channel	α	p_0	p_1	n_0	n_1	t
Partial Width (keV)	0.2	0.2	0.1	0.2	0.1	0.04
Channel	τ	d_0	d_1	γ	Total	
Partial Width (keV)	0.03	3.8	0.3	0.016	4.9	

of the state derived from the known mass of the ground state of ${}^8\text{He}$ (a mass excess of 31.65 ± 0.12 MeV) and Coulomb energy differences, obtained from shell model wave functions, have given an energy of 27.33 MeV in agreement with Harrison et al. (see references [Ce 66, Ba 66]). Calculations of partial widths for the $T = 2$ state not only depend upon $T = 0$ and $T = 1$ admixtures but also on the spectroscopic factors for the various particle decay channels. These calculations are also dependent on the single particle reduced widths for each channel which are not well known but, in the case of Barker and Kumar, were obtained by fitting the observed widths of states in ${}^8\text{Be}$, ${}^7\text{Be}$ and ${}^7\text{Li}$. The calculations are also based on the assumption that the lowest $T = 2$ state is a 0^+ state and belongs to the lowest shell model configuration $1s^4 1p^4$.

3.3 EXPERIMENTAL SEARCH FOR THE LOWEST $T = 2$ STATE IN ${}^8\text{Be}$

Following the failure of Harrison et al. [Ha 68] to find the lowest $T = 2$ state in ${}^8\text{Be}$ using the ${}^7\text{Li} + p$ channel, it was decided to search for the state using the ${}^6\text{Li} + d$ channel. This decision was made following the preliminary calculations of Barker

and Kumar [Ba 69] which indicated that the d_0 width of the state was likely to be a substantial fraction of the total width. Thus, measurements of the excitation functions for the reactions ${}^6\text{Li}(d,p_0)$, ${}^6\text{Li}(d,p_1)$, ${}^6\text{Li}(d,\alpha)$ and ${}^6\text{Li}(d,d_0)$ were made using a deuteron beam provided by the EN tandem accelerator at A.N.U.

3.3.1 Experimental Details

Enriched ${}^6\text{Li}$ metal targets were made by evaporation of the metal onto thin layers of formvar which had been picked up on $15 \mu\text{g}/\text{cm}^2$ carbon foils prior to evaporation. The targets were transferred from the evaporator to the target chamber in vacuo. The 51 cm diameter scattering chamber (figure 3.3.1, [Po 70]) was used for these measurements. This chamber permits solid state counters to be placed at various distances from the target and to be rotated to any desired angle. A cooling ring is attached to the base of the chamber enabling counters to be cooled.

Excitation function measurements were made at seven angles using silicon surface barrier detectors to detect both alpha particles and protons from the reactions together and separately. The angles ranged from 25° to 165° in the lab-frame. In a typical run, counters of 1000 μ and 700 μ depletion depths were used at various angles as set out in table 3.3.1. As can be seen from the table, an aluminium foil of 0.008 inches thickness was placed in front of the counter at 25° to absorb alpha particles and so permit a clean proton spectrum to be observed. A typical spectrum from this counter is shown in figure 3.3.2.

Figure 3.3.3 shows a typical spectrum observed using a 1000 μ counter with no aluminium absorber foil.

The excitation functions were measured for each counter simultaneously using the 8-way routing system associated with the

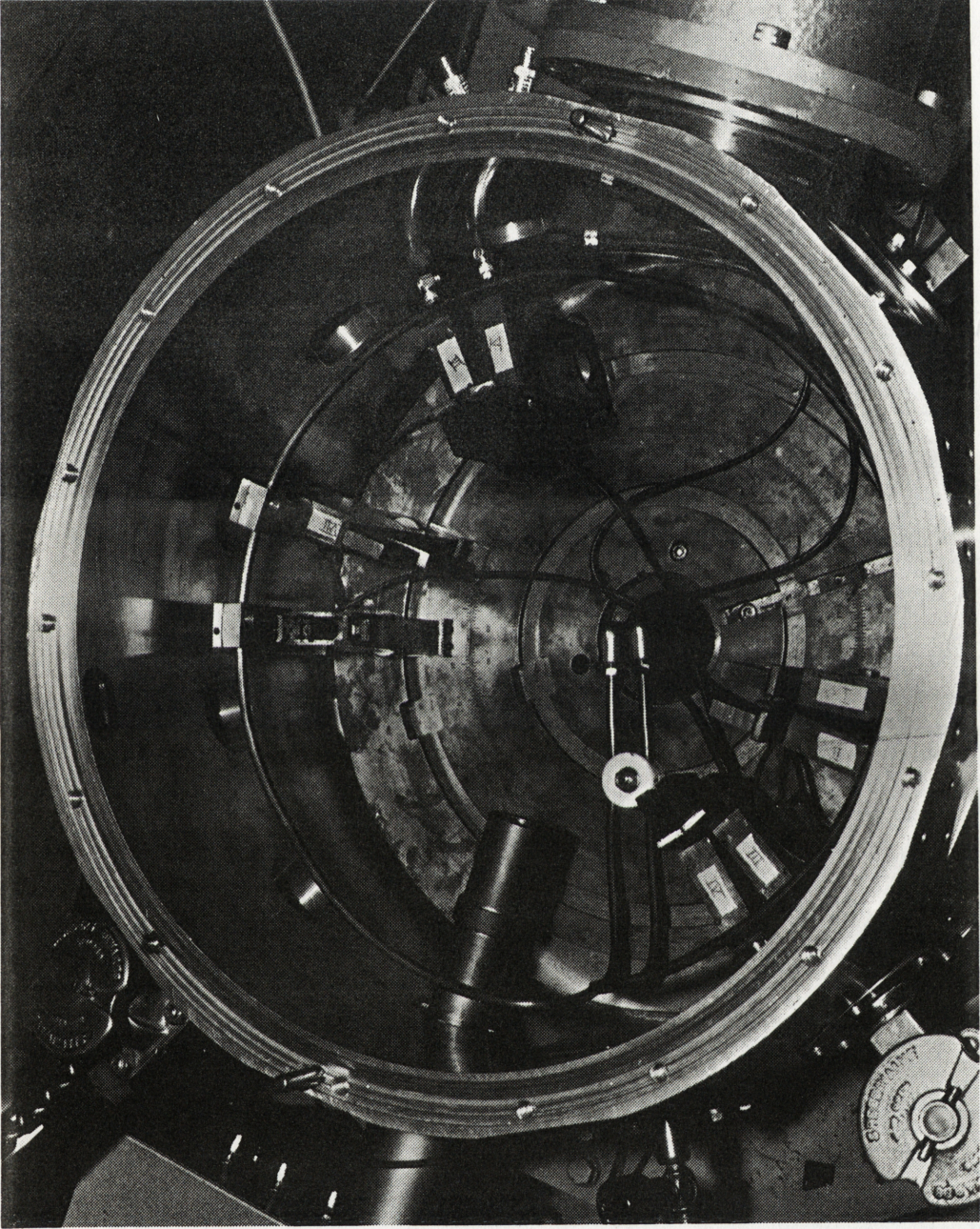


Figure 3.3.1: The 51 cm diameter scattering chamber [Po 70].

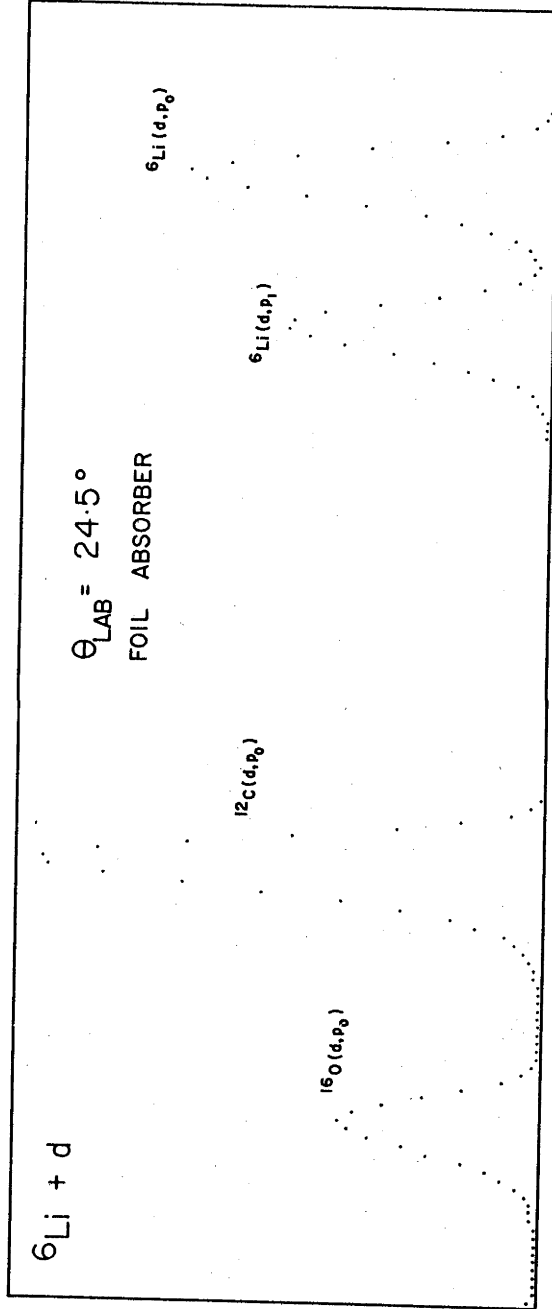


Figure 3.3.2: Spectrum from 1000 μ depletion depth counter at $\theta_{\text{LAB}} = 24.5^\circ$ with aluminium foil cover.

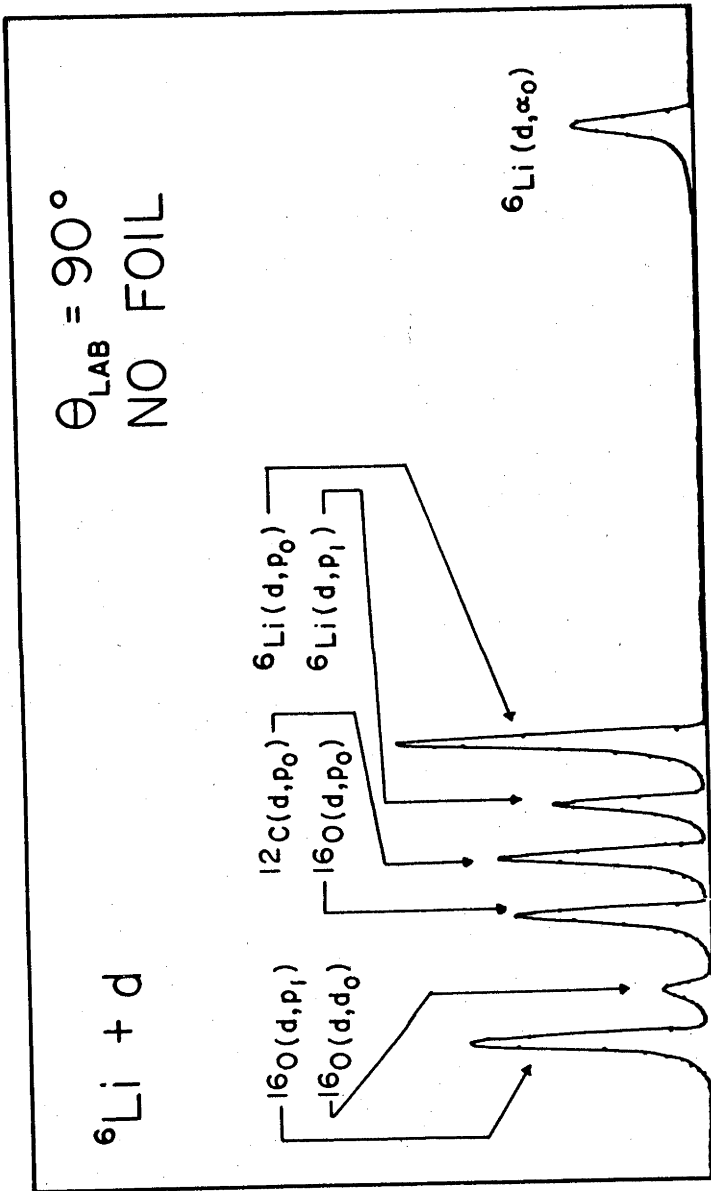


Figure 3.3.3: Spectrum from 1000 μ depletion depth counter at $\theta_{\text{LAB}} = 90^\circ$ with no aluminium foil cover.

Table 3.3.1

Typical Counter Assembly for T = 2 in ^8Be

Lab. Angle	Counter Depth in Microns	Foil Cover (Yes or No)
25°	1000	Yes
44.8°	1000	No
62.8°	1000	No
90°	1000	No
111.4°	1000	No
145° (LHS)	1000	No
145° (RHS)	700	No
165°	700	No

IBM 1800 data acquisition system. Standard "ORTEC" electronics modules were used for each counter. A block diagram of the electronics used as well as the routing system for the computer is given in figure 3.3.4. Subsequent to the collection of the data each set of spectra was transferred to disk and some preliminary analysis done while the next set of spectra was being recorded. This procedure was made possible because of the time-sharing operating system of the IBM 1800 system which enables high and low priority programs to be run by sharing the same area of machine memory. Whenever a high priority job is activated from disk, the low priority job currently in memory is "rolled-out" to disk storage while the high priority job is "rolled-in" for execution. On completion of the high priority job the interrupted low priority job is restored from disk and execution continues. At the same time that the system is performing these tasks data collection may continue [Ca 69].

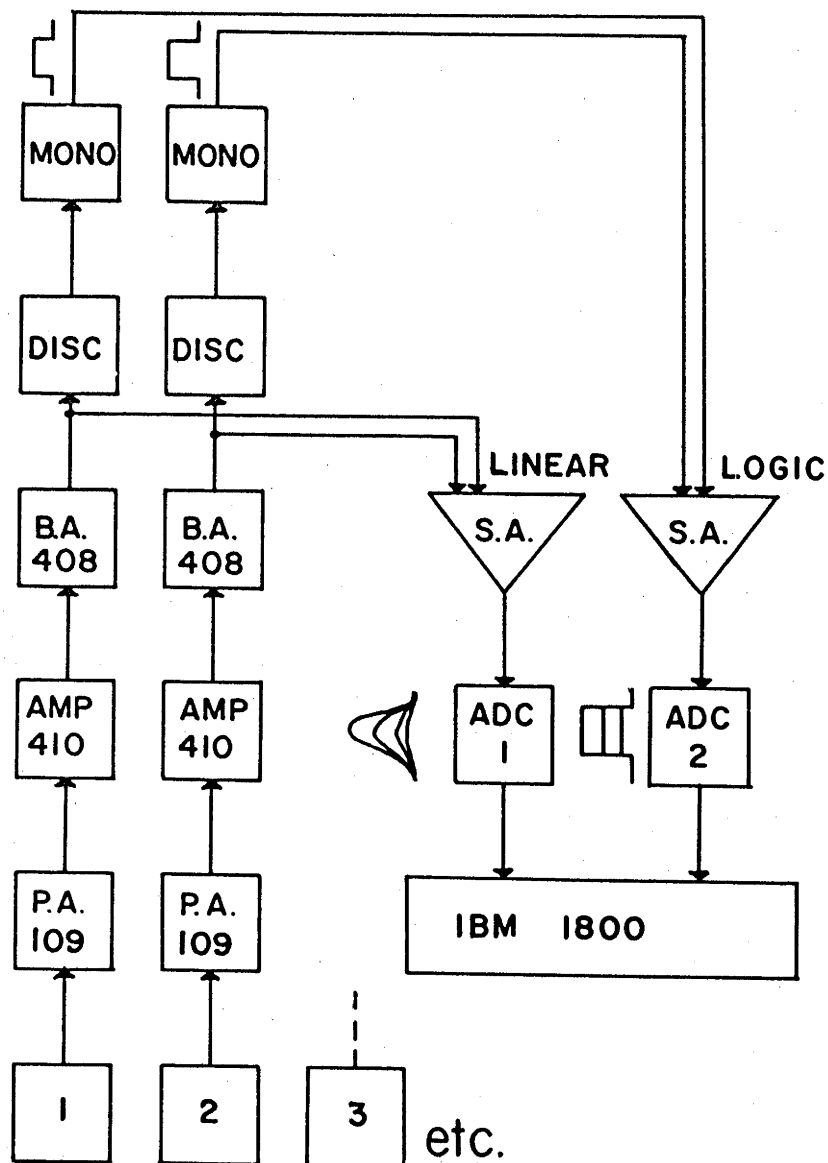


Figure 3.3.4: Block diagram of electronics system used to collect 8 particle spectra simultaneously. Abbreviation are as follows:

- Mono - Monostable circuit
- Disc - Integral discriminator
- B.A. - Biassed amplifier
- S.A. - Summing amplifier
- Amp - Linear amplifier
- P.A. - Pre-amplifier
- A.D.C. - Analog-to-digital converter.

Numbers in boxes refer to "ORTEC" electronics modules.

3.3.2 Excitation Functions

The excitation functions were measured simultaneously in deuteron bombarding energy steps of 3 keV (2.25 keV in excitation energy) from deuteron energies of 6.33 MeV ($E_x = 27.03$ MeV) to 7.14 MeV ($E_x = 27.63$). Since the $T = 2$ state resonance anomaly was expected to be small, it was considered most satisfactory to measure the ratios of differential cross sections. This technique ensures that the results are independent of small target non-uniformities and changes, dead time corrections and beam integration, these factors being possibly able to mask any weak resonance expected. The ratios $(d,p_1)/(d,p_0)$ and $(d,\alpha)/(d,p_0)$ were extracted at forward angles in the range 25° to 90° . These ratios could not be obtained at backward angles due to the masking of one or more of the particle groups by groups from reactions involving oxygen and carbon. For all angles and reactions, moreover, the particle yields were normalised to the yield of the (d,p_0) reaction at $\theta_{\text{LAB}} = 25^\circ$ which corresponds to the peak of the $\ell_n = 1$ stripping pattern.

Over the first half of the energy range covered (up to approximately 6.73 MeV deuteron bombarding energy), no significant resonance was seen in the excitation functions at any angle. Any variations were inside statistics, in this case ± 3 to 5%, (see figure 3.3.5). In the upper half of the range (deuteron bombarding energy range 6.73 to 7.14 MeV) an anomaly was observed at $\theta_{\text{LAB}} = 90^\circ$ in the $(d,p_1)/(d,p_0)$ ratio at a deuteron bombarding energy of 6.945 MeV (figure 3.3.5). The figure also shows the observed values for the ratio at $\theta_{\text{LAB}} = 45^\circ$ in the same region as the observed anomaly. These data exhibit an anomaly of opposite sign in the same region as the 90° data. The data shown in figure 3.3.5 were obtained with a target thickness corresponding to 2.5 keV energy loss for the

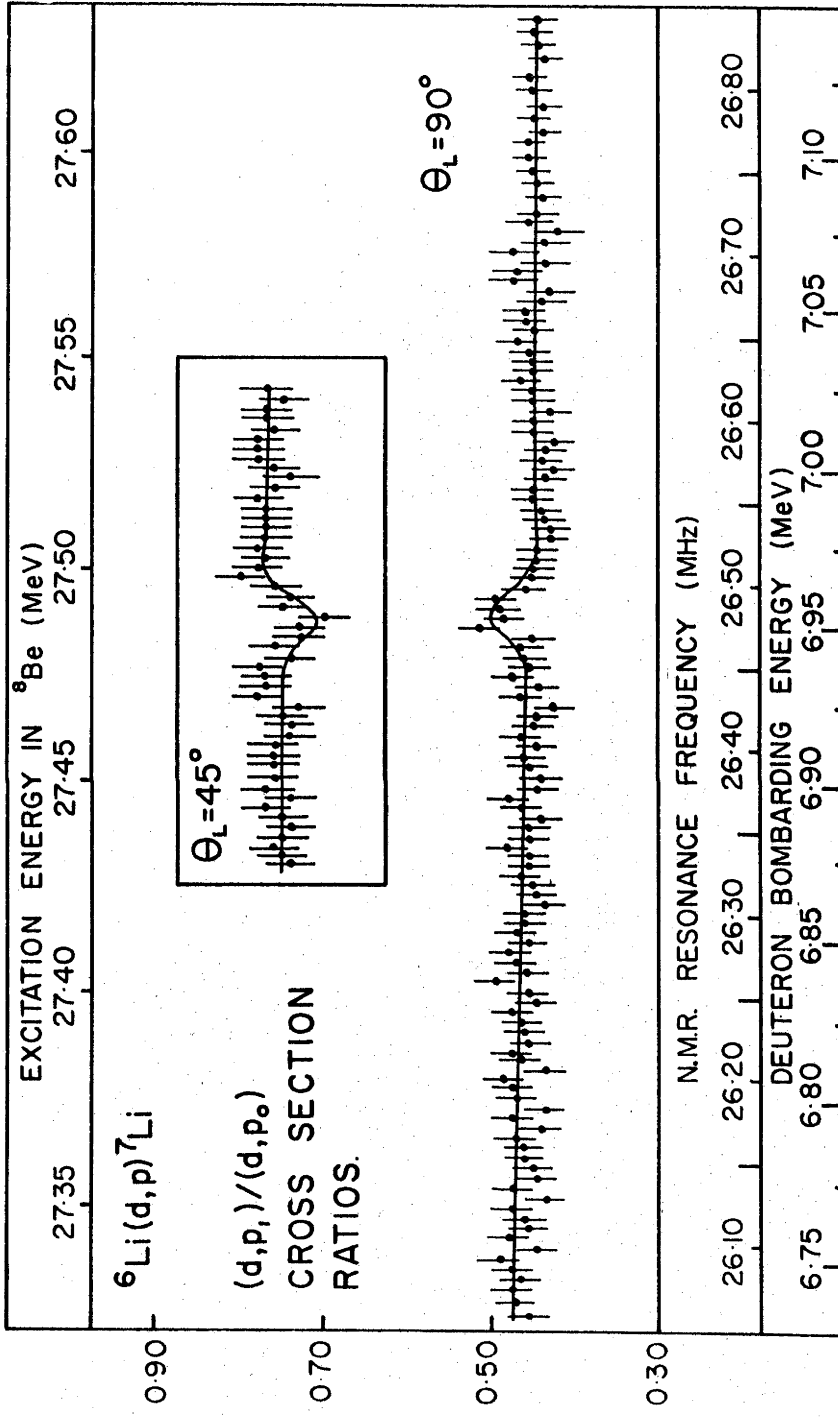


Figure 3.3.5: The ratio of the differential cross sections for the ${}^6\text{Li}(d,p){}^7\text{Li}^*$ and ${}^6\text{Li}(d,p_0){}^7\text{Li}$ reactions at $\theta_{\text{LAB}} = 90^\circ$ as a function of deuteron bombarding energy. The inset shows the same ratio at $\theta_{\text{LAB}} = 45^\circ$. The target thickness used for these measurements corresponded to a deuteron energy loss of 2.5 ± 1 keV.

bombarding deuterons. This is substantially smaller than the width of the resonance seen. Figure 3.3.6 shows data from a repeat of the experiment over the region of the resonance using thicker targets (energy loss for deuterons of around 8 keV). The region was re-investigated a number of times and figure 3.3.6 gives the data from one series of runs. The ratios $d\sigma/d\omega[{}^6\text{Li}(d,p_1)]/d\sigma/d\omega[{}^6\text{Li}(d,p_0)]$ for four lab. angles 25° , 45° , 73° and 90° are shown on the left of figure 3.3.6 and the normalised (d,α) yields at five angles, 45° , 73° , 90° , 152° and 165° , are shown on the right of the figure.

3.3.3 Observed Resonance

The $(d,p_1)/(d,p_0)$ ratio shows a resonance of $-2.4 \pm 0.5\%$ relative to background at $\theta_{\text{LAB}} = 25^\circ$ while, at $\theta_{\text{LAB}} = 90^\circ$, the anomaly has increased in size to $+12 \pm 2\%$ after allowing for target thickness. It is to be noted that the direction of the anomaly has changed over the range of angles observed. In the (d,α) case the anomaly is very weak near $\theta_{\text{LAB}} = 73^\circ$ ($\theta_{\text{CM}} \approx 90^\circ$) becoming a maximum of $+11 \pm 2\%$ near $\theta_{\text{LAB}} = 165^\circ$ ($\theta_{\text{CM}} = 168.7^\circ$). The (d,α) angular distribution must be symmetric about $\theta_{\text{CM}} = 90^\circ$ and so the observed anomaly must be equally strong at forward angles as it is at backward angles.

3.3.4 Basis for Using Ratios

As has been already discussed, the use of particle group ratios is useful for detecting resonances since such ratios are independent of many experimental parameters. In the cases discussed in the previous section, the ${}^6\text{Li}(d,p_0)$ reaction was used for obtaining ratios. This reaction, at angles of 45° , 73° , 90° and 111.4° showed no anomaly in the yield normalised to integrated

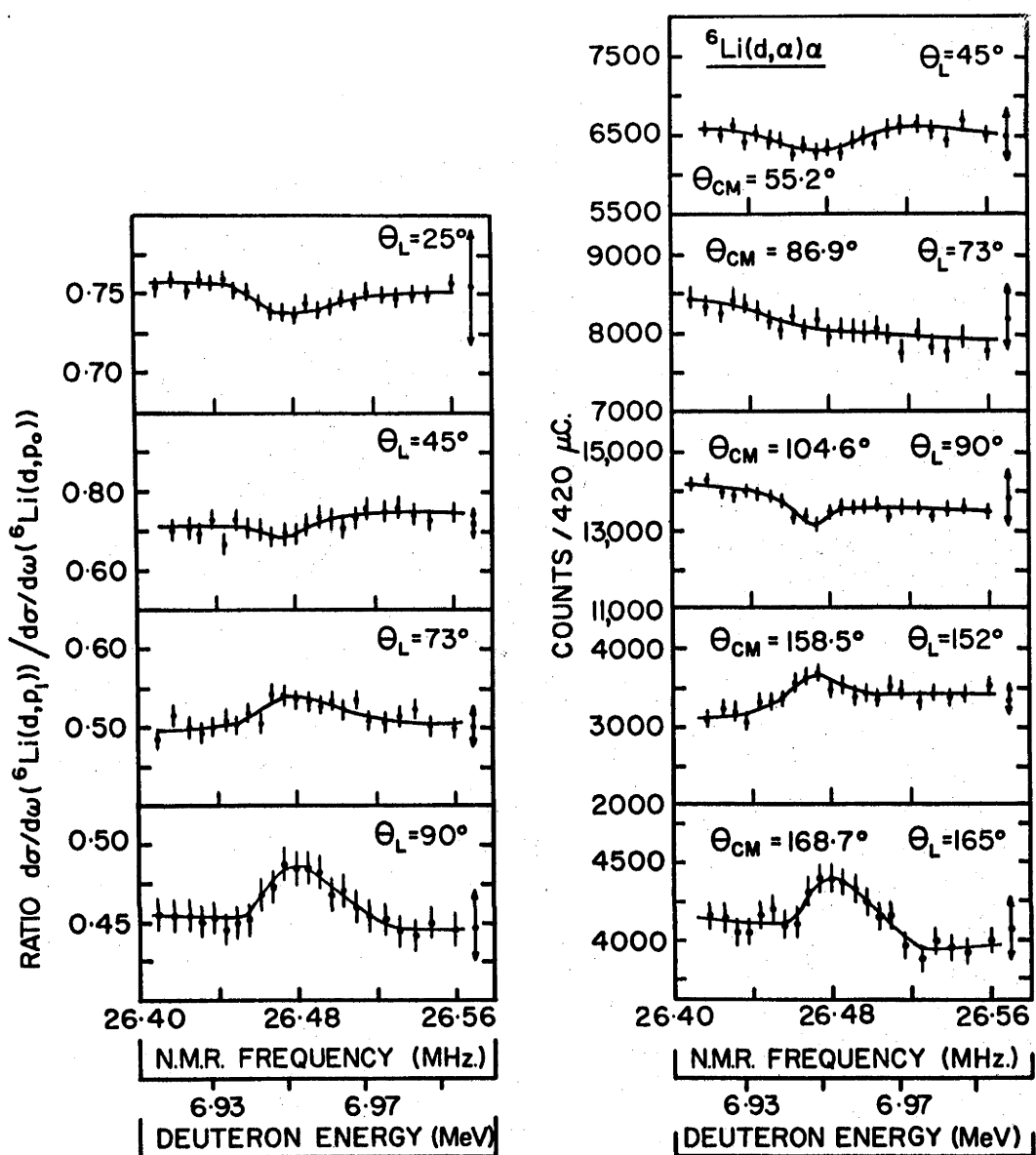


Figure 3.3.6: Left: The $(d, p_1)/(d, p_0)$ ratio over a region spanning the anomaly.

Right: The (d, α) excitation function obtained by normalising the yield against that from $^6\text{Li}(d, p_0)$ at $\theta_{\text{LAB}} = 25^\circ$.

The target thickness corresponded to a deuteron energy loss of 8 ± 3 keV. The arrows on the right of each figure show $\pm 5\%$ as a guide to the size of the anomaly in each case.

charge, greater than 2%; the 25° (d,p₀) yield, used for the above ratio calculations, showed no anomaly greater than 1.5% of background over the region of the "T = 2" resonance. A check was made by normalising the ⁶Li(d,p₀) yield at 25° against the ¹⁶O(d,p₁) yield observed at the same angle. Again no anomaly was seen, as expected.

3.4 CALCULATIONS AND DISCUSSION

It is to be noted that, due to masking by contaminant peaks, the ⁶Li(d,d₀) groups could only be extracted at θ_{LAB} = 73° and 90°. However, in both cases the backgrounds were very high and so extracted yields were subject to errors of ±5%. This reaction may be a favourable one to use for a search for the lowest T = 2 state due to the predicted high d₀ width of the state, as has been explained [Ba 69]. At the two angles at which it was observed, no anomaly exceeding the quoted errors of ±5% was observed.

The anomaly seen (figure 3.3.5) is narrow and superimposed upon a smooth background. A program was written for the IBM S/360-50 at A.N.U. to evaluate the effects of interference on this resonance width and shape. These interference calculations assumed an energy dependence of the cross section of the form:

$$\frac{d\sigma}{d\omega} = a + \left| be^{i\delta} + \frac{c}{(E_r - E) - \frac{i\Gamma}{2}} \right|^2$$

where the parameters a, b, c and δ are independent of energy. The parameter c is proportional to the square root of the product of the partial widths for the entry and exit channels while parameter b is the amplitude of the section of the background that interferes with the state. The above expression was evaluated for various

values of the above parameters. After allowing for target thickness and straggling, good fits to the data were obtained with the constant values $E_r = 27.483$ MeV and total width $\Gamma = 10$ keV. These calculations verified that the shapes of the observed resonances are in agreement with interference concepts. It should be noted, however, that no fit to the data could be obtained which provided a unique set of parameters.

No unique set of partial widths for the state can be presented from this analysis. Since no notable anomaly was seen in the ${}^6\text{Li}(d,p_0)$ excitation function at any angle observed from $\theta_{\text{LAB}} = 25^\circ$ to 111° , and, since such a resonance was seen in the ${}^6\text{Li}(d,p_1)$ reaction (see figure 3.3.5), it follows that Γ_{p_0} is most likely much smaller than Γ_{p_1} . Clark et al. [Cl 67] have shown that the ${}^6\text{Li}(d,\alpha)$ angular distribution is strongly peaked near 90° for excitation energies in the range 26 to 29 MeV. This helps to explain the fact that the observed relatively strong resonance (compared to background) in the (d,α) reaction appears only at angles far removed from 90° where the off-resonance background is low.

3.5 SUMMARY

Anomalies in the ${}^6\text{Li}(d,p_1)$ and ${}^6\text{Li}(d,\alpha)$ reactions excitation functions have been found by taking ratios between these reaction yields and the ${}^6\text{Li}(d,p_0)$ yield. The anomalies occur at an excitation energy in ${}^8\text{Be}$ of 27.483 ± 0.010 MeV in agreement with predictions for the position of the lowest $T = 2$ state in ${}^8\text{Be}$. A total resonance width measurement produced a value of 10 ± 3 keV again in reasonable agreement with the calculations of Barker and Kumar. The predictions that Γ_{d_0} for the state should be much greater than Γ_{p_0} , have been experimentally verified from the

appearance of the state in ${}^6\text{Li} + d$ experiments compared to previous work on ${}^7\text{Li} + p$ induced reactions [Ha 68]. The data from this experiment have been incorporated in table 2.14.1.

CHAPTER 4

SEARCH FOR THE LOWEST $T = 2$ STATE
OF ^{12}C VIA ISOSPIN-FORBIDDEN REACTIONS

4.1 PREVIOUS WORK

The lowest $T = 2$ state in ^{12}C is the analogue of the ground state of the $|T_z| = 2$ nuclei ^{12}O and ^{12}Ne . The $T = 2$ multiplet, then, consists of the $|T_z| = 0$ to 2 nuclei ^{12}Be , ^{12}B , ^{12}C , ^{12}N and ^{12}O . The existence of a narrow level in ^{12}C at $E_x = 27.5 \pm 0.1$ MeV, presumed to be the lowest $T = 2$ state of ^{12}C with $J^\pi = 0^+$, was reported by Cerny [Ce 68] from a study of the isospin allowed direct reaction $^{14}\text{C}(p,t)^{12}\text{C}^*$ ($T = 2$). Barnes et al. [Ba 70] have recently repeated this experiment and located the state with greater accuracy at $E_x = 27.585 \pm 0.020$ MeV. Its total width Γ was found to be less than 50 keV. These results agree well with those of Cerny. Excitation of the state via an isospin-forbidden reaction had not been reported in the literature until the current work. An energy level scheme for ^{12}C is shown in figure 4.1.1.

4.2 THEORETICAL CALCULATIONS

Extending theoretical predictions made for the lowest $T = 2$ state of ^8Be , Barker [Ba 69] at A.N.U. repeated the calculations for the case of ^{12}C . As before the calculations were performed to obtain the admixtures of $J^\pi = 0^+$, $T = 1$ and $T = 0$ states in the $T = 2$ state. The results indicated the following:

- a) the total width of the state could be very small, of the order of 1 keV or less;
- b) the alpha and ^3He partial widths for the state should be very small; and
- c) Γ_{p_0}/Γ , Γ_{n_0}/Γ , Γ_{d_0}/Γ and Γ_{d_1}/Γ could be of the order of 0.1.

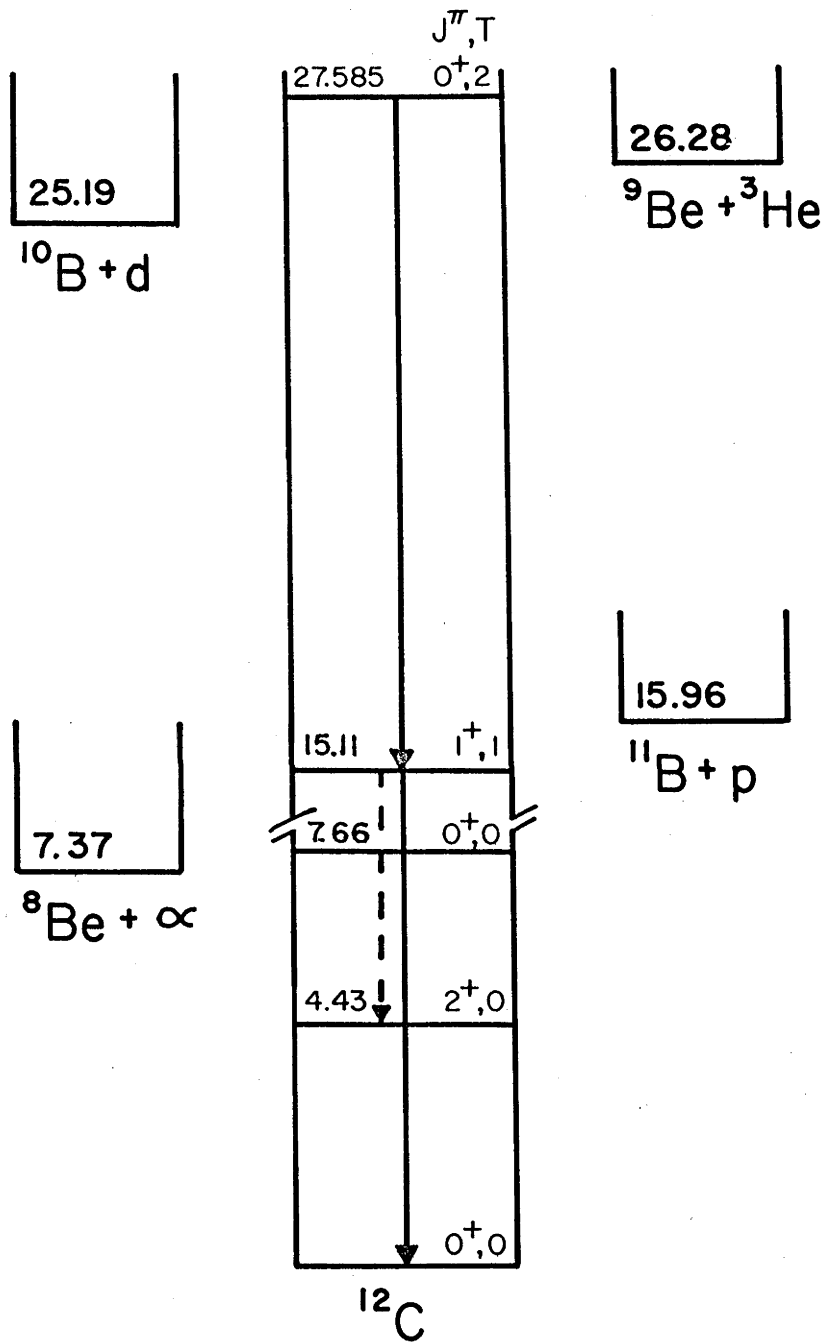


Figure 4.1.1: Energy level scheme for ^{12}C .

4.3 EXPERIMENTAL WORK - $^{10}\text{B}(\text{d},\text{p})$; (d,α)

Following the successful search for the lowest $T = 2$ state in ^8Be (see previous chapter) via the $^6\text{Li} + \text{d}$ reaction, it was decided to search for the lowest $T = 2$ state in ^{12}C via the $^{10}\text{B} + \text{d}$ reaction channel. The deuteron beam was again supplied by the A.N.U. EN tandem accelerator.

The ^{10}B targets for this experiment were made by electron-gun evaporation of the isotopically enriched metal. Boron 10 targets of $30 \mu\text{g}/\text{cm}^2$ thickness were deposited onto $15 \mu\text{g}/\text{cm}^2$ thick carbon foils. The ^{10}B target thickness corresponded to a deuteron energy loss of 6 keV. Again, as for ^8Be , the charged particles from the (d,p) and (d,α) reactions were detected using silicon surface barrier detectors of 1000μ and 120μ depletion depths respectively. The (d,p) spectra were obtained by placing aluminium foil in front of the counters. The foils were varied in thickness from 0.0076 to 0.015 cm depending upon the counter angles. These foils stopped alpha particles and also elastically scattered deuterons. Table 4.3.1 gives a characteristic set-up of counters used in a given accelerator run.

Figure 4.3.1 shows a typical spectrum obtained using a foil covered counter, while figure 4.3.2 shows a similar spectrum from a counter without a foil. Figure 4.3.3 also shows a spectrum recorded using the 120μ depletion depth counters used for α particle detection. No foils were used in front of these counters. The excitation functions measured extended 50 keV either side of Cerny's stated range of 27.5 ± 0.1 MeV for the position of the lowest $T = 2$ state in ^{12}C .

Excitation functions for the reactions $^{10}\text{B}(\text{d},\text{p}_0)$, $^{10}\text{B}(\text{d},\text{p}_1)$, $^{10}\text{B}(\text{d},\text{p}_2)$ and $^{10}\text{B}(\text{d},\text{p}_3)$ were measured at four angles,

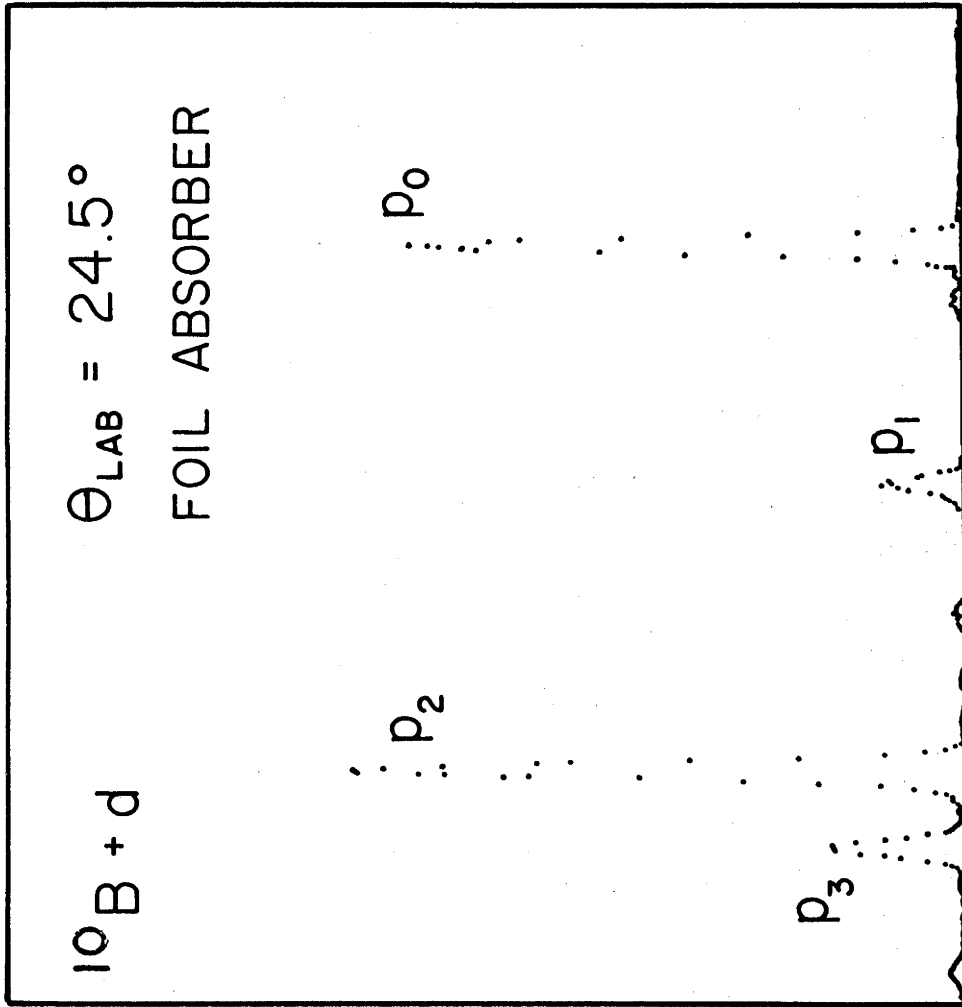


Figure 4.3.1: Spectrum from 1000 μ counter at $\theta_{\text{LAB}} = 24.5^\circ$ with aluminium foil cover.

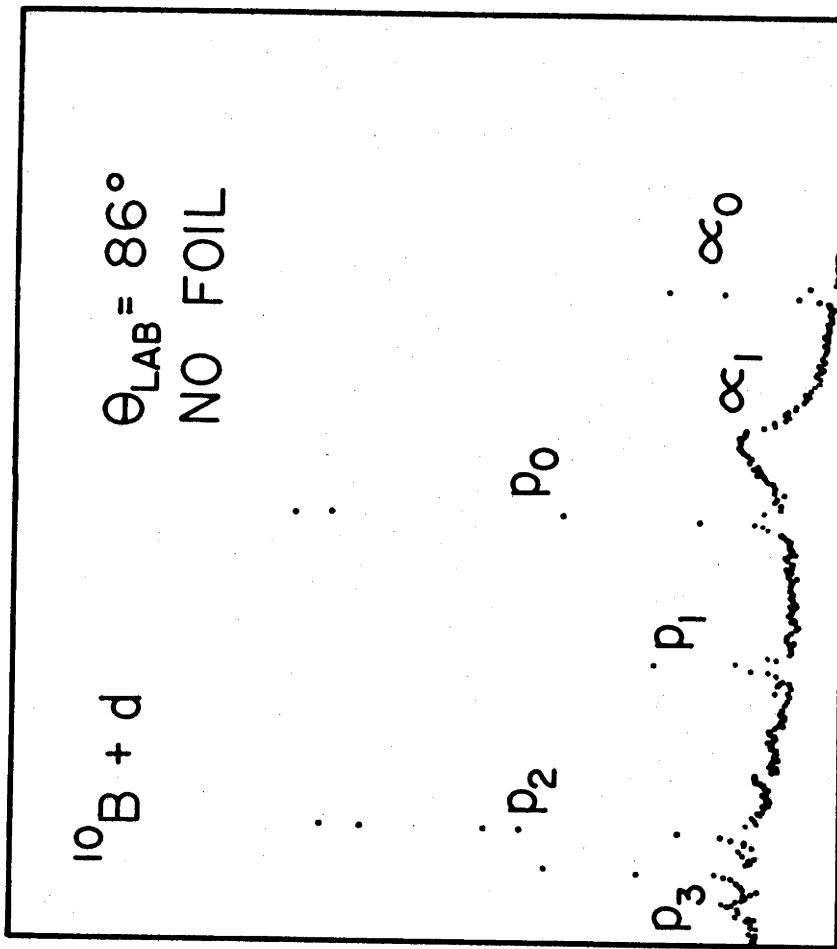


Figure 4.3.2: Spectrum from 1000 μ counter at $\theta_{\text{LAB}} = 86^\circ$ without aluminium foil cover.

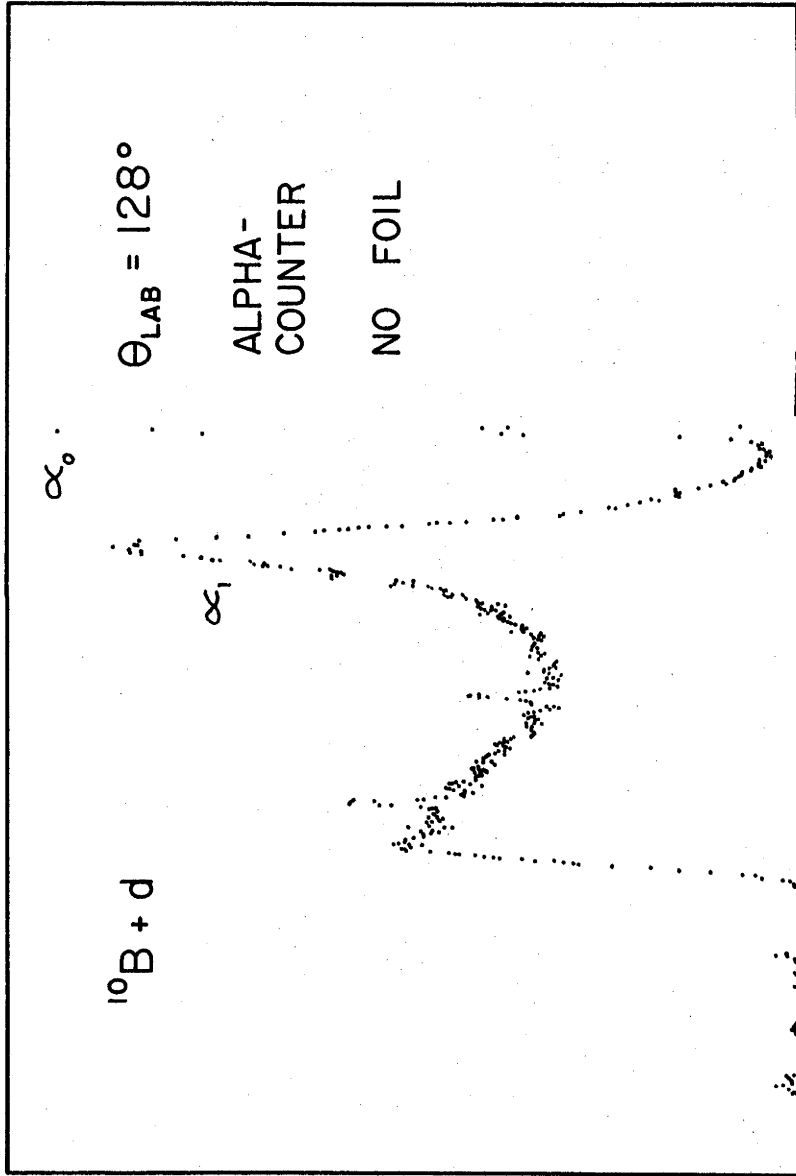


Figure 4.3.3: Spectrum from 120 μ alpha-particle counter at

$\theta_{\text{LAB}} = 128^\circ$.

Table 4.3.1

Counter Set-up for a Given Accelerator Run

Lab. Angle	Counter Depletion Depth in Microns	Particles Counted	Foil (Thickness in Thous. of Inch)
24.5°	1000	p	5
52°	1000	p	5
86° (RHS)	1000	p	5
86° (LHS)	1000	all	-
128°	120	α	-
146°	1000	p	4
165° (RHS)	120	α	-
165° (LHS)	1000	p	3

$\theta_{\text{LAB}} = 24.5^\circ, 52^\circ, 86^\circ$ and 165° . The excitation functions were, as for the ^8Be case, measured simultaneously using the "routing" mode of the on-line IBM 1800 data acquisition system [Ca 69] and the electronics system shown in figure 3.3.4. Measurements were made in deuteron bombarding energy steps of 2 keV from $E_d = 2.605$ MeV to $E_d = 2.960$ MeV corresponding to excitation energies in ^{12}C of 27.35 MeV to 27.65 MeV, i.e. a range extending 300 keV centred on the reported excitation energy of the $T = 2$ state [Ba 70]. The $^{10}\text{B}(d, \alpha_0)$ and $^{10}\text{B}(d, \alpha_1)$ excitation functions were also measured at $\theta_{\text{LAB}} = 165^\circ$ over the broad range. The data for these (d,p) and (d, α) reactions are shown in figure 4.3.4.

Again, as was the case for ^8Be , it was decided to derive cross section ratios, as shown in figure 4.3.4. The same reasons apply in this case as for the ^8Be case, viz. ratios are independent of any target non-uniformities, etc. In the case of the proton data ratios against the $^{10}\text{B}(d, p_2)$ reaction are shown in figure

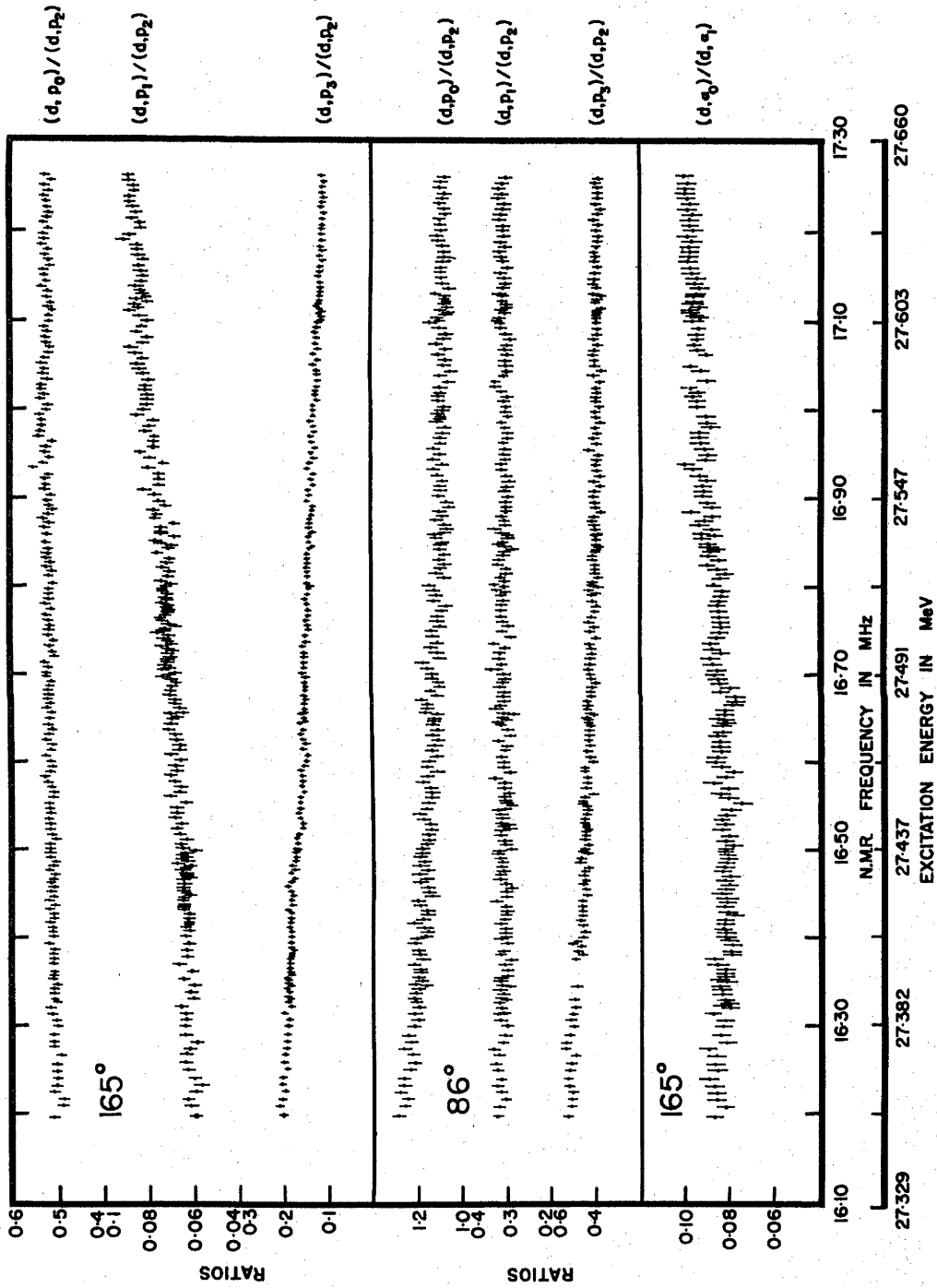


Figure 4.3.4: Ratios of differential cross sections for $^{10}\text{B}(d,p)$ and $^{10}\text{B}(d,\alpha)$ reactions in the expected [Ce 68] excitation energy range for the lowest $T = 2$ state of ^{12}C .

4.3.1. For the alpha particle data, the $(d,\alpha_0)/(d,\alpha_1)$ ratio is shown for the angle $\theta_{\text{LAB}} = 165^\circ$.

As can be seen no narrow anomaly that could be associated with the lowest $T = 2$ state of ^{12}C was observed in the (d,p) or (d,α) reactions anywhere within the ranges suggested by Barnes and Cerny. It is to be noted that it is difficult to observe a state as a thick target resonance if the width of the state is very small since the yield is proportional to $\Gamma_i \Gamma_f / \Gamma$. This could explain the lack of a resonance in the charged particle reaction data since it could be necessary to distinguish a very small anomaly from a large cross section stripping background. Accordingly, it could be expected that a more favourable method would be to search for the state as a resonance in the $^{10}\text{B}(d,\gamma\gamma)$ reaction since in this case the off-resonance background should be low.

4.4 THE $^{10}\text{B}(d,\gamma\gamma)$ REACTION

As has been stated elsewhere, it is possible that a search for the lowest $T = 2$ state in ^{12}C could be effected by observing the γ -decay of the state following its population through the $^{10}\text{B} + d$ channel. Since dipole transitions in self-conjugate nuclei obey $\Delta T = \pm 1$ [Ha 70a], it is likely that the lowest $T = 2$ state in ^{12}C will γ -decay primarily through the lowest $T = 1$, $J^\pi = 1^+$ state of ^{12}C at an excitation energy of 15.1 MeV. Garwin [Ga 59, Aj 68] has assigned a value of 0.9 to $\Gamma_{\gamma_0} / \Gamma$ for this state. Ajzenberg-Selove and Lauritsen [Aj 68] assign to this $T = 1$ state a total width (Γ) of 39.4 ± 1.5 eV. An extremely small $\Gamma_{\gamma_1} / \Gamma$ value of 3.2 ± 2.5 eV is also reported. Particle decay of the state appears to be negligible with Γ_α / Γ of approximately $5 \pm 8\%$.

In order to measure the γ -decay cascade of the $T = 2$

state through this $T = 1$ state, two NaI(Tl) detectors were used to measure coincidences between γ -rays of energy approximately 12.5 MeV and 15.1 MeV, the former arising from the M1 transition from the $J^\pi = 0^+$, $T = 2$ state to the $J^\pi = 1^+$, $T = 1$ state at 15.1 MeV. The two detectors had dimensions of 12.7 cm diameter by 10.2 cm thick. They were coupled to RCA 8075 photomultiplier tubes. The coincidence system used standard "ORTEC" electronic modules. Energy windows were set from 9 to 14 MeV in one counter and from 11 to 18 MeV in the other. The coincidence resolving time was 30 ns. The coincidence system used is outlined in the block diagram in figure 4.4.1. The $10 \mu\text{g}/\text{cm}^2$ ^{10}B targets were made by evaporation onto 0.05 cm thick tungsten discs which completely stopped the beam.

The coincidence measurements were made in two series. The first series covered the lower half of Cerny's quoted range and extended up to an excitation energy in ^{12}C of 27.55 MeV. The second series covered Barnes' range from $E_x = 27.55$ to 27.61 MeV. This second series of data was measured with much better statistical accuracy, each point taking four hours to measure.

The excitation functions thus measured are shown in figure 4.4.2. It is to be noted that one point in the data taken in Barnes' range fell well outside statistical variations, i.e. approximately 4 standard deviations from the mean. The inset in the figure shows a repeat measurement of the data in this area. This second set of measurements did not reproduce the high point indicating that the original variation must have arisen from normal statistical deviations. It was thus considered that the $^{10}\text{B}(d,\gamma\gamma)$ data displayed no narrow anomaly outside of normal statistical variations.

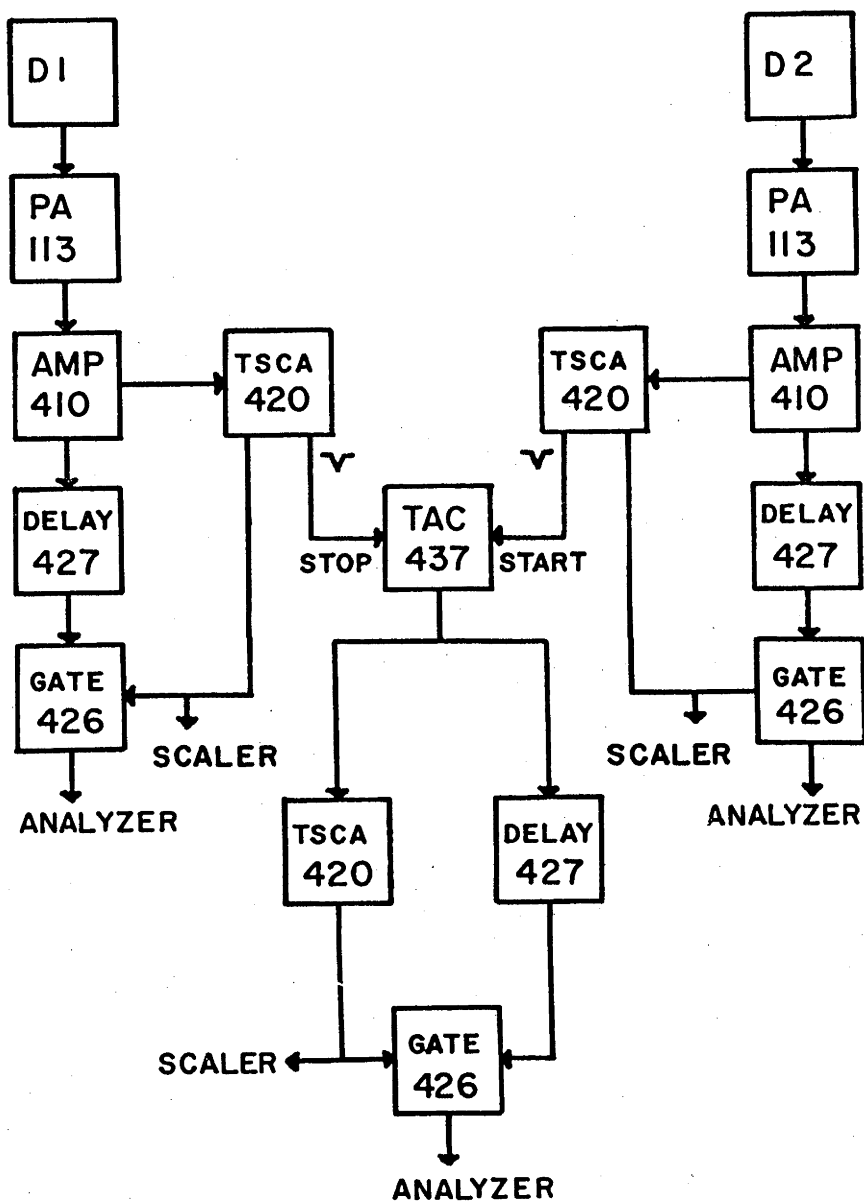


Figure 4.4.1: γ - γ coincidence system used for $^{10}\text{B}(d,\gamma\gamma)$ experiment.
 (Numbers in boxes refer to "ORTEC" module numbers; D1 and D2 refer to the two NaI(Tl) detectors.)

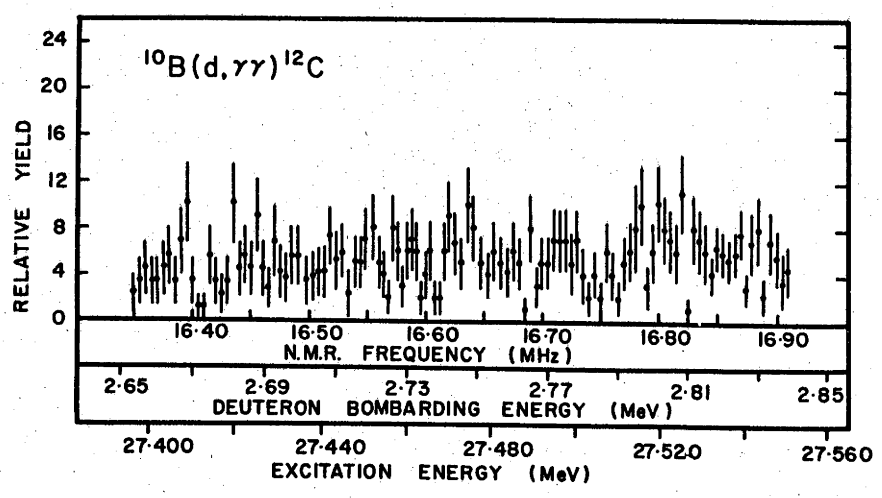
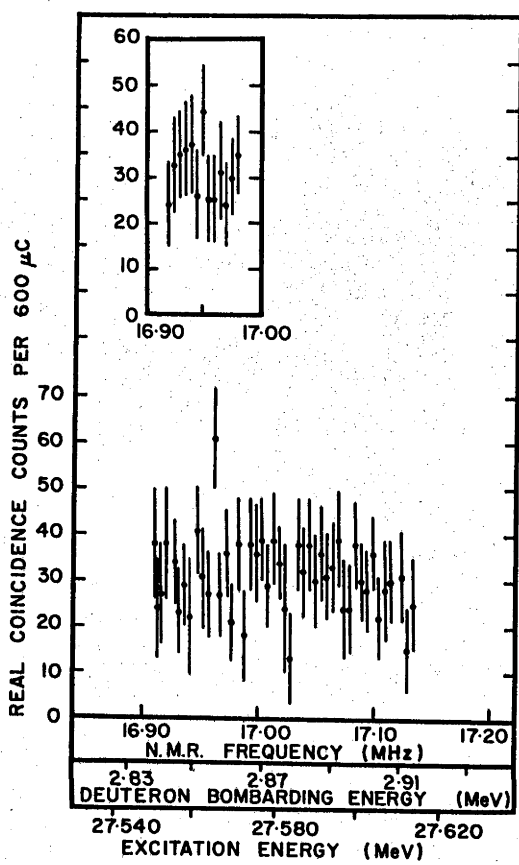


Figure 4.4.2: Excitation functions for the reaction $^{10}\text{B}(d, \gamma)$.

4.5 THE ${}^9\text{Be}({}^3\text{He},\gamma\gamma)$ REACTION

The only other open channel available for the formation of the lowest $T = 2$ state of ${}^{12}\text{C}$ is ${}^9\text{Be} + {}^3\text{He}$. Thus, the reaction ${}^9\text{Be}({}^3\text{He},\gamma\gamma)$ was investigated using the same technique as that used in the ${}^{10}\text{B}(\text{d},\gamma\gamma)$ work. The two NaI(Tl) detectors used, however, had dimensions 12.7 cm diameter by 10.2 cm thick and 23.8 cm diameter by 25.4 cm thick. Accordingly the sensitivity of the experiment was much higher than that of the $(\text{d},\gamma\gamma)$ experiment. A detailed description of the operation of the 23.7×25.4 cm NaI(Tl) crystal is provided in an A.N.U. internal report [B1 70]. A photograph of the detector itself along with a 12.7×10.2 cm NaI crystal is provided in figure 4.5.1. The plastic scintillator anti-coincidence shield for the large crystal is not shown in that photograph. A diagram of the structure of the large crystal is shown in figure 4.5.2.

The ${}^9\text{Be}$ targets were 2 to 6 $\mu\text{g}/\text{cm}^2$ in thickness and were prepared by evaporation onto tungsten discs. In order to populate a state at an excitation energy of 27.585 MeV a ${}^3\text{He}$ beam of energy 1.748 MeV is required, (see figure 4.5.3). This beam was supplied by the 2 MV AK Van de Graaff accelerator at A.N.U. The coincidence excitation function was measured over Barnes' range. Three sets of data in this range are shown in figure 4.5.3. The target used for the series of runs at the top of the diagram was approximately twice as thick as that used for the lower two sets. A very weak resonance appears in the data at an excitation energy of 27.585 ± 0.005 MeV, in very good agreement with Barnes' energy for the $T = 2$ state from the allowed (p,t) reaction. It seems likely that this resonance can be identified with the lowest $T = 2$ state. The width of the state is less than 1.5 keV.

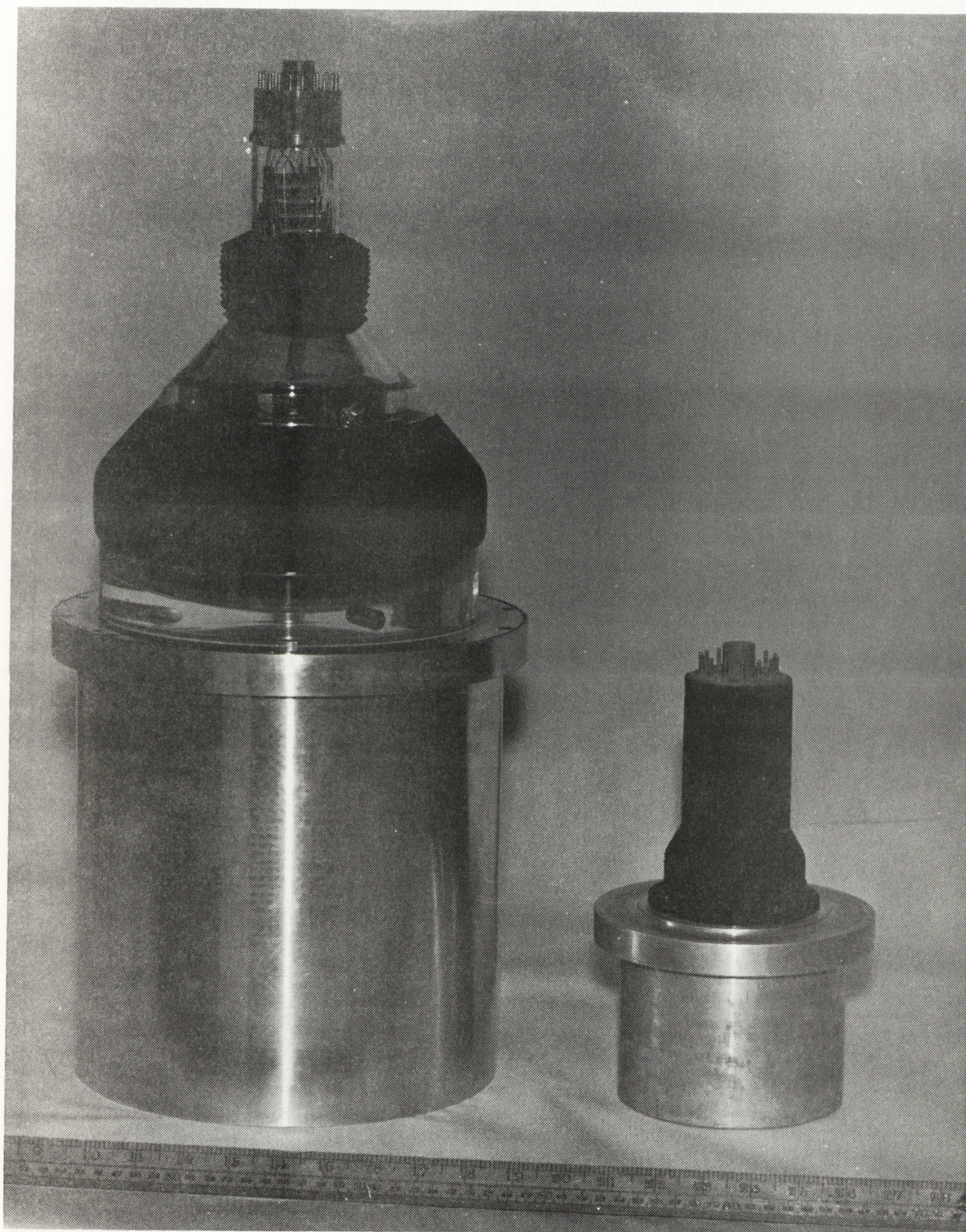


Figure 4.5.1: The A.N.U. 23.7 cm \times 25.4 cm NaI(Tl) crystal beside a 12.7 cm \times 10.2 cm NaI(Tl) crystal.

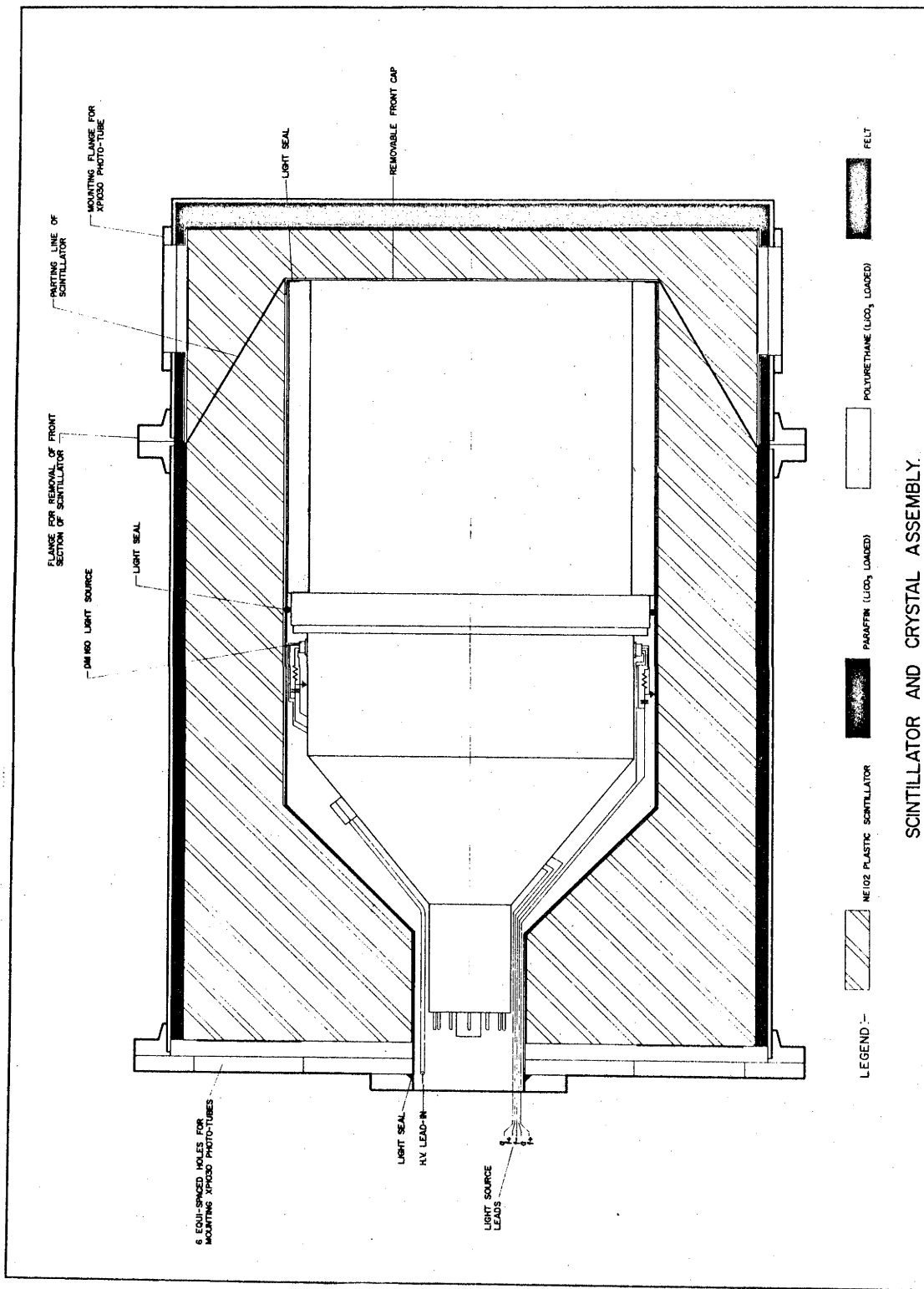


Figure 4.5.2: The A.N.U. 10" crystal system showing the NaI(Tl) crystal inside the anticoincidence plastic scintillator shield. The crystal alone was used for the experiments described in chapter 4.

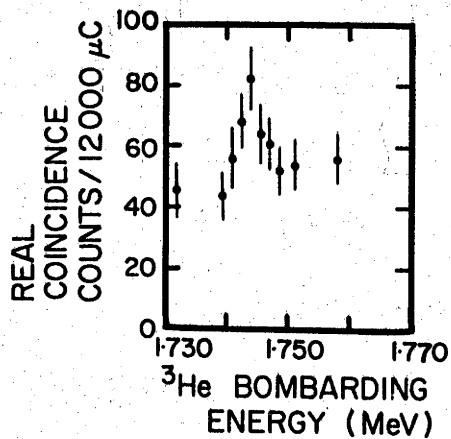
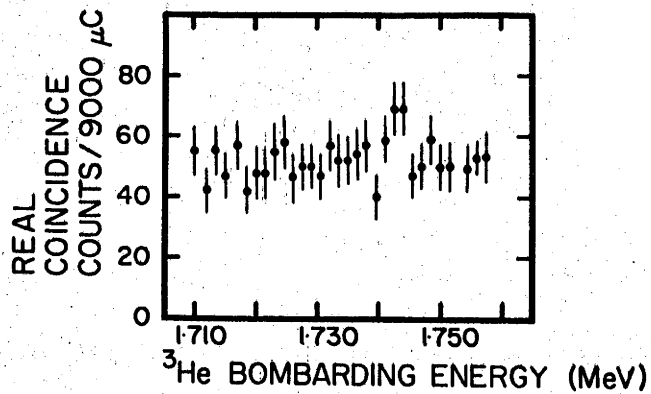
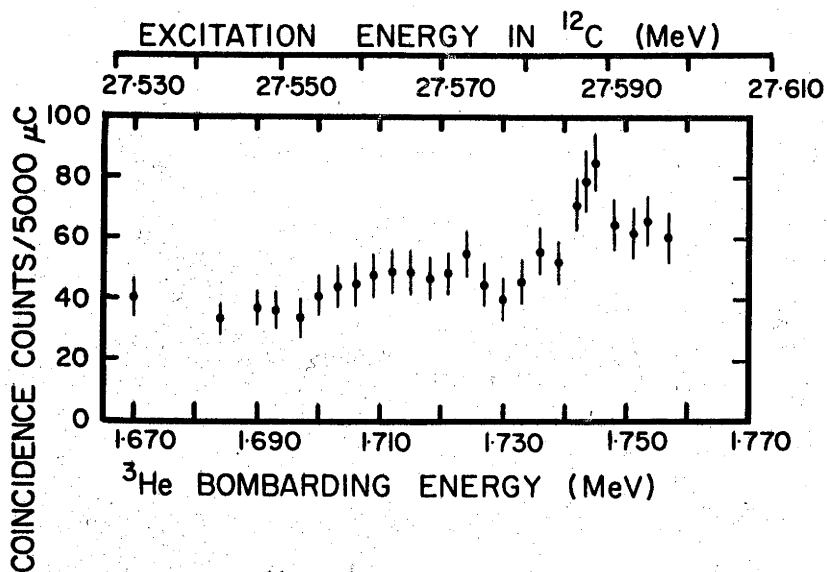


Figure 4.5.3: Three measurements of the excitation function for $^9\text{Be}(^3\text{He}, \gamma\gamma)$ in the expected [Ba 70] excitation energy region for the lowest $T = 2$ state in ^{12}C . The top data set was taken with 6 - 8 keV resolution, the lower two sets with 2 - 3 keV resolution.

4.6 ESTIMATES OF PARTIAL WIDTHS

From the theory of thick target yields [Fo 48] various upper limits and estimates of partial widths for the lowest $T = 2$ state in ^{12}C could be obtained. From the possible observation of the state in the $^9\text{Be}(^3\text{He}, \gamma\gamma)$ experiment the following estimate was made, viz. $\Gamma_{^3\text{He}_0} \Gamma_{\gamma} / \Gamma = 8 \pm 5$ meV. If Γ_{γ} is of the order of 1 Weisskopf unit then we obtain $\Gamma_{^3\text{He}_0} / \Gamma \approx 1/3000$, an extremely small width indeed. (1 W.u. is equivalent to 41 eV in this case.)

From the $^{10}\text{B}(d, p)$, (d, α) and $(d, \gamma\gamma)$ reaction studies the following upper limits for partial widths of the state could be made (table 4.6.1). From the $(d, \gamma\gamma)$ data the following upper limit could also be made, viz. $\Gamma_{d_0} \Gamma_{\gamma} / \Gamma \lesssim 200$ meV. Again, if we assume $\Gamma_{\gamma} \approx 1$ Weisskopf unit, then $\Gamma_{d_0} / \Gamma \lesssim 0.005$.

Table 4.6.1

Upper Limits for Partial Widths of
Lowest $T = 2$ State in ^{12}C

Partial Width	Upper Limit in eV
$\Gamma_{d_0} \Gamma_{p_0} / \Gamma$	225
$\Gamma_{d_0} \Gamma_{p_1} / \Gamma$	100
$\Gamma_{d_0} \Gamma_{p_2} / \Gamma$	120
$\Gamma_{d_0} \Gamma_{p_3} / \Gamma$	125
$\Gamma_{d_0} \Gamma_{\alpha_0} / \Gamma$	100
$\Gamma_{d_0} \Gamma_{\alpha_1} / \Gamma$	300

It is to be noted that the resonance observed in the $(^3\text{He}, \gamma\gamma)$ experiment could be from a very weakly excited state of lower isospin. This is unlikely, however, since no other reson-

ances were seen in the $^{10}\text{B} + \text{d}$ reactions over the whole of the range quoted by Cerny. From the data obtained over the lower half of Cerny's range, smaller limits could be placed on partial widths (table 4.6.2) over that range.

Table 4.6.2

Upper limits on partial widths for the lowest $T = 2$ state in ^{12}C from data taken over the lower half of Cerny's Range

Partial Width	Upper Limit in eV
$\Gamma_{d_0} \Gamma_{p_0} / \Gamma$	80
$\Gamma_{d_0} \Gamma_{p_1} / \Gamma$	35
$\Gamma_{d_0} \Gamma_{p_2} / \Gamma$	45
$\Gamma_{d_0} \Gamma_{p_3} / \Gamma$	40

For the upper half of Cerny's range the results are those stated previously, i.e. $\Gamma_{d_0} \Gamma_{p_1} / \Gamma \leq 225$ eV, etc. From the alpha-particle data, $\Gamma_{d_0} \Gamma_{\alpha_0} / \Gamma \leq 100$ eV and $\Gamma_{d_0} \Gamma_{\alpha_1} / \Gamma \leq 300$ eV over the whole of Cerny's range. From data obtained in the $^{10}\text{B}(d, \gamma\gamma)$ experiment we obtained the upper limits quoted previously for measurements taken in the smaller Barnes' range. Outside this range, but within Cerny's range we have obtained $\Gamma_{d_0} \Gamma_{\gamma} / \Gamma \leq 500$ meV. Again, if it is assumed that $\Gamma_{\gamma} \approx 1$ Weisskopf unit then $\Gamma_{d_0} / \Gamma \leq 0.012$. If the total width of the suspected $T = 2$ state were as large as 15 keV, the upper limit on Γ_{d_0} / Γ would increase to 0.06.

4.7 SUMMARIES AND CONCLUSIONS

The above data on partial widths for the lowest $T = 2$ state in ^{12}C are summarised in table 2.14.1. A recent measurement

of the $^{11}\text{B}(p,\gamma\gamma)$ excitation function [Sn 69a] over the whole of Cerny's quoted range (27.5 ± 0.1 MeV) did not show any resonance. This result yielded an upper limit for Γ_{p_0}/Γ of 0.03. This value was calculated assuming a resonance width of less than 5 keV and again assuming that $\Gamma_\gamma \approx 1$ Weisskopf unit. These estimates for upper limits of relative widths would increase if Γ_γ were substantially smaller than a Weisskopf unit. However, from results of the study of the γ -decay of $T = 2$ states in other self-conjugate even-even nuclei [Ha 70a], the assumption would appear to be quite reasonable. For example, in the case of the γ -decay of the lowest $T = 2$ state in ^{20}Ne at $E_x = 16.73$ MeV via a cascade through the 1^+ , $T = 1$ state at 11.2 MeV, the Γ_γ value for the state was found to be approximately 5 eV. This compares well with the Weisskopf estimate of 3.4 eV for Γ_γ , in this case a strong M1 transition.

These results are interesting in relation to the theoretical estimates of Barker and Kumar for the lowest $T = 2$ state in ^{12}C and bear out the fact that the d_0 partial width of the state must be small. It is to be noted that the lowest $T = 2$ state in ^{12}C most likely has substantial width for decay into channels not studied thus far, e.g. deuterons to excited states of ^{10}B or alpha particles to excited states of ^8Be .

The above observation and measurement of the lowest $T = 2$ states in ^8Be and ^{12}C have added information on these states to that already existing for $T = 2$ states in higher even-even nuclei, (table 2.14.1). The data on these states now present a systematic set of measurements in the low-mass region. Even though these states appear to have no obvious simple relationships over this mass range, further theoretical research on them should prove to be interesting.

CHAPTER 5

INELASTIC PROTON SCATTERING FROM ^{103}Rh , ^{107}Ag and ^{109}Ag

5.1 INTRODUCTION - CORE-EXCITATION MODEL

The core-excitation model of de-Shalit [Sh 61] describes the low-lying negative-parity states of odd-mass nuclei of masses 103, 107 and 109 as the coupling of an odd $2p_{1/2}$ proton or proton hole to the collective vibrational states of a doubly-even core. In this single particle, core-excitation model, then, the odd-mass nucleus is considered as an odd particle weakly coupled to an even-mass core. The ground state spin should thus equal the angular momentum of the odd nucleon in the average potential created by the even mass core of A nucleons, say. If the next state occupied by the single particle is high in excitation compared to the lowest excitation energy of the core, then the lowest excitations in the nucleus $A + 1$ should be described by the extra-core nucleon staying in its lowest state while the core is excited to its low excitation collective states. In this way collective excitations of the core occur in the same way as for even-mass nuclei but are split into a number of states in the $A + 1$ nucleus by the coupling of the single particle to the core.

Using the notation of de-Shalit [Sh 61] the zeroth-order wave functions of an odd-mass nucleus are described by the wave function $|J_c j, JM\rangle$, where:

- i) J_c is the core angular momentum,
- ii) j is the angular momentum of the odd particle, and
- iii) J is the total angular momentum with $J_z = M$.

From these concepts, it follows:

- a) For each collective core state J_c there will be a multiplet of

$2j + 1$ states in the odd mass nucleus with spins $J = J_c - j,$

$J_c - j + 1, \dots, J_c + j.$

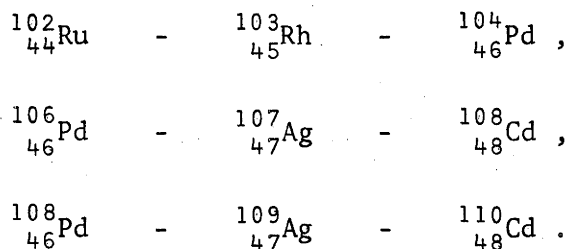
b) The $B(E2; J \rightarrow \text{g.s.})$ value for each state of a given multiplet should equal the $B(E2; J \rightarrow \text{g.s.})$ value for the neighbouring doubly even core nucleus.

c) The $B(M1; J \rightarrow \text{g.s.})$ values should be zero if there is no configuration mixing.

d) The "centre of gravity" of the multiplet of states associated with a particular core state J_c should be at approximately the same energy as the excitation energy of the state J_c in the neighbouring nucleus [La 57].

e) For E2 transitions, there should be no cross-over from two phonon states to the ground state, although transitions involving a phonon number change of one unit are allowed, [B1 67].

For the cases to be considered in this chapter, the weak coupling of a $p_{1/2}$ proton or proton hole to the neighbouring even-even core nucleus is of interest. The three cases are as follows:



In each case the odd-mass nucleus has a ground state spin of $J^\pi = 1/2^-(2p_{1/2})$. If the weak coupling model applies, for each core state J_c , there should be a multiplet of 2 states in the odd-mass nucleus. In the limit that there is no coupling between the single particle motion of the odd proton or proton hole and the collective excitation of the core, the states of a multiplet based on a given core state J_c will be degenerate. In the general case

the splitting between the states is proportional to the coupling strength, [Al 56, Sh 61, Da 68].

5.2 USE OF THE BUECHNER BROAD-RANGE SPECTROGRAPH

Proton spectra from the reactions $^{103}\text{Rh}(p,p')^{103}\text{Rh}^*$, $^{107}\text{Ag}(p,p')^{107}\text{Ag}^*$ and $^{109}\text{Ag}(p,p')^{109}\text{Ag}^*$ were obtained using the 65 cm broad-range Buechner spectrograph in conjunction with the EN tandem accelerator. This spectrograph is similar to that outlined by Browne and Buechner [Br 56] and has been fully described by Scarr [Sc 66]. This magnet system has a pole radius of 65 cm and a pole gap of 3.2 cm. The useful focal plane length is 107 cm where the charged particles may be detected using either photographic plates or position-sensitive detectors. The magnet can be rotated to a maximum angle of 153° with respect to the beam direction and can also be rotated through the 0° position. The solid angle subtended varies along the focal plane from 0.6×10^{-3} sr to 0.35×10^{-3} sr.

Calibration of the spectrograph had been performed by a number of groups within the laboratory. This often involved the use of a ^{210}Po source which emits alpha particles of energy 5.3042 ± 0.0016 MeV [Sc 66]. These calibrations were used to determine proton energies from proton group positions along the focal plane of the magnet. In order to perform these calculations, computer programs for the magnet were used with the IBM System/360-50 of the A.N.U. Computer Centre. These programs had been developed by Dr. H.J. Hay of the Department of Nuclear Physics.

The magnetic field strength of the system is measured and controlled using a proton nuclear magnetic resonance system. The field uniformity is quoted as being 1 part in 4000 below 7000 gauss

decreasing to 1 part in 1000 at 14000 gauss. A resolution figure of $E/\Delta E \approx 1000$ is quoted as being attainable but the actual value is limited by target and beam conditions. Nuclear emulsion plates are held in position along the magnet's focal plane by means of a 45 inch long plate holder which carries as many as $4\frac{1}{2}$ emulsion plates, each approximately 25 cm in length. A mask has been placed in the camera section of the magnet system to define a 10 mm wide exposure path across the 2 inch wide plate holder. This path position can be altered in position across the emulsion plates and normally, in these experiments, three equally spaced exposures were made across the plates.

The associated target chamber has an internal diameter of 13.7 cm. A solid state monitor counter can be mounted outside the chamber to detect particles through a thin mylar window in the side wall of the chamber. For the experiments discussed in this chapter Ilford K2 nuclear emulsion plates of thickness 25 μm were employed for charged particle detection. Sufficient plates were mounted ($4\frac{1}{2}$ plates) to fill the plate holder and thus cover the whole of the focal plane length. Proton scattering from each target will be discussed in separate sections as set out below.

5.3 THE REACTION $^{103}\text{Rh}(p,p')^{103}\text{Rh}^*$

To perform this experiment ^{103}Rh targets were made by vacuum evaporation of the naturally occurring (100%) target material from a tungsten boat. Two $15 \mu\text{g}/\text{cm}^2$ carbon foils were used to sandwich the $270 \mu\text{g}/\text{cm}^2$ rhodium target, one on the back and one on the front surface. This technique was adopted to prevent target instability problems which were apparent with the metal deposited directly onto a single carbon foil. The rhodium target

thickness corresponded to a proton energy loss of 6 keV for

$$E_p = 10 \text{ MeV.}$$

The $^{103}\text{Rh}(p,p')^{103}\text{Rh}^*$ reaction was studied at proton bombarding energies of 10 MeV and 11.75 MeV. At 10 MeV bombarding energy proton spectra were recorded at lab. angles of 100° , 120° and 140° . At 11.75 MeV bombarding energy a lab. angle of 130° only was used. These backward angles were chosen since the kinematic difference between proton groups due to the $^{103}\text{Rh}(p,p)^{103}\text{Rh}$ and $^{12}\text{C}(p,p)^{12}\text{C}$ reactions was large. The proton elastic peak from carbon was, for example, shifted down by 1.5 MeV with respect to the rhodium elastic peak at the most forward angle of 100° . Due to the small effective solid angle of the Buechner spectrograph (see section 5.2) and the small cross section for proton inelastic scattering long exposures were needed. The exposures used for each angle and bombarding energy are given in table 5.3.1.

Table 5.3.1

Exposures Used for the $^{103}\text{Rh}(p,p')^{103}\text{Rh}^*$ Reaction

Proton Bombarding Energy	Lab. Angle	Number of Microcoulombs of Deposited Charge
10 MeV	100°	20,100
	120°	47,000
	140°	37,600
11.75 MeV	130°	7,540

Beam integration was performed using an Elcor A3093 current integrator.

The nuclear emulsion plates were scanned in steps of 0.5 mm. The data obtained from the 10 MeV bombarding energy experi-

ments are shown in figure 5.3.1. Similarly the data recorded at $E_p = 11.75$ MeV are shown in figure 5.3.2. For presentation purposes the data are plotted in scan units of 1 mm obtained by adding together track counts from adjoining 0.5 mm scans. Peaks from the $^{103}\text{Rh}(p,p')^{103}\text{Rh}^*$ reaction were identified by their energy shifts with observation angle. These peaks have been labelled with their corresponding excitation energy in ^{103}Rh . Similarly contaminant groups from ^{37}Cl , ^{35}Cl , ^{32}S , ^{28}Si , ^{16}O , ^{14}N , ^{13}C and ^{12}C were identified and have also been indicated in figures 5.3.1 and 5.3.2.

5.4 THE REACTIONS $^{107}\text{Ag}(p,p')^{107}\text{Ag}^*$ AND $^{109}\text{Ag}(p,p')^{109}\text{Ag}^*$

5.4.1 $^{107}\text{Ag}(p,p')^{107}\text{Ag}^*$

The ^{107}Ag targets were prepared by vacuum deposition of the isotopically enriched material onto carbon foils. Targets of 100-150 $\mu\text{g}/\text{cm}^2$ were used for inelastic proton scattering measurements. As was the case for the $^{103}\text{Rh}(p,p')^{103}\text{Rh}^*$ experiment, the broad-range Buechner spectrometer was used. The nuclear emulsion plates (Ilford K2 plates) were the same as those used for the ^{103}Rh experiment. Data were obtained at three angles of $\theta_{\text{LAB}} = 100^\circ$, 120° and 140° at a proton bombarding energy of 10 MeV. The plates were scanned in steps of 0.5 mm. Data from adjoining 0.5 mm scans were added for presentation of the spectra in figure 5.4.1. These three spectra were recorded on one set of nuclear emulsion plates, the 10 mm magnet slit being moved across the plates for each exposure. Details of the three accelerator runs producing these results in figure 5.4.1 are given in table 5.4.1. Contaminant peaks have been identified and are indicated in figure 5.4.1.

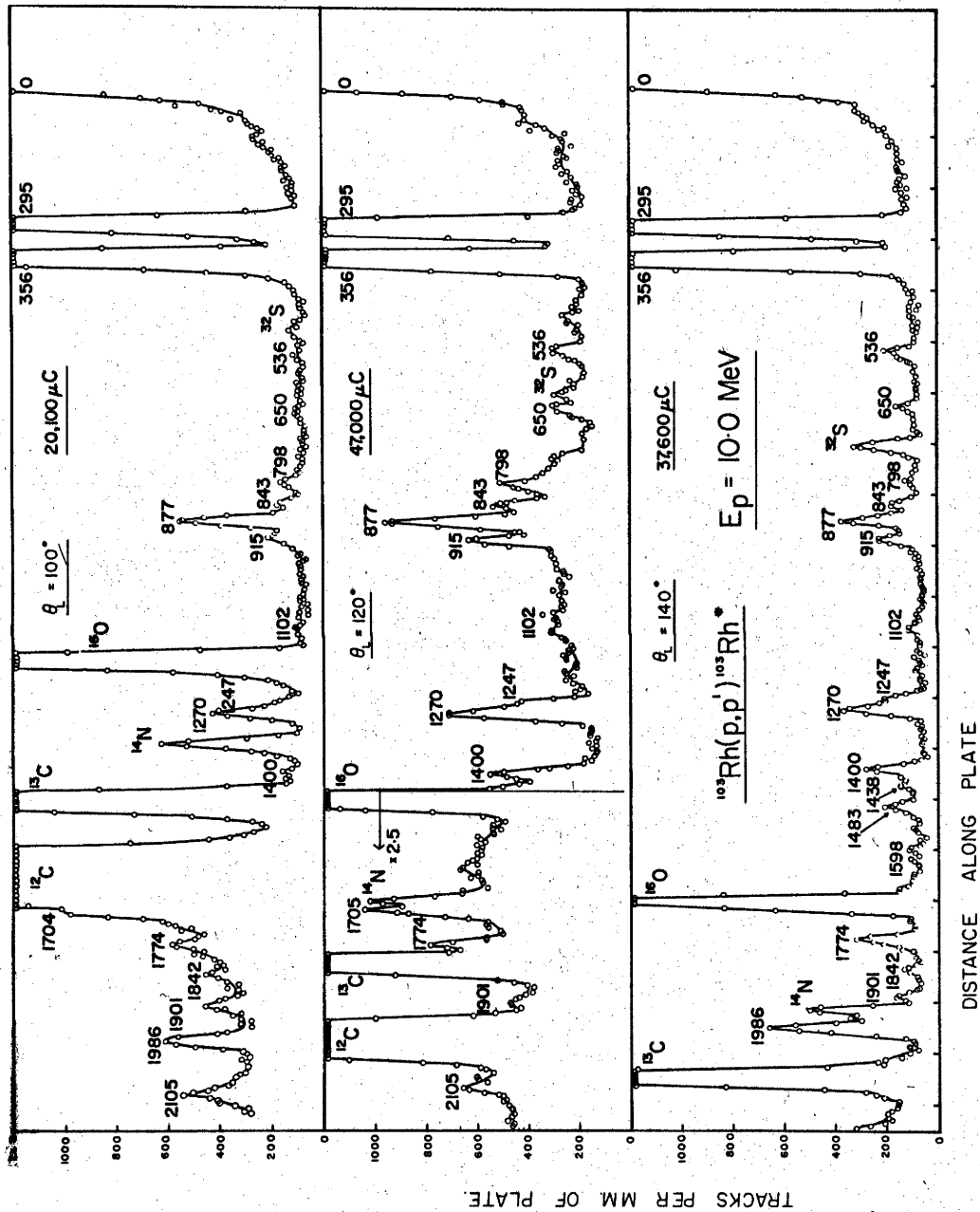


Figure 5.3.1: Proton spectra from the reaction $^{103}\text{Rh}(p,p')^{103}\text{Rh}^*$ at $\theta_{LAB} = 100^\circ, 120^\circ$ and 140° with $E_p = 10 \text{ MeV}$.

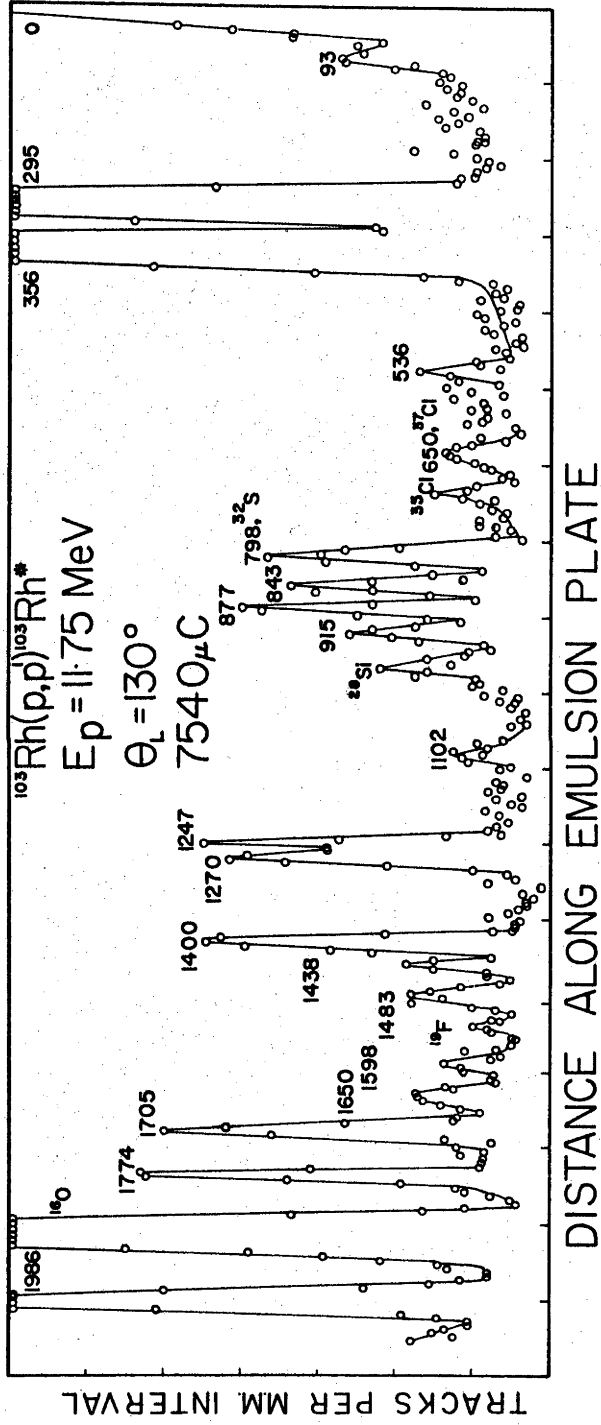


Figure 5.3.2: Proton spectrum from the reaction $^{103}\text{Rh}(p,p')^{103}\text{Rh}^*$ at $\theta_{\text{LAB}} = 130^\circ$ with $E_p = 11.75 \text{ MeV}$.

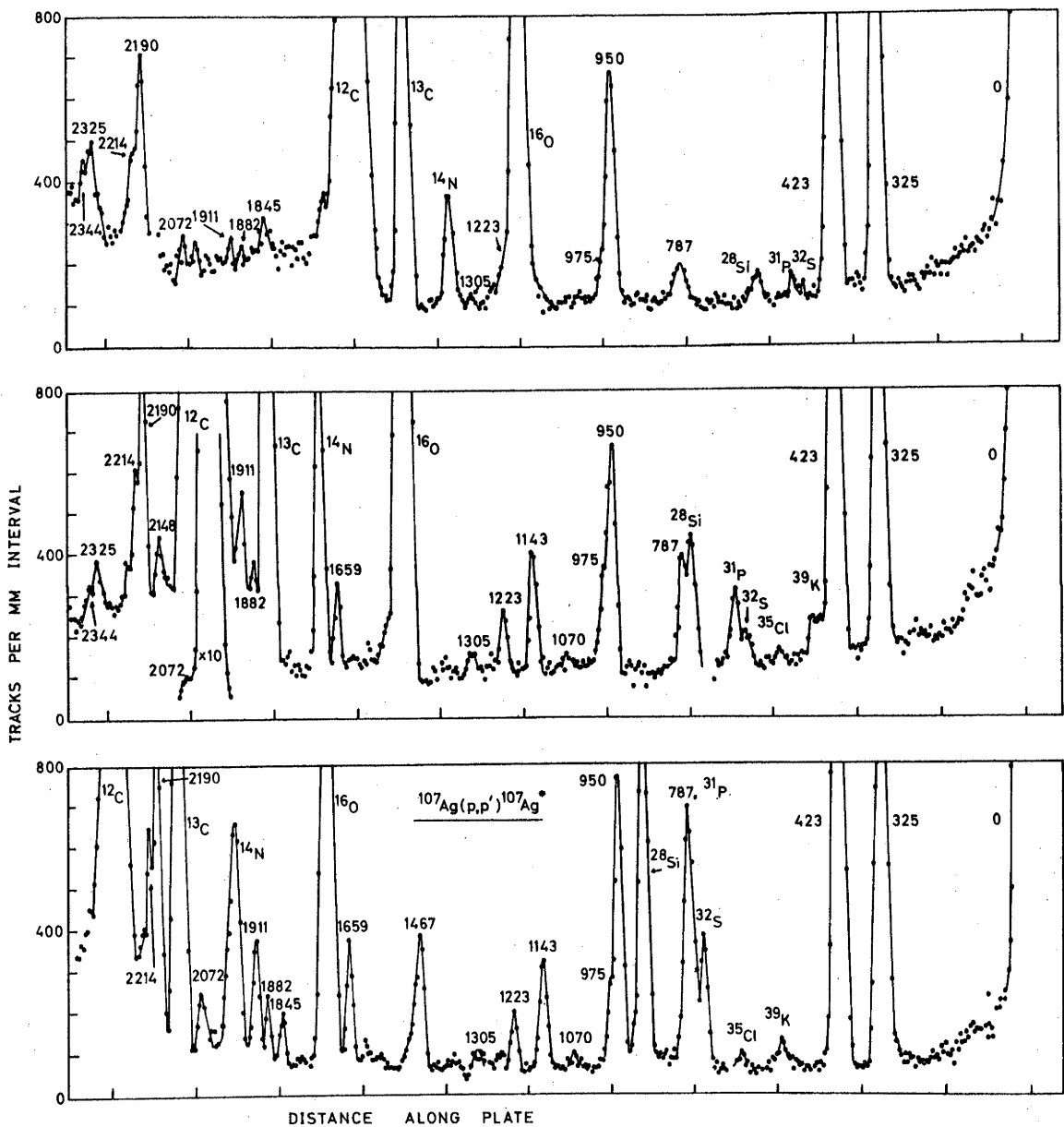


Figure 5.4.1: Proton spectra from the reaction $^{107}\text{Ag}(p,p')^{107}\text{Ag}^*$ at $\theta_{\text{LAB}} = 100^\circ, 120^\circ$ and 140° with $E_p = 10.0$ MeV.

Table 5.4.1

Experimental Details of $^{107}\text{Ag}(p,p')^{107}\text{Ag}^*$ Spectra

Lab. Angle	Proton Bombarding Energy	Path No. on Plates	Deposited Charge in Microcoulombs
100°	10.0 MeV	1	13,602
120°	10.0 MeV	2	40,000
140°	10.0 MeV	3	37,500

5.4.2 $^{109}\text{Ag}(p,p')^{109}\text{Ag}^*$

These measurements were performed concurrently with the $^{107}\text{Ag}(p,p')^{107}\text{Ag}^*$ experiment. Experimental conditions were in general the same as those outlined in section 5.4.1 above. Targets of ^{109}Ag were prepared by vacuum deposition of the isotopically enriched material. The targets used were of $150 \mu\text{g}/\text{cm}^2$ thickness. In this experiment, however, spectra were recorded at two angles only, viz. $\theta_{\text{LAB}} = 120^\circ$ and 140° at a proton bombarding energy of $E_p = 10 \text{ MeV}$. However, an additional spectrum was obtained at $\theta_{\text{LAB}} = 120^\circ$ at a proton bombarding energy of 11.75 MeV. The plates were again scanned as described above and the spectra obtained are given in figure 5.4.2. Experimental details relating to these spectra are given in table 5.4.2. Contaminant peaks were again observed and are identified in figure 5.4.2.

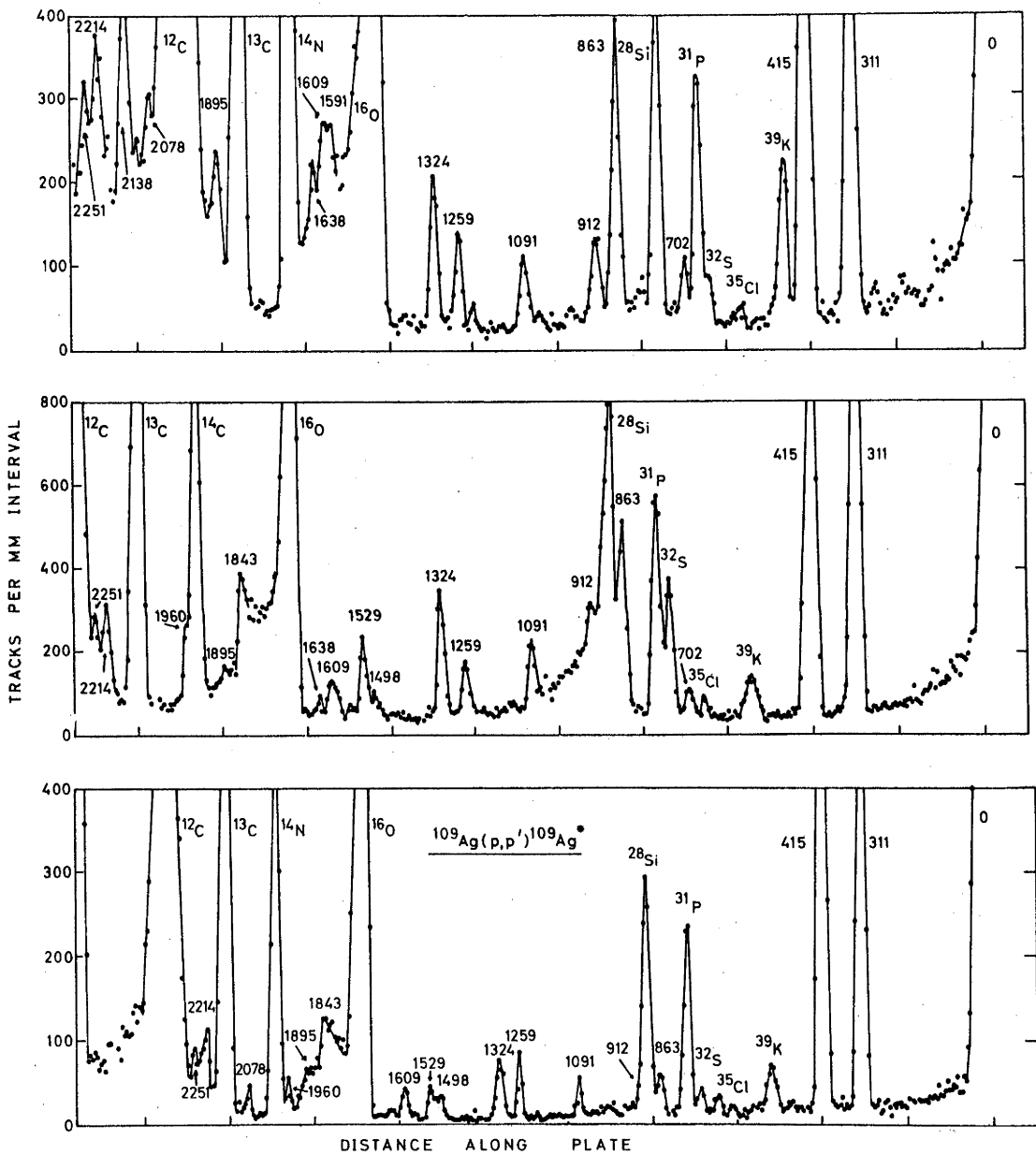


Figure 5.4.2: Proton spectra from the reaction $^{109}\text{Ag}(p,p')^{109}\text{Ag}^*$ at $\theta_{\text{LAB}} = 140^\circ$ and 120° with $E_p = 10.0$ MeV, and at $\theta_{\text{LAB}} = 120^\circ$ with $E_p = 11.75$ MeV.

Table 5.4.2

Experimental Details of $^{109}\text{Ag}(p,p')^{109}\text{Ag}^*$ Spectra

Lab. Angle	Proton Bombarding Energy	Path No. on Plates	Deposited Charge in Microcoulombs
140°	10.0 MeV	1	42,500
120°	10.0 MeV	2	25,000
120°	11.75 MeV	3	8,710

CHAPTER 6

COULOMB EXCITATION OF ^{103}Rh

6.1 INTRODUCTION

The Coulomb excitation of states in ^{103}Rh was performed in order to measure electromagnetic decay rates for the low-lying states in ^{103}Rh . Detailed treatments of Coulomb excitation have been given by a number of authors, e.g. Biedenharn and Brussard [Bi 65] and the reprint collection edited by Alder and Winther [Al 66]. The increased use of heavy-ions to induce nuclear reactions over the last few years [Ne 69] has led to increased interest in Coulomb excitation with heavy-ions.

The term "Coulomb excitation" has been defined by Alder and Winther [Al 66] to mean "the excitation of atomic nuclei through the electromagnetic field of impinging charged particles which do not penetrate into the region of nuclear forces". In this way the nuclear properties enter through the matrix elements for electric and magnetic moments which are identical to those describing the spontaneous electromagnetic transitions between the same nuclear states. Using first order perturbation theory it is possible [Al 56] to derive expressions for the thin target Coulomb excitation cross section for electric multipole excitation as:

$$\sigma_{E_\lambda} = c_{E_\lambda} \frac{E_{\text{MeV}}^{\lambda-2}}{\text{MeV}} (E_{\text{MeV}} - \Delta E'_{\text{MeV}})^{\lambda-1} \cdot B(E_\lambda) \cdot f_{E_\lambda}(\eta_1, \xi),$$

where

$$c_{E_\lambda} = (Z_1^2 A_1 / 40.03) \cdot [0.07199(1 + A_1/A_2 Z_1 Z_2)]^{-2\lambda+2} \text{ barns},$$

where

- i) A_1, Z_1, A_2 and Z_2 are the mass numbers and atomic numbers of the projectile and target respectively,
- ii) $\Delta E' = (1+A_1/A_2)\Delta E$ where ΔE represents the excitation energy,
- iii) λ represents the multipolarity,
- iv) $B(E_\lambda)$ is the reduced nuclear transition probability in units of $e^2 (10^{-24} \text{ cm}^2)^\lambda$, and
- v) $f(\eta_i, \xi)$ is a quantum mechanical excitation function tabulated by Alder et al. [Al 56] where ξ is a complex function of E and ΔE .

From these equations the thick target Coulomb excitation cross section can be derived.

Coulomb excitation is important in the study of the de-Shalit weak coupling model in that E2 transition probabilities for excitation of excited states can be measured by analysis of the γ -ray yields and angular distributions following Coulomb excitation [Da 68]. In addition to obtaining these excitation $B(E2)$ values for excited states it is also possible to obtain information on the spins of the states, E2/M1 mixing ratios (δ) and reduced transition probabilities for decay of the states. These $B(E2)$ values are important in discussion of the core-excitation model of de-Shalit.

6.2 EXPERIMENTAL DETAILS - CALIBRATION

OF Ge(Li) γ -RAY SPECTROMETER

For the Coulomb excitation of ^{103}Rh both thick and thin targets were used. The thick ^{103}Rh targets consisted of 0.75 mm thick discs of the chemically pure metal. The thin ^{103}Rh targets were the carbon-rhodium-carbon sandwich targets used for the $^{103}\text{Rh}(p,p')^{103}\text{Rh}^*$ experiments. An oxygen beam was provided by the EN tandem accelerator. This beam was produced by feeding a mixture of 5% CO_2 and 95% H_2 gases to the duoplasmatron ion source of the

accelerator. Using this gas mixture it was possible to obtain a beam on target of approximately 1.5 μA of O^{4+} beam at approximately 20 MeV. Similarly, 300 nA of O^{5+} beam was obtained at an approximate bombarding energy of 34 MeV. A 300 V electron suppression system was used during charge collection for these experiments. A glass target chamber consisting of a 1" diameter glass tube was fabricated. The tube was sealed at the bottom and another tube of smaller diameter was placed perpendicular to it about half way along its length. This second tube connected the chamber to the beam line via a glass to metal seal. A small target ladder holder fitted into the top of the chamber and supported the target ladder and targets. The beam was dumped in the target, in the case of the thin rhodium targets, by placing a thick tantalum plate behind the target. Gamma-rays from Coulomb excitation of ^{103}Rh were detected with a 40 cm^3 Nuclear Diodes Ge(Li) spectrometer with a resolution of 8 keV for γ -rays of the order of 500 keV. An additional 12.7 cm \times 10.2 cm NaI(Tl) crystal was used for the γ - γ coincidence measurements. The NaI crystal was identical in performance to that outlined in chapter 4 of this thesis in the description of the $^9\text{Be}(^3\text{He},\gamma\gamma)^{12}\text{C}$ reaction.

In order to derive $B(E2)$ values from the data, it was necessary to know the photopeak efficiency of the Ge(Li) counter as a function of γ -ray energy. A measurement of this efficiency was made using radioactive sources which emitted two or more gamma-rays of known relative intensity. The sources used and the associated gamma-rays are given in table 6.2.1 below. For the ^{60}Co , ^{24}Na and ^{46}Sc sources, the two gamma-rays are in one to one correspondence since they arise from β -decay to the upper state only with a subsequent decay sequence $J^\pi = 4^+ \rightarrow 2^+ \rightarrow 0^+$. The ^{24}Na , ^{46}Sc and $^{180\text{m}}\text{Hf}$

Table 6.2.1
Sources Used for Photopeak Efficiency Measurement

Source	Half Life	Gamma-Rays Emitted	Relative Intensities	References
^{24}Na	15 hr	2.752 MeV	1	
		1.368 MeV	1	
^{60}Co	5.2 yr	1.333 MeV	1	
		1.173 MeV	1	
^{22}Na	2.6 yr	1.274 MeV	0.9994 ± 0.0011	Al 56
		0.511 MeV	1.8114 ± 0.0011	Al 56
^{46}Sc	84 d	1.120 MeV	1	
		0.889 MeV	1	
$^{180\text{m}}\text{Hf}$	5.5 hr	0.0575 MeV	291 ± 7	Ed 61
		0.0933 MeV	100 ± 2	Ed 61
		0.2153 MeV	500 ± 14	Ed 61
		0.3325 MeV	567 ± 24	Ed 61
		0.4438 MeV	490 ± 26	Ed 61

sources for this calibration were prepared by activating thin samples of hafnium, sodium carbonate and scandium in the HIFAR reactor at the Australian Atomic Energy Commission Research Establishment at Lucas Heights, N.S.W. The reactor provides a slow neutron flux of $9 \times 10^{12} \text{ n.cm}^{-2}.\text{sec}^{-1}$. After activation these sources were brought to Canberra and the γ -ray spectra were measured with the Ge(Li) detector. The spectra were obtained using the IBM 1800 data acquisition system in a single parameter mode with 2048 channels of resolution. Characteristic spectra for ^{46}Sc and ^{22}Na are shown in figure 6.2.1. From these spectra and the known relative intensities (see table 6.2.1) the measured photopeak efficiency curve was determined. This curve is shown in figure 6.2.2.

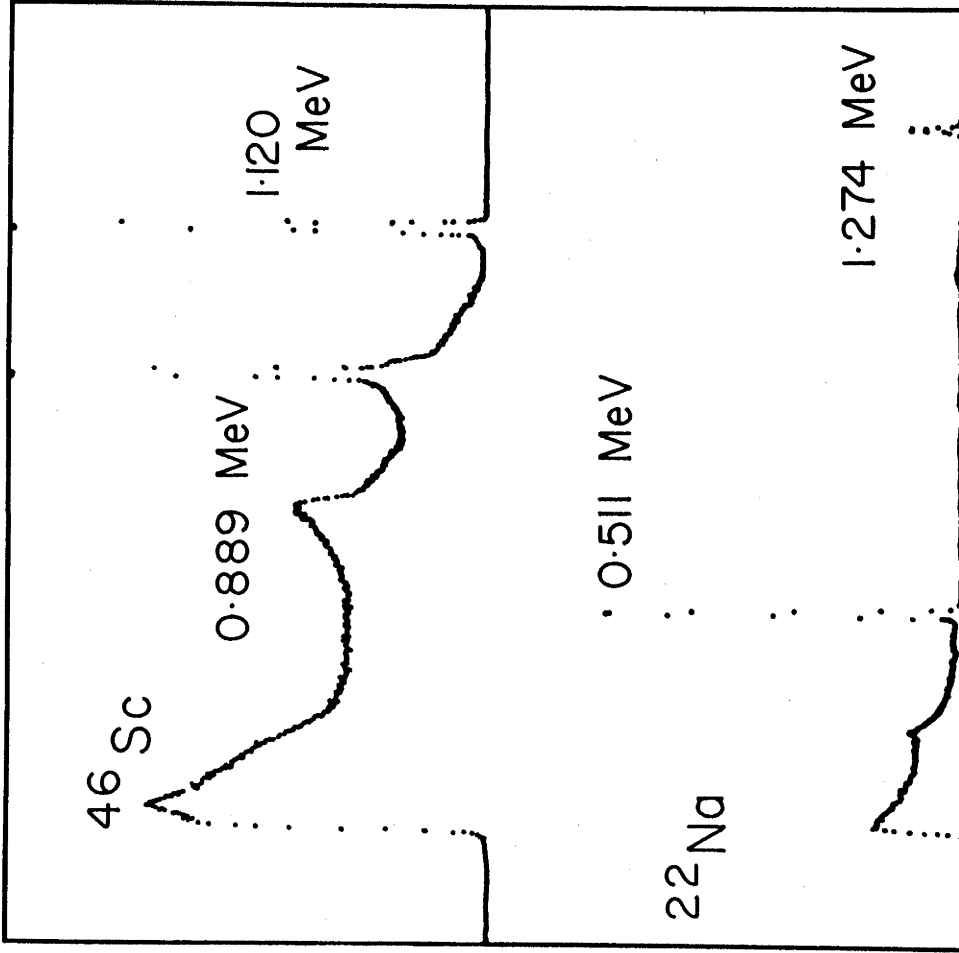


Figure 6.2.1: Characteristic spectra from ^{46}Sc and ^{22}Na used for relative efficiency measurements on Ge(Li) counter.

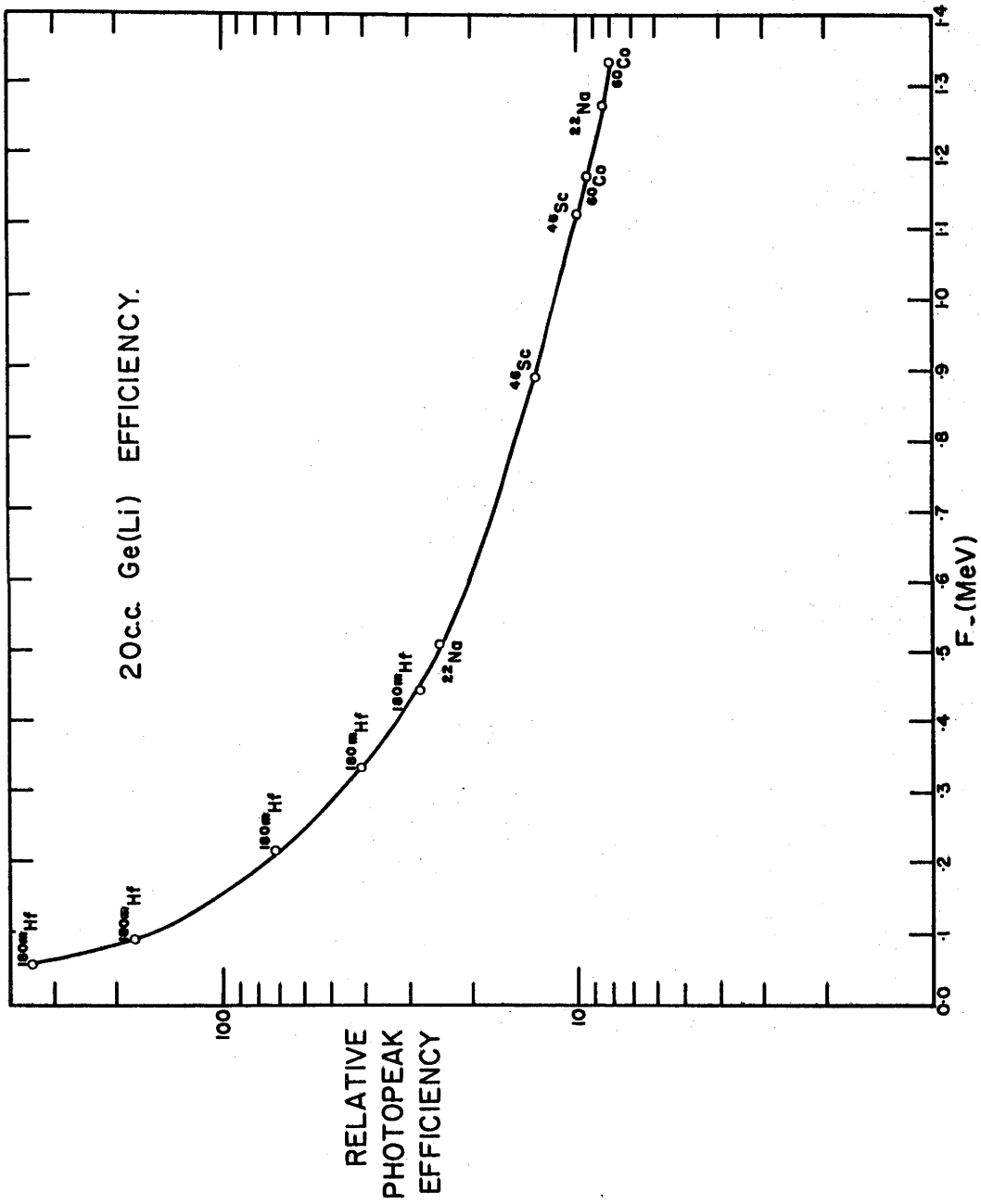


Figure 6.2.2: Relative photopeak efficiency for the 20 cm³ Nuclear Diodes Ge(Li) detector.

6.3 COULOMB EXCITATION USING OXYGEN IONS

Coulomb excitation of ^{103}Rh using oxygen ions was performed using both the thick and thin Rh targets. Both single parameter spectra and γ - γ coincidence spectra were obtained using a Ge(Li) counter and a NaI(Tl) counter.

A γ -ray spectrum from the bombardment of the thick disc of ^{103}Rh had been previously taken by Black and Gruhle [Bl 67a] at Stanford University using ^{16}O ions of 40 MeV bombarding energy supplied by the Stanford FN tandem accelerator. A spectrum obtained is shown in figure 6.3.1. A similar spectrum was taken in this laboratory using 100 nA of ^{16}O beam at a bombarding energy of 34 MeV. In this case an $^{16}\text{O}^{5+}$ beam was used. A spectrum is shown in figure 6.3.2. Gamma-ray energies shown in figure 6.3.2 are considered to be accurate to ± 3 keV. In both the cases of spectra recorded in this laboratory and at Stanford, calibration of the Ge(Li) detectors was performed using γ -ray sources. Also, in both these cases, spectra were taken at an observation angle of $\theta_{\text{LAB}} = 55^\circ$ with respect to the beam direction, where $P_2(\cos \theta) = 0$. Delayed γ -rays from the thick ^{103}Rh target were identified by recording a spectrum for 20 minutes after beam off time following bombardment of the target for 24 hours using 34 MeV oxygen ions.

The thick rhodium target was used for γ - γ coincidence measurements using the Ge(Li) and NaI(Tl) counters. The coincidence spectra were obtained using oxygen ions of 34 MeV bombarding energy. The resolution of the 12.7 cm \times 10.2 cm NaI(Tl) counter (FWHM $\approx 8.5\%$) enabled γ -rays of energy 295 keV and 356 keV (third and fourth excited states of ^{103}Rh) to be separated. Energy windows set around these γ -rays were used to gate the Ge(Li) detector. A spectrum from the NaI(Tl) detector is shown in figure 6.3.3 with

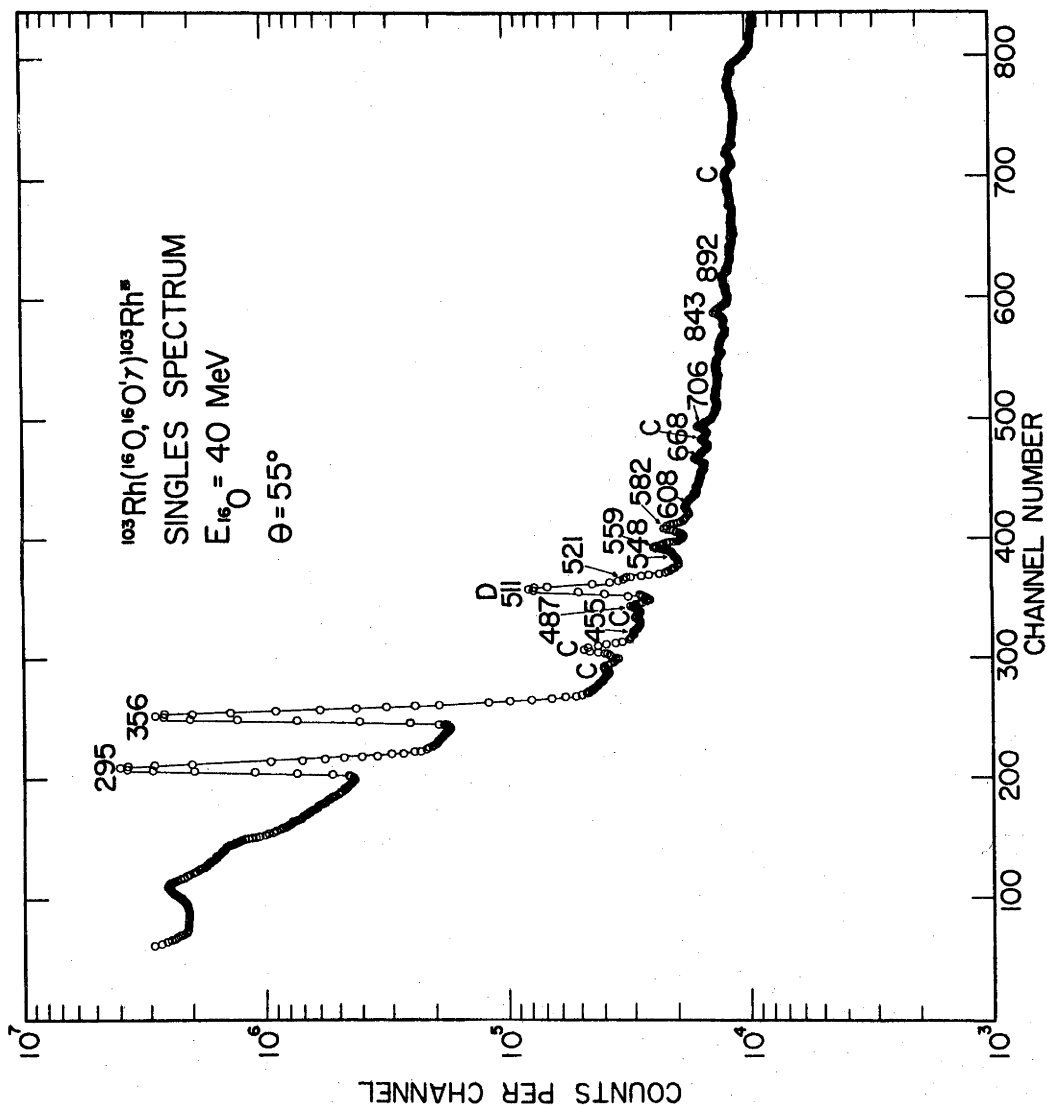


Figure 6.3.1: Singles γ -ray spectrum from the bombardment of the thick rhodium target with 40 MeV O^{6+} ions, (Stanford).

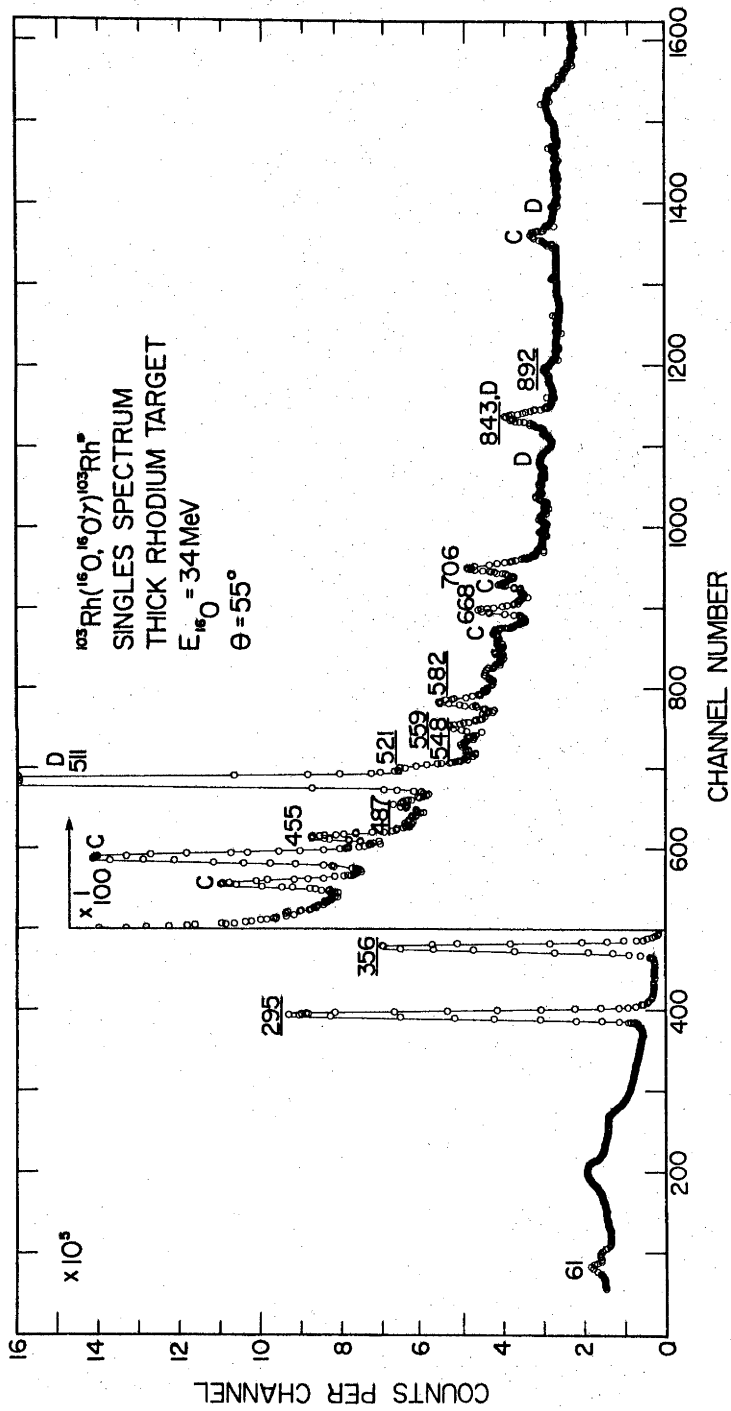


Figure 6.3.2: Singles γ -ray spectrum from bombardment of the thick rhodium target with 34 MeV O^{5+} ions. Delayed γ -rays and γ -rays arising from reactions with carbon are labelled.

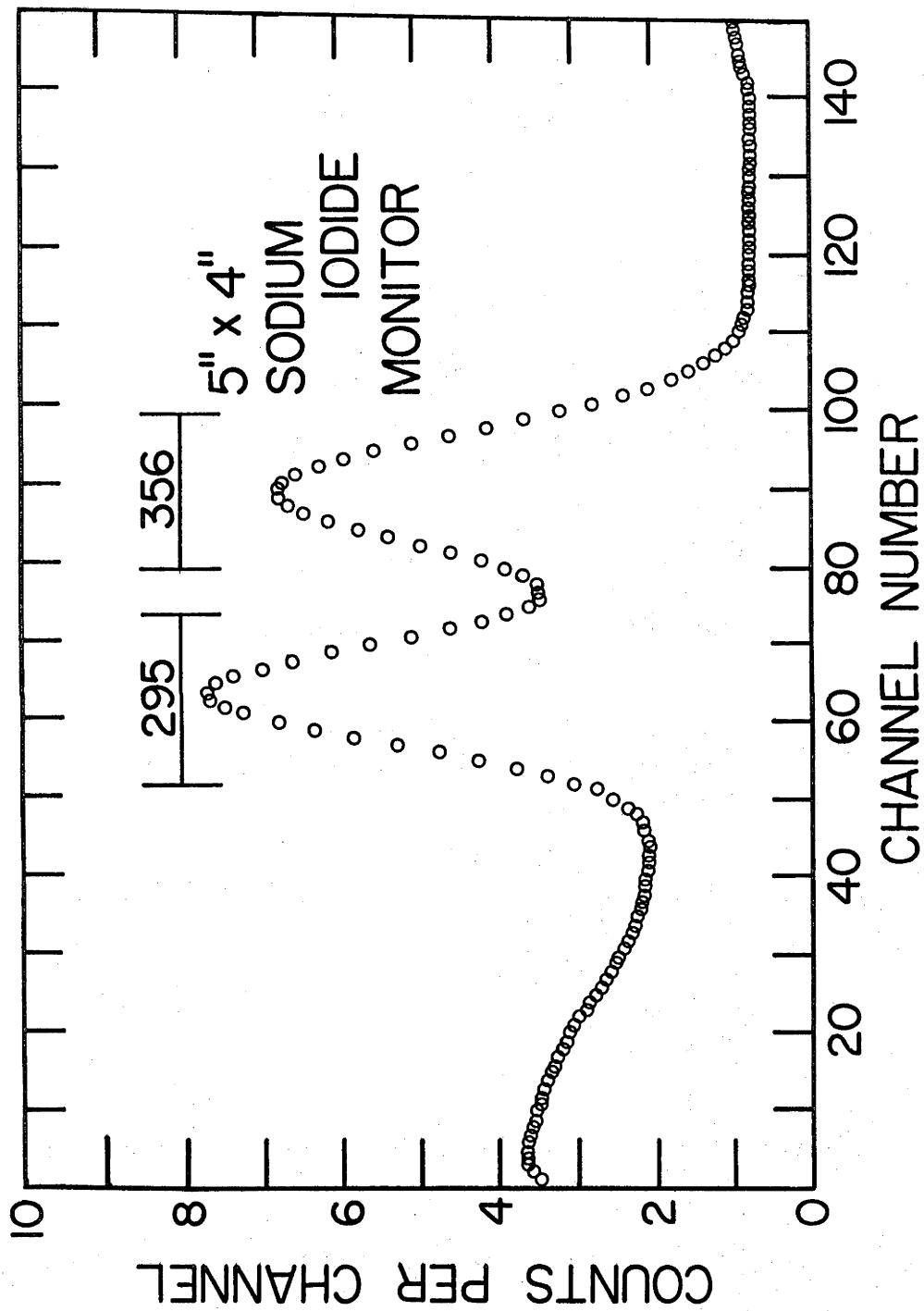


Figure 6.3.3: Singles γ -ray spectrum from bombardment of the thick rhodium target with $34 \text{ MeV } O^{5+}$ ions. Detector was $12.6 \times 10.2 \text{ cm NaI(Tl)}$ crystal. Windows used for gating Ge(Li) detector are shown.

the windows indicated. A slow-fast coincidence system based on Ortec electronic modules, with a resolving time $2\tau = 75$ ns, was used (figure 6.3.4). Timing single channel analysers (ORTEC module no. 420) were used to sense the cross-over timing of the γ -ray pulses subsequent to energy selection. Using the resolving time above, a real/random coincidence rate of approximately 8/1 was obtained. Coincidence spectra were obtained of the Ge(Li) detector output gated in turn by the 295 keV and 356 keV γ -rays detected by the NaI(Tl) counter. These spectra are shown in figures 6.3.5 and 6.3.6 respectively. Each of these spectra were accumulated over a 48 hour period.

Gamma-ray singles spectra were obtained using the thin rhodium targets already described. A spectrum obtained with the Ge(Li) detector is shown in figure 6.3.7. In order to identify γ -rays seen in this spectrum it was decided to also bombard a carbon target with oxygen ions of 34 MeV bombarding energy. The resulting spectrum obtained from this experiment is shown in figure 6.3.8. The carbon targets used were of $20 \mu\text{g}/\text{cm}^2$ thickness.

Finally a spectrum was recorded using the thin rhodium targets wherein the Ge(Li) counter was gated by backscattered oxygen ions from the reaction. A surface barrier detector was used at 130° to the beam direction. The Ge(Li) detector was, as usual, positioned at $\theta_{\text{LAB}} = 55^\circ$. A particle-gamma coincidence system, similar to that used for the γ - γ coincidence work (see figure 6.3.4), was used for these measurements. This system had a resolving time of $2\tau = 100$ ns yielding a real/random ratio of 6/1 with 40 nA of O^{5+} beam. The spectrum obtained revealed only the 295 keV and 356 keV γ -rays. These both appeared strongly as compared to their strength in the ungated spectrum from the same target (figure

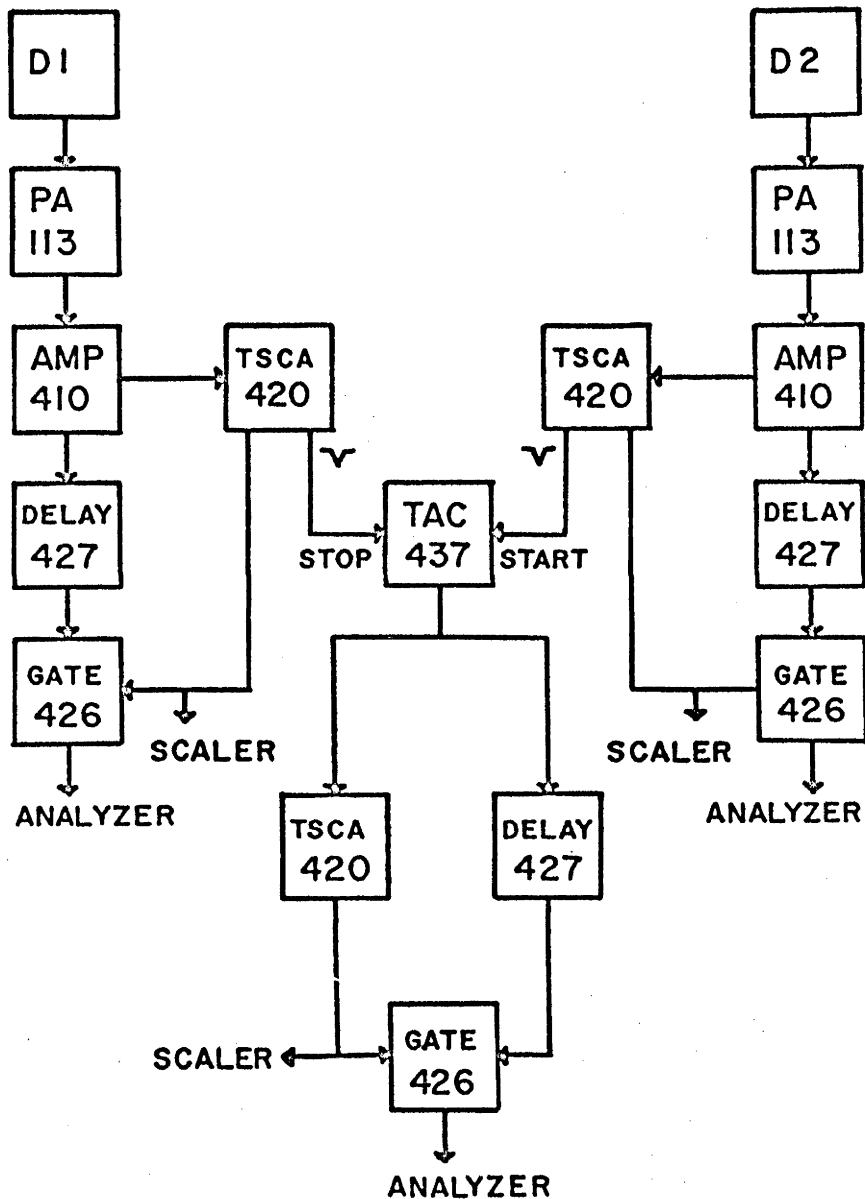


Figure 6.3.4: Logic diagram for slow-fast coincidence system used for NaI(Tl) and Ge(Li) detectors coincidence measurements (see also figure 4.4.1).

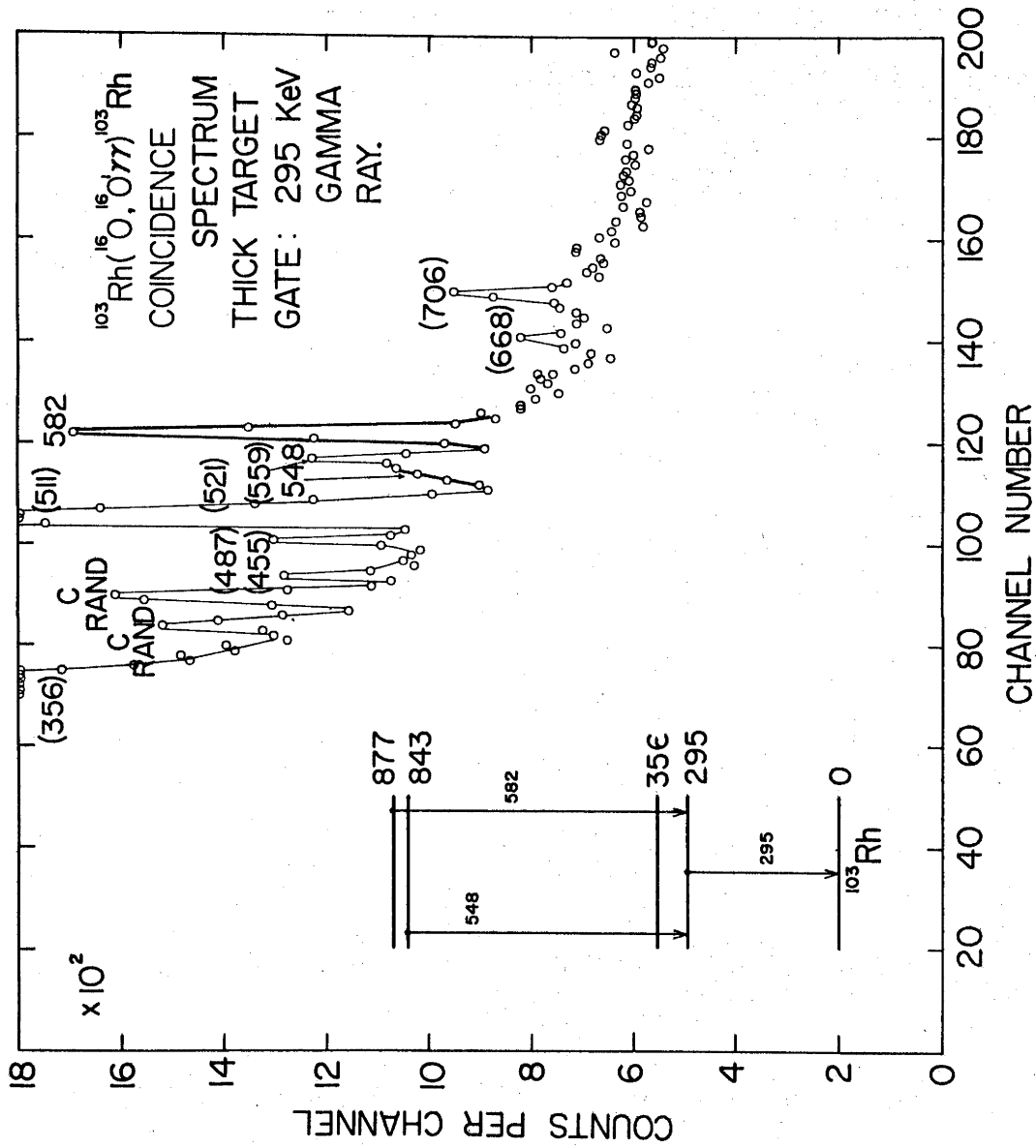


Figure 6.3.5: γ - γ coincidence spectrum from ^{103}Rh gated with the 295 keV line. Bracketed peaks arise from random coincidences.

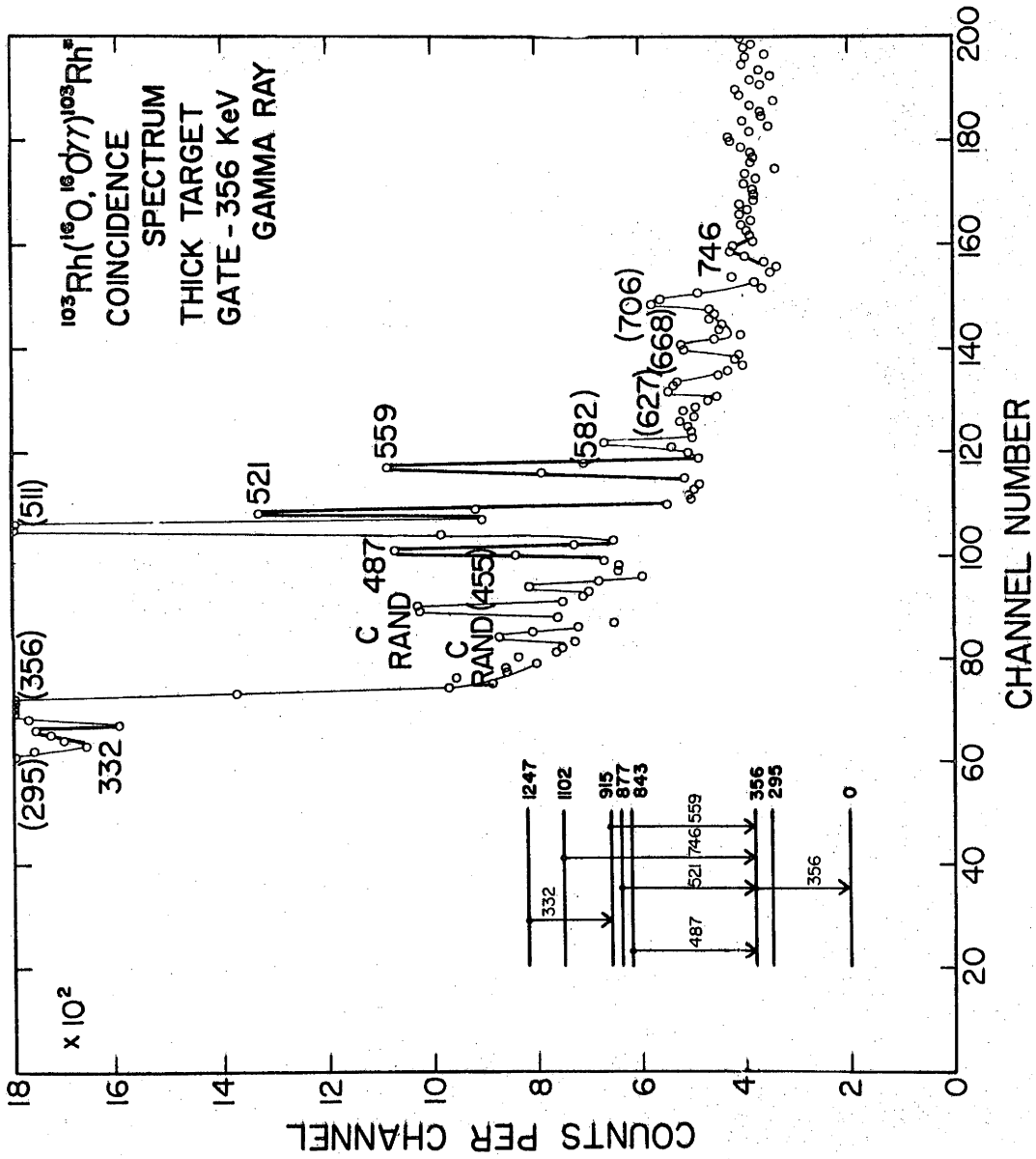


Figure 6.3.6: γ - γ coincidence spectrum from ^{103}Rh gated with the 356 keV line. Bracketed peaks arise from random coincidences.

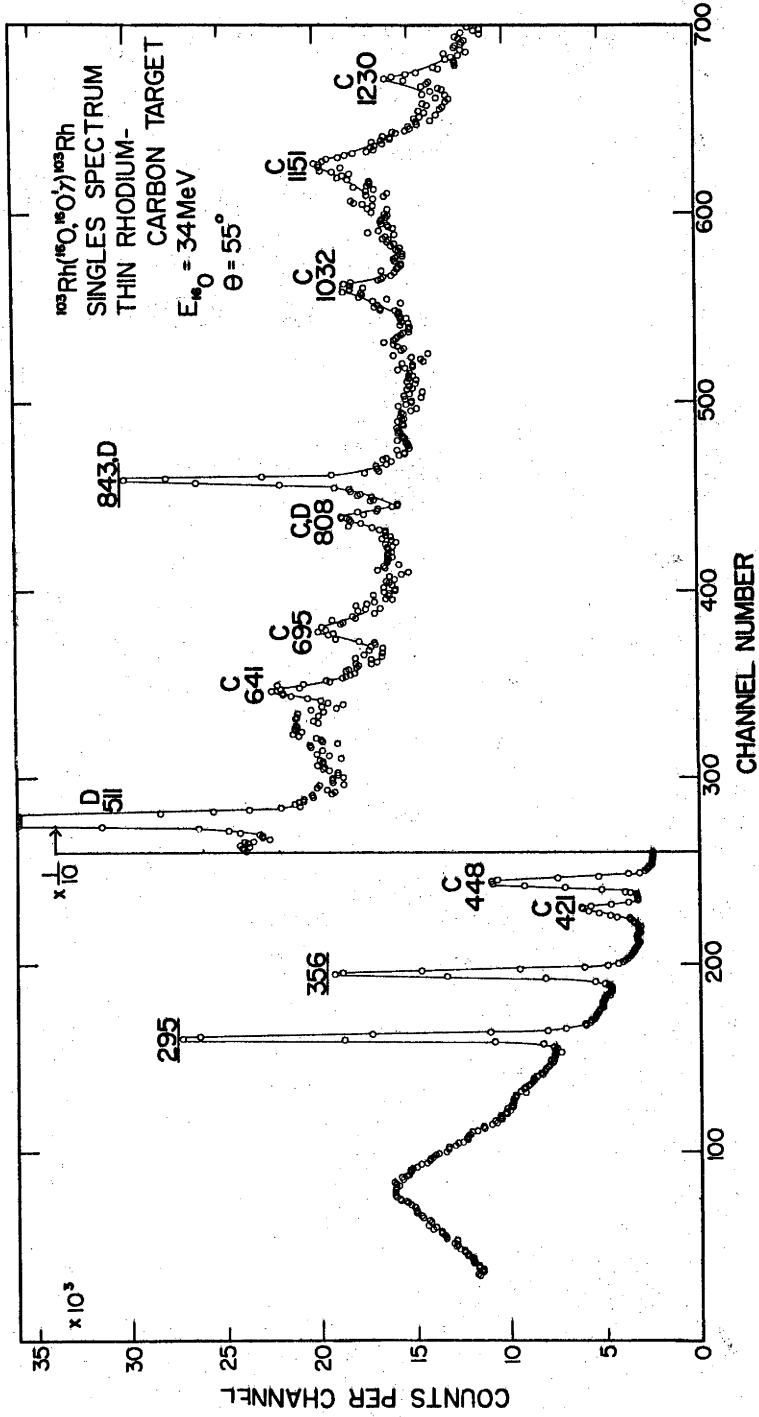


Figure 6.3.7: Singles γ -ray spectrum from the bombardment of the thin rhodium target with 34 MeV O^{5+} ions.

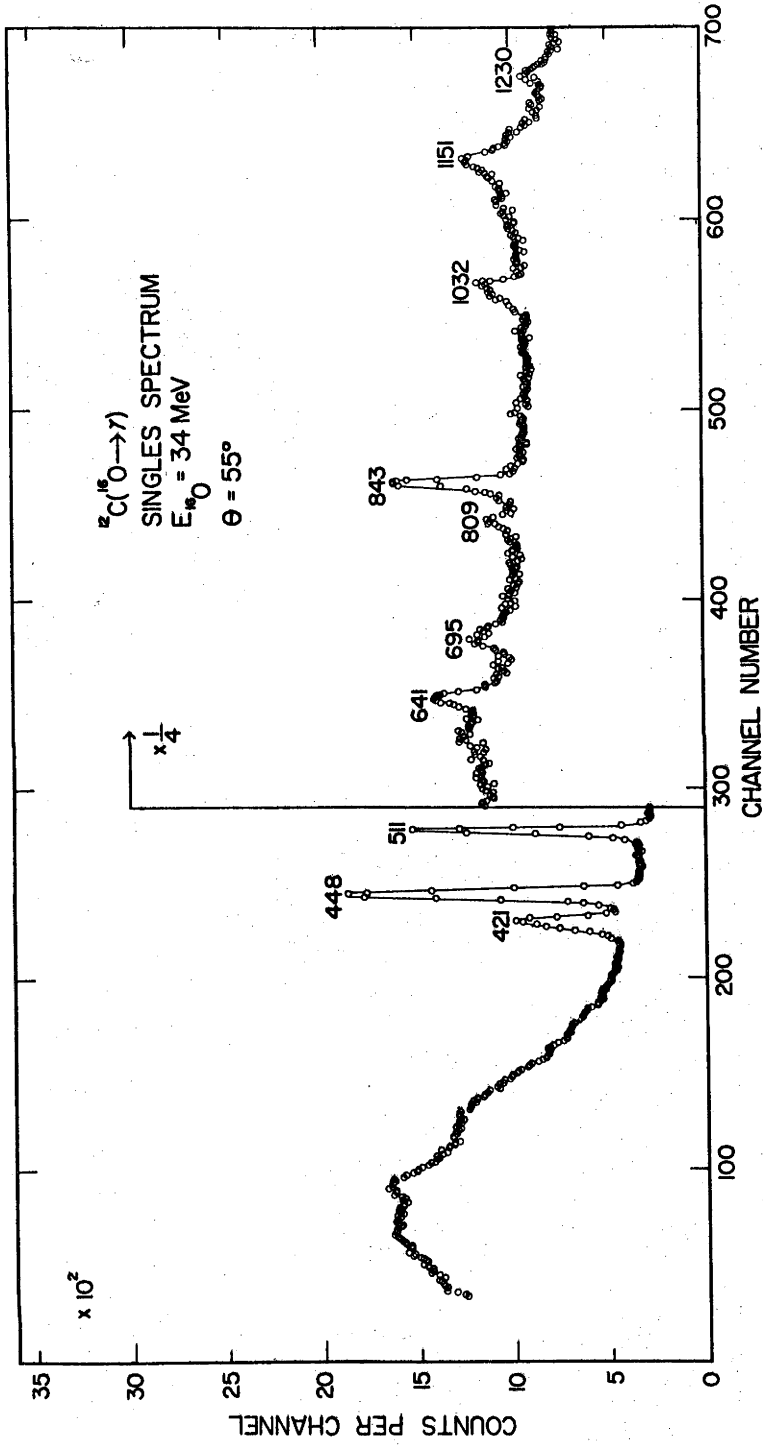


Figure 6.3.8: Singles γ -ray spectrum from bombardment of a
 20 $\mu\text{g}/\text{cm}^2$ carbon foil target with 34 MeV O^{5+} ions.

6.3.7). In the coincidence spectrum, the ratio of the 356 keV γ -ray to the 448 keV γ -ray was found to be 40/1 as compared to 1.9/1 in the ungated spectrum. All spectra taken in these experiments were taken using the IBM 1800 data acquisition system in the EN tandem laboratory at A.N.U. [Ca 69].

CHAPTER 7

STATES OF ^{103}Rh , ^{107}Ag and ^{109}Ag 7.1 ^{103}Rh STATES

The study of the $^{103}\text{Rh}(p,p')^{103}\text{Rh}^*$ reaction permitted the observation of many previously unreported levels in ^{103}Rh at low excitation energies. In many cases, states were not observed at all angles in the (p,p') study due to masking by contaminant peaks. The levels are tabulated in figure 7.1.1. In this table of energy levels only levels which appear at two or more angles have been included. The 1650 keV state has been bracketed as doubtful because it only appears in the (p,p') spectrum obtained at a proton bombarding energy of 11.75 MeV. The proton group could not be explained by the usual contaminants and so it has been included. The excitation energies in figure 7.1.1 are considered to be accurate to ± 10 keV. The observed energy levels are in good agreement with the subsequent results of Sayer et al. [Sa 70] who observed the de-excitation γ -rays from states in ^{103}Rh following Coulomb excitation with 7 - 10 MeV alpha particles. This group was able to assign B(E2) values to a number of states.

Absolute cross section calculations were made for the $^{103}\text{Rh}(p,p')^{103}\text{Rh}^*$ reaction. These came from a knowledge of the effective magnet solid angle and of the target thickness, which was obtained by weighing. The (p,p') cross sections for the 295, 356 and 877 keV states were determined from both the data taken at 10 MeV and 11.75 MeV proton bombarding energy. The results are shown in table 7.1.1. These calculated values are estimated to be accurate to about $\pm 30\%$.

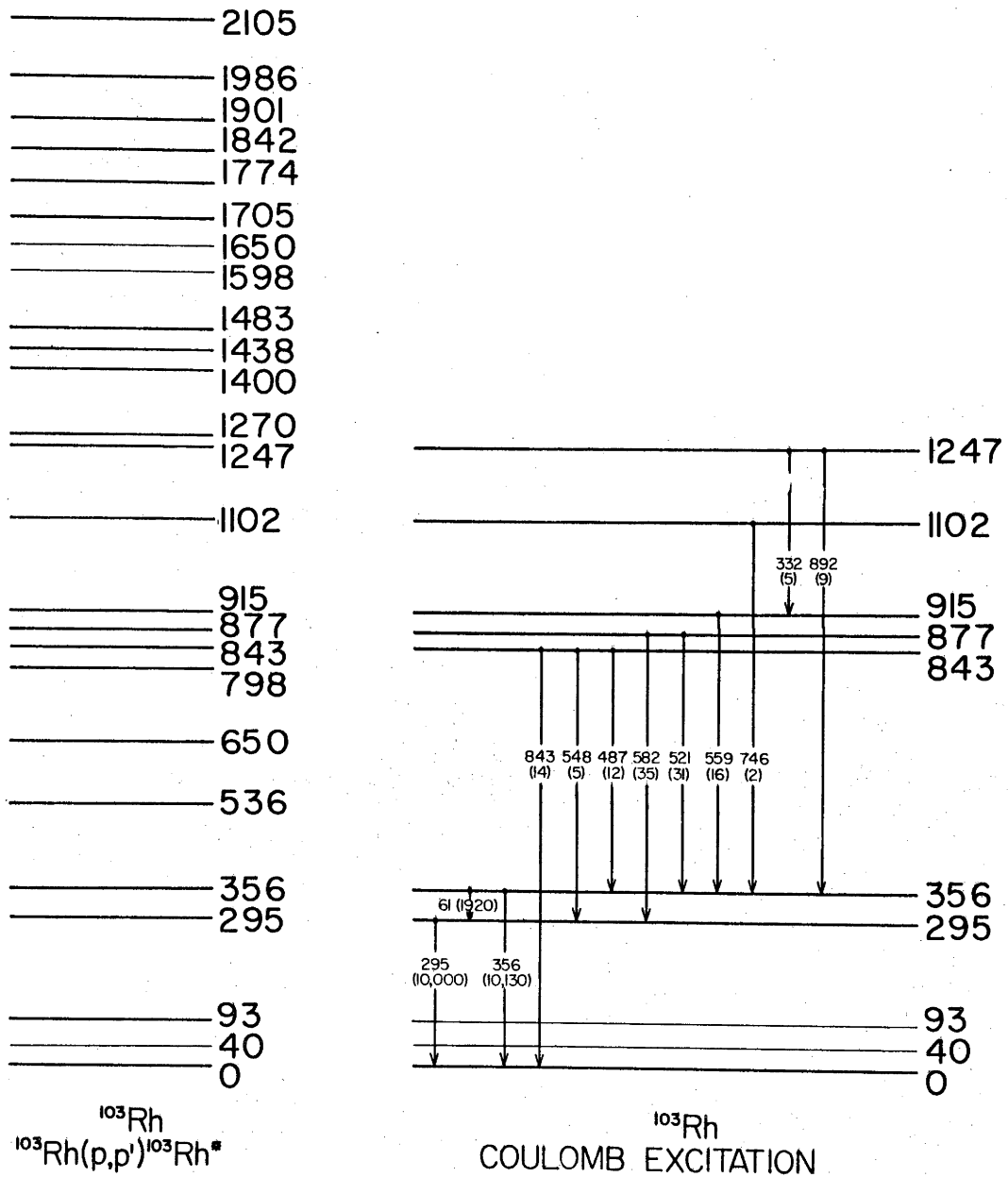


Figure 7.1.1: Excited states of ^{103}Rh .

Table 7.1.1
(p,p') Cross Sections for States in ^{103}Rh

State Excitation in keV	Cross Section in $\mu\text{b}/\text{sr}$ ($\pm 30\%$)	Lab. Angle	Proton Bombarding Energy
295	157	100°	10 MeV
356	226		
877	29		
295	244	130°	11.75 MeV
356	345		
877	7		

7.2 STATES OF ^{103}Rh AND DECAY SCHEMES - EXPERIMENT

The decay scheme, as interpreted from the (p,p'), Coulomb excitation and coincidence measurements is shown in figure 7.1.1. The excitation energies of the states observed via the (p,p') reaction and Coulomb excitation agree very well, as is evident in figure 7.1.1. The states observed in the (p,p') work extend to an excitation energy approximately twice that of the levels seen via Coulomb excitation. This is because the Coulomb excitation cross section [Al 56, Bi 65, pg. 96] falls off rapidly as the excitation energy increases. Figure 7.1.1 shows the γ -decay scheme and branching ratios, (γ -ray transition energies in keV and branching ratios inside brackets). These are to be compared to the results obtained by Sayer et al. [Sa 70] shown in table 7.3.3.

The gamma decay information was obtained from the Coulomb excitation experiment using both the singles and coincidence data. The well-established 295 keV and 356 keV states decay to ground. The γ - γ coincidence data obtained by gating with these γ -rays produced the following information:

a) The 295 keV γ -ray is in coincidence with γ -rays of energy 548 keV and 582 keV. The resulting decay scheme for states de-exciting through the 295 keV state is unambiguous and is shown in figure 7.1.1.

b) The 356 keV γ -ray is in coincidence with γ -rays of energy 332, 487, 521, 559 and 746 keV. The states decaying through the 356 keV state are again shown in figure 7.1.1. It is to be noted that the 843 and 877 keV states decay through both the 295 and 356 keV states.

A number of γ -rays apparent in the singles spectra were not observed in the coincidence spectra and are interpreted as arising from reactions with carbon. Gamma-rays with energies of 420 and 440 keV, present in all of the singles spectra and very strong in the $^{12}\text{C} + ^{16}\text{O}$ spectrum, were not observed in the oxygen backscattering measurement. A 1386 keV γ -ray, likewise found in all singles spectra, is interpreted as arising from the reaction $^{12}\text{C}(^{16}\text{O}, \alpha_1\gamma)^{24}\text{Mg}$. The peaks associated with carbon were very weak in the spectra obtained with the thick rhodium discs (figure 6.3.2). Their presence is due to a small build-up of carbon on the target surface during bombardment. The spectrum obtained by bombardment of the thin rhodium target (figure 6.3.7) clearly shows only γ -rays of energies 295 and 356 keV from the Coulomb excitation of rhodium. Several γ -rays found in the thick target spectrum were present in the spectrum taken after bombardment. In order to interpret these γ -rays a similar delayed spectrum was recorded with the thin carbon target. The same γ -rays appeared in the latter spectrum. It is thus concluded that they cannot arise from isomeric transitions in ^{103}Rh . Of particular note are the two γ -rays of energies 808 and 845 keV which appeared in the thin target singles spectra and the

delayed spectra. The γ -rays were also observed in a background spectrum measured with beam off and with the targets removed from the chamber. The 845 keV γ -ray is identified as coming from radioactivity in the chamber caused by the $^{56}\text{Fe}(p,n)^{56}\text{Co}(\beta^+)^{56}\text{Fe}$ reaction. This populates the first excited state of ^{56}Fe at 845 keV which then γ -decays to ground. The β -decay has a half-life of 77 days.

Careful analysis showed that the 843 keV peak in the thin rhodium target spectrum was somewhat stronger than in the pure carbon target spectrum suggesting that an 843 keV γ -ray results from Coulomb excitation of rhodium. It thus appears that the 843 keV state has a weak γ -decay to ground. However, due to the presence of the γ -ray from activation of the chamber an estimation of the intensity of this gamma ray is liable to large error (table 7.3.1). A ground state decay of this state was not observed by Sayer et al. [Sa 70] supporting the proposition that the ground state γ -decay of this 843 keV state is, at the most, extremely weak. The origin of γ -rays at 455, 668 and 706 keV remains in doubt. It has not been possible to fit these γ -rays into the suggested decay scheme. It is assumed that they arise from Coulomb excitation or nuclear reactions with light contaminant elements in the target. It is possible that a 706 keV γ -ray could arise by the decay of the 798 keV state (seen in the (p,p') experiment) to the 93 keV state. However, there is no supporting evidence for the Coulomb excitation of this 798 keV state.

7.3 INTENSITIES OF γ -DECAYS IN ^{103}Rh AND B(E2) VALUES

7.3.1 γ -Ray Intensities

Using the thick target spectra, γ -ray intensities were

obtained by summing the counts under each peak and subtracting a background derived from smooth interpolation. Corrections were made for the following effects:

- a) the variation of photopeak efficiency with γ -ray energy;
- b) γ -ray attenuation in the walls of the glass target chamber, and in the target backing (0.075 cm nickel); and
- c) γ -ray self-attenuation in the thick ^{103}Rh target.

Total transition strengths were obtained by correcting the γ -ray intensities for internal conversion. The total internal coefficients (α) for the 61, 295 and 356 keV γ -rays were taken from the paper by McGowan and Stelson [Mc 58] and those for the higher energy transitions from Hager and Seltzer's tabulations [Ha 68a]. These led to the calculation of γ -ray intensities observed by Coulomb excitation as shown in table 7.3.1.

Table 7.3.1
Intensities of γ -Rays Observed in the
Coulomb Excitation of ^{103}Rh

γ -Ray Energy (keV)	Intensity Normalized to 295 keV γ -Ray Intensity	Error (\pm %)
62	1920	30
295	10000	
332	5	50
356	10130	0.25
487	12.0	5
521	30.7	40
548	4.7	6
559	15.9	4
582	34.7	3
747	2	50
843	14	100
892	8.6	6

7.3.2 B(E2) Values

If it is assumed that the Coulomb excitation of states is due to a pure electric interaction, reduced electric quadrupole transition probabilities, i.e. B(E2) values, can be obtained. The Coulomb excitation cross section for thin targets has been obtained by Alder et al. [A1 56] using first order perturbation theory. This assumes first order Coulomb excitation, i.e. Coulomb excitation from the ground state only and not through higher order Coulomb excitation via excited states. Since the Coulomb excitation work was performed using a thick target it becomes necessary to integrate the expressions of Alder et al. with respect to energy. The B(E2) \uparrow values from the thick target experiment can be obtained using the equation:

$$B(E2)\uparrow \propto N/Y$$

where N is the total number of excitations for a given state per μC of oxygen beam and Y is the thick target Coulomb excitation integral defined by:

$$Y = K^2 \int_{E_{\min}}^{E_{\max}} \frac{(E - \Delta E/K) f(\xi)}{S(E)} \cdot dE .$$

In this case:

- a) S(E) is the rate of energy loss of the projectile in the target;
- b) f(ξ) is an excitation cross section tabulated by Alder et al. [A1 56, section IIC.2];
- c) $K = A_2/(A_1 + A_2)$, where A_1 and A_2 are the mass numbers of the projectile and target nuclei respectively;
- d) ΔE is the excitation energy of the state being populated via Coulomb excitation; and

e) ξ is a complex function of E and ΔE again given by Alder et al. [A1 56, section IIC.1].

The thick target integration must be performed from the bombarding beam energy (E_{\max}) down to an energy where the contribution to the integral is negligible.

In order to perform this integration numerically a Fortran program was written. This program used Simpson's rule for numerical integration and the integral was calculated for each state populated. Stopping cross sections were obtained from the data of Booth [Bo 65] and Northcliffe [No 63]. $B(E2)\downarrow$ values were derived from the $B(E2)\uparrow$ values using the equation [A1 56]:

$$B(E2; J \rightarrow 0) = B(E2; 0 \rightarrow J) \frac{2J_0 + 1}{2J + 1}$$

where J_0 and J are the spins of the ground and particular excited state respectively. The ratios:

$$B(E2)\downarrow/B(E2)_{\text{SINGLE PARTICLE}}$$

were obtained again using the definition of Alder et al. [A1 56]:

$$B(E2)_{\text{S.P.}} = R_0^4 (9/100 \pi)$$

where R_0 has been taken as $1.2 A^{1/3}$ fm. Quadrupole distortion parameters (β_2) have also been extracted in addition to the ground state $B(E2)$ values. Since the $E2/M1$ mixing ratios for the transitions from the 295 and 356 keV states to ground are known, the lifetimes of these states could be calculated from the β_2 values. Table 7.3.2 contains, then, level energies and J^π values, values for the thick target Coulomb excitation integral Y , $B(E2)\uparrow$ and $B(E2)\downarrow$ values, $B(E2)\downarrow/B(E2)_{\text{S.P.}}$ values, mean lifetimes (where applicable) and quadrupole distortion parameters (β_2). Spins and

Table 7.3.2

Properties of Excited States of ^{103}Rh

Level E (keV)	J^π	Integral Y (arb. units)	$B(E2)^\dagger$ ($e^2 \cdot 10^{-49} \text{ cm}^4$)	$B(E2)^\dagger$ ($e^2 \cdot 10^{-49} \text{ cm}^4$)	$\frac{B(E2)^\dagger}{B(E2) \text{ S.P.}}$	Mean Lifetime (psec)	β_{20}
0	$1/2^-$					g.s.	
40	$7/2^+$						
93	$5/2^+, 7/2^+, 9/2^+$						
295	$3/2^-$	61.03	2.09	1.045	36	9.6	0.139
356	$5/2^-$	50.31	3.78	1.26	44	94	0.190
536	$3/2^\pm, 5/2^-, 5/2^+, 7/2^\pm$						
650	$3/2^\pm, 5/2^\pm, 7/2^-, 7/2^+$						
798							
843	$3/2^-, 5/2^-$	8.76	0.055	$3/2^- 0.028$ $5/2^- 0.018$	0.96, 0.64		0.023
877	$1/2^-, 3/2^-, 5/2^-, 7/2^-$	7.77	0.133	$5/2^- 0.044$	1.5		0.035
915	$5/2^-, 7/2^-, 9/2^-$	6.62	0.026	$5/2^- 0.009$	0.3		0.015
1102	$5/2^\pm, 7/2^\pm, 9/2^-$	3.17	0.010	$5/2^- 0.003$	0.1		0.010
1247	$5/2^\pm, 7/2^\pm, 9/2^-$	1.65	0.131	$5/2^- 0.044$	1.5		0.035

parities included in this table have been obtained by examining the branching ratios for γ -decay and on the assumption that the Coulomb excitation process proceeds via pure E2 excitation.

These results compare well with those of Sayer et al. [Sa 70]. A comparison of our ^{103}Rh data to that of Sayer et al. is given in table 7.3.3. The only major difference occurs for the $B(E2)\uparrow$ value of the 843 keV transition (847 keV to Sayer et al.) for which the Sayer et al. result is a factor of 10 larger than the present value. On this matter the following comments can be made. Our experiment was hampered by the presence of an 843 keV background γ -ray from the radioactive decay to ^{56}Fe previously mentioned. Also, as pointed out by Sayer [Sa 70], the 843 keV level is strongly excited by double E2 excitation with ^{16}O , possibly with the result that a first order perturbation analysis overestimates the $B(E2)$ value. It is considered, however, that the main reason for the overestimating was due to the difficulties encountered in estimating and extracting out the very large contribution from the β -decay.

7.4 STATES OF ^{103}Rh - DISCUSSION

The low-lying states in ^{103}Rh have been studied by a number of groups using both (p,p') and β -decay experiments. The β -decay work [Kn 52, Ra 55, Sa 55, Mu 65, Po 66, Ma 68] has been necessarily restricted by the small amount of energy available for β -decay from ^{103}Ru (750 keV) and for orbital electron capture in ^{103}Pd (560 keV). This β -decay work gives broad agreement for the first six excited states. The more recent work using γ -rays [Po 66, Ra 68] or internal conversion electrons [Ma 68] following β -decay of ^{103}Ru show that the 40 keV state has $J^\pi = 7/2^+$. The

Table 7.3.3

Comparison of Results for State in ^{103}Rh (Black et al. [Bl 69] and Sayer et al. [Sa 70])

Ex. State from (p,p')	Black, Caelli, Watson		Sayer, Temperly, Eccleshall	
	Ex State from C.E. using ^{16}O	$B(E2)^\dagger$ ($e^2 \cdot 10^{-50} \text{ cm}^4$)	Ex State from C.E. using ^4He	$B(E2)^\dagger$ ($e^2 \cdot 10^{-50} \text{ cm}^4$)
0	-		-	
40	-		-	
93	-		-	
295	295	20.9	295	21.8
356	356	37.8	357	39.2
536	-		-	
650	-		-	
798	-		-	
843	843	0.55	848	0.057
877	877	1.3	880	1.3
915	915	0.26	-	-
1102	1102	0.10	1107	0.16
1247	1247	1.31	-	-
1270	-		1277	0.99

evidence for the assignment is the long lifetime of the 40 keV state (57 min.) which is consistent with the γ -ray transition to ground being of E3 character. The 93 keV state has $J^\pi = 5/2^+$, $7/2^+$ or $9/2^+$ since [Ma 68] $\alpha_K = 1.84$ for the 53 keV transition from the 93 keV state to the 40 keV state. This α_K value is consistent with a pure M1 transition [Ro 58]. Coupled with this the absence of a β -branch to the 93 keV state from the ^{103}Ru ground state ($J^\pi = 5/2^+$) favours a $J^\pi = 9/2^+$ assignment for the 93 keV state.

The 295 and 356 keV states have been extensively studied using (p,p') and (d,d') reactions [Co 58, Co 61] and Coulomb excitation using protons, α -particles and ^{14}N ions [Mc 58, Th 67, Ko 64, Al 65, Sa 70] as well as β -decay [Po 66]. The $J^\pi = 3/2^-$ and $5/2^-$ assignments for these two states respectively have been obtained from measurements of angular distributions of γ -rays following Coulomb excitation [Ed 61, Sa 70]. The E2/M1 mixing ratio for the transition from the 295 keV state to the $J^\pi = 1/2^-$ ground state was found to be $\delta = (E2/M1)^{1/2} = -0.17$. The cascade/cross-over ratio for the decay of the 356 to 295 keV state was found to be 0.19 [Mc 58].

The 538 keV state and the 650 keV state have [Ma 68] J^π values of $(3/2, 5/2, 7/2)^\pm$. The log ft data from β -decay favour $J^\pi = 5/2^+$ for the 538 keV state and $J^\pi = 7/2^+$ for the 650 keV state. From a study of γ -rays from (p,p' γ), Thosar et al. [Th 67] suggest that the 650 keV state has positive parity. Rama Rao et al. [Ra 68] measured the lifetime of the 538 keV state and found it to be $\tau = (5.6 \pm 1.8) \times 10^{-11}$ sec. This result is said to be consistent with $J^\pi = 5/2^+$ for the state. These authors suggest that the 538 keV state (possibly $J^\pi = 5/2^+$) and the 650 keV state (possibly $J^\pi = 7/2^+$) arise through the coupling of a phonon to the 40 keV state.

Little evidence for the existence of higher excited states exists in the literature prior to the data reported herein. In summary, then, the existing evidence arises from studies of (p,p') and (d,d') experiments [Co 58, Co 61], Coulomb excitation with α -particles [Ko 64, Sa 70] and ^{14}N ions [Al 65] and a study of the reaction $^{103}\text{Rh}(p,p'\gamma)^{103}\text{Rh}^*$ using proton bombarding energies up to 4.5 MeV [Th 67]. The states shown in table 7.4.1 were obtained from the (d,d') and (p,p') work.

Table 7.4.1

High Excited States of ^{103}Rh
Found via (p,p') and (d,d') Reactions

(p,p') [Co 58]	(d,d') [Co 61]
870 keV	880 keV
1.32 MeV	1.27 MeV
2.04 MeV	1.48 MeV
	2.01 MeV
	2.10 MeV

The Coulomb excitation work using α -particles [Ko 64] reported two states at 840 keV ($J^\pi = 3/2^-$ or $5/2^-$) and 1.04 MeV ($J^\pi = 3/2^-$ or $5/2^-$). Alkhazov et al. [Al 65] reported states at 840 keV and 1.32 MeV which were observed in Coulomb excitation using ^{14}N ions at 45 MeV. The further α -particle Coulomb excitation work of Sayer et al. reported states at 848, 880, 920, 1107 and 1277 keV and a possible state at 804 keV. Angular distributions gave J^π values as follows: 880 keV, $J^\pi = 5/2^-$; 920 keV, J^π possibly $9/2^-$; 1107 keV, $J^\pi = 3/2^-$ or $5/2^-$; and 1277 keV, $J^\pi = 3/2^-$. Thosar et al. [Th 67] found evidence for states at 880, 1275, 1320 and 2040 keV from a study of the γ -rays from the reac-

tion $^{103}\text{Rh}(p,p'\gamma)^{103}\text{Rh}^*$.

The work reported in this thesis is in good agreement with that published. However, many new states at higher excitation energy have been identified. Angular distribution measurements on the 295 and 356 keV γ -rays from the states of the same energy gave J^π values of $3/2^-$ and $5/2^-$ as indicated by Stelson and McGowan [Mc 58] and Sayer et al. [Sa 70]. The 536 and 650 keV states were populated in (p,p') but not in Coulomb excitation. Above 650 keV eighteen more excited states have been identified up to an excitation energy of 2.105 MeV. There is some disagreement with Thosar et al. [Th 67] and Sayer et al. [Sa 70]. Both these groups report that the 880 keV has a three way γ -decay, and 880 keV γ -decay to ground, a 586 keV γ -decay to the 295 keV state and a 523 keV γ -decay to the 356 keV state. This 880 keV decay to ground was not seen in the work reported here. From the data of Sayer et al. [Sa 70] and assuming that the observed decays of the 880 keV total 100% of its decay, then the branching ratios of the state are as given in table 7.4.2. The ratio of the intensities of the 523 and 586 keV γ -rays is 1.30 ± 0.13 from the data of Sayer et al. [Sa 70].

Table 7.4.2

Decays of the 880 keV state [Sa 70]

Transition	γ -Energy (keV)	Branching Ratio (100% for all Observed Decays)
880 \rightarrow 356	523	$50 \pm 3\%$
880 \rightarrow 295	586	$38 \pm 2\%$
880 \rightarrow g.s.	880	$12 \pm 1\%$

This compares well with the ratio of intensities reported in the

experiment, as 0.90 ± 0.36 . In our experiment the ground state transition was immeasurably weak compared to either the 523 or 586 keV γ -rays.

7.5 STATES OF ^{107}Ag AND ^{109}Ag

7.5.1 ^{107}Ag

The states of ^{107}Ag and their γ -decay schemes have been well studied by a number of groups [Bl 67, Fo 67, Ro 69]. Black and Gruhle [Bl 67] studied these states with both Coulomb excitation using oxygen ions and β^+ -EC decay of ^{107}Cd . The data on the ^{107}Ag level scheme obtained by these techniques are shown in figure 7.5.1 [Bl 67]. The present data (see figure 7.5.2) support the level scheme of Black and Gruhle [Bl 67]. The $3/2^-$ and $5/2^-$ states at 325 and 423 keV were again strongly populated in the (p,p') experiment at all three angles of observation. The $3/2^-$ state at 788 keV was also seen. The next states observed in the data were then taken at 950 keV ($J^\pi = 5/2^-$, [Ro 69]) and 975 keV ($J^\pi = 7/2^-$ or $5/2^-$, [Bl 67]). As can be seen from figure 7.5.2 no evidence for a 922 keV state was found at any angle. The existence of this state had been confirmed by another group, Lark et al. [La 62a] who assigned it a J^π of $5/2^+$. This assignment is stated by Black and Gruhle to be consistent with their γ -decay scheme. The 950 keV state had been previously populated using the (p,p') reaction [Ro 66] and the (d,d') reaction [Co 61]. The 975 keV state was reported by Black and Gruhle in both β -decay and Coulomb excitation studies. Gamma-decay of the state via the 423 and 325 keV states was also reported by these authors. The γ -decay of the 950 keV state through these same levels was also studied by Robinson et al. [Ro 69]. From the present data the

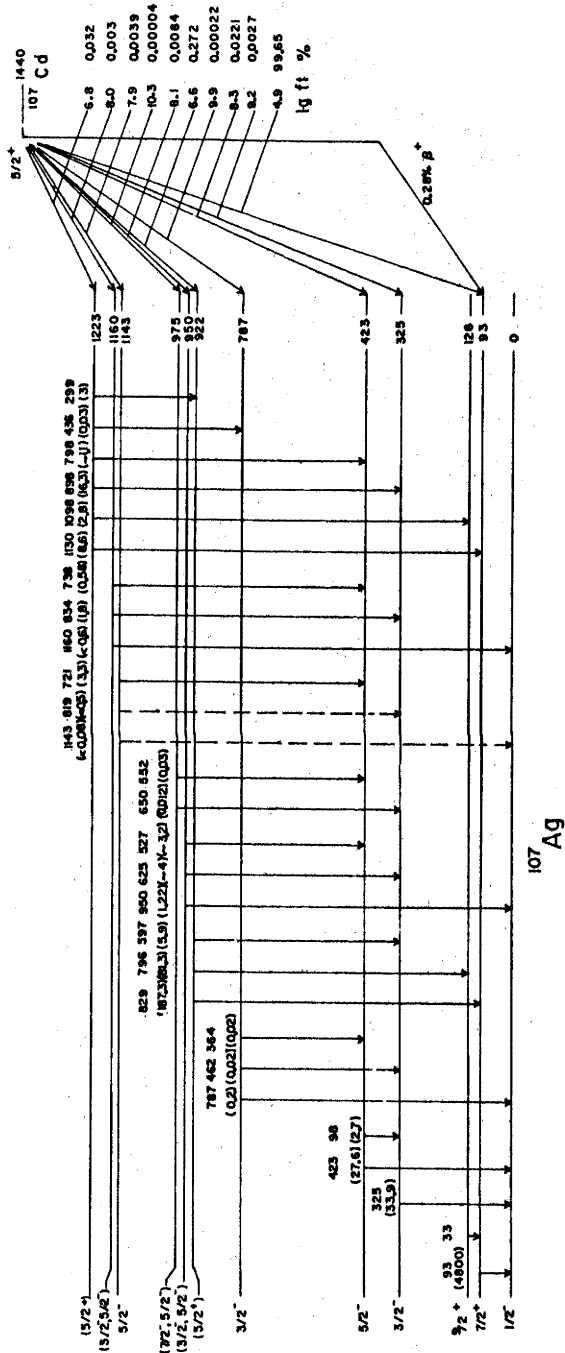


Figure 7.5.1: Excited states and decay scheme of ^{107}Ag from β -decay and Coulomb excitation measurements [Black and Gruhle, BI 67].

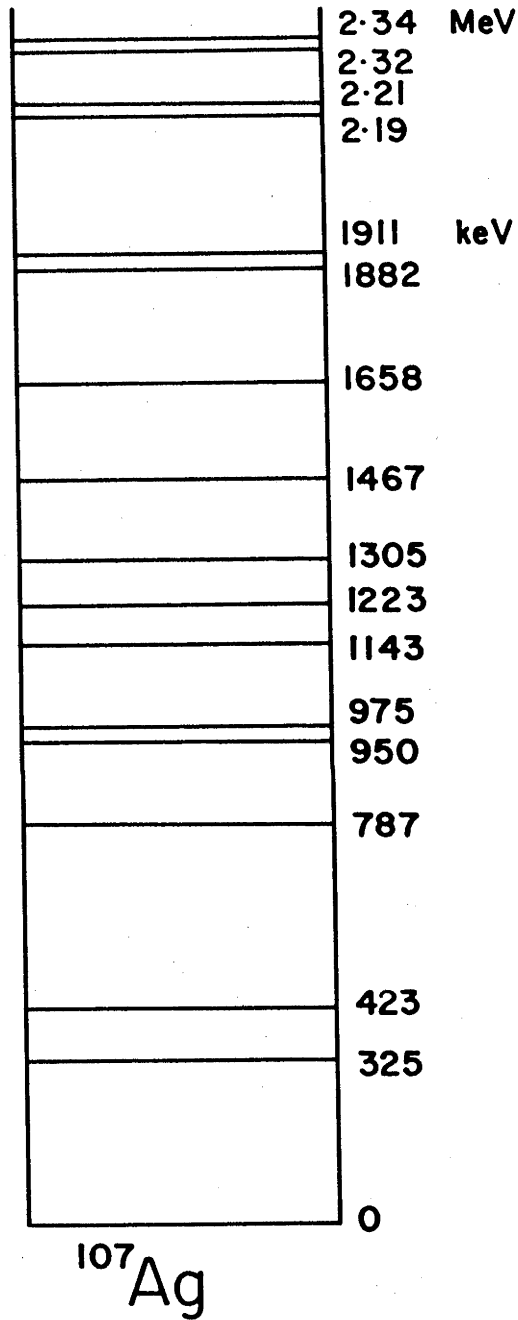


Figure 7.5.2: Excited states of ^{107}Ag from the reaction $^{107}\text{Ag}(p,p')^{107}\text{Ag}^*$.

existence of a state at 1070 keV is suggested. However, due to the poor statistics in this peak compared to background and since it is only observed at two angles, (it could have been obscured by the 160 peak at the third angle), it has not been included in a list of the identified excited states. The state at 1143 keV has been reported by other groups [Fo 67, Ro 69] and its existence is confirmed by the present work.

A peak is also seen at an excitation energy of 1223 keV. The peak appears with good statistics at all three angles studied, its relative intensity to the 1143 keV peak remaining the same at 120° and 140° . At 100° , the 1223 keV peak only appears as a shoulder on the side of the 160 peak. The state has not been reported by Ford et al. [Fo 67] nor by Robinson et al. [Ro 69] but it has been observed by Black and Gruhle [Bl 67] who also report its γ -decay through the first six excited states of ^{107}Ag .

The peak at 1305 keV appears weakly at all three angles of observation. Since, however, it has appeared at all angles of observation it is included in the list of levels. The 1467 keV peak appears strongly at $\theta = 140^\circ$ but is masked at both 100° and 120° by contaminant peaks. Robinson et al. [Ro 69] have already reported the existence of a state at 1470 keV. Our data support that observation. Beyond this excitation energy, the only known levels are from the work of Ford et al. [Fo 67] using the (p,p') reaction. Ford et al. report a state at 1.50 MeV which possibly corresponds to the present level at 1467 keV. The next state at 1658 keV confirms the observation of a level at 1.66 MeV by Ford et al. However, no evidence for the 1.57 MeV state reported by that group was obtained. The possibility of three states at 1845, 1882 and 1911 keV is suggested by the present data. The existence

of the 1845 keV state was rejected because of poor statistics while those at 1882 and 1911 keV appear to be populated at all three angles. The 1882 keV state has not been previously reported but the 1911 keV state has been reported by Ford et al. at 1.92 MeV. The states at 2.19 MeV and 2.21 MeV are clearly defined, the 2.19 MeV state agreeing with Ford et al. The levels at 2.32 and 2.34 MeV were identified at two angles, being obscured by the ^{12}C contaminant peak at 140° . The energy level diagram summarising these data is given in figure 7.5.2. To conclude it appears that a possible 8 new states have been identified up to an excitation energy of 2.34 MeV. The existence of a state at 975 keV has been confirmed. This is the first set of data which separates the 950 and 975 keV states due to sufficiently high resolution (p,p') study using the Buechner magnet. Four higher excitation states reported by Ford et al. have also been reported.

7.5.2 ^{109}Ag

As was the case with ^{107}Ag , the states of ^{109}Ag have been extensively studied by a number of groups [Bl 67, Fo 70, Gr 68, Ro 69]. Black and Gruhle [Bl 67], as part of their joint study of ^{107}Ag and ^{109}Ag , populated states in ^{109}Ag via Coulomb excitation using oxygen ions. Their level scheme is contained in figure

7.5.3. Robinson et al. [Ro 69] again populated states in ^{109}Ag using Coulomb excitation by alpha particles. Graeffe and Gordon [Gr 68] populated low-lying states in ^{109}Ag via β - and γ -decay of ^{109}Pd . Their level scheme is also given in figure 7.5.3 along with that of Ford et al. [Fo 70] obtained by the reaction $^{109}\text{Ag}(p,p')^{109}\text{Ag}^*$. Agreement exists between all these groups, on the states up to 912 keV, with one exception. Black and Gruhle [Bl 67] report the possible existence of a level at 728 keV from

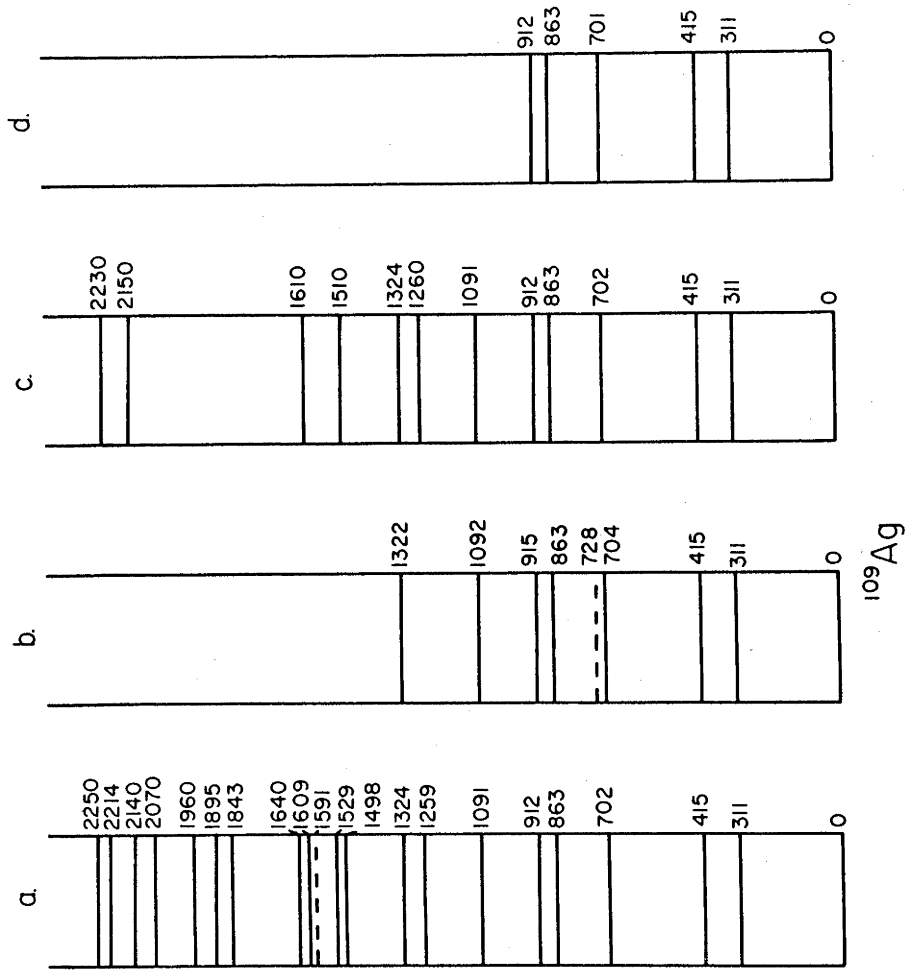


Figure 7.5.3: Excited states of ^{109}Ag as determined by, (a) present work, (b) Black and Gruhle [B1 67], (c) Ford et al. [Fo 70] and (d) Graeffe and Gordon [Gr 68].

the observation of a 728 keV γ -ray in their Coulomb excitation spectrum. They suggest support from previous studies by Starner [St 59] and Brandhorst and Cobble [Br 62]. No evidence for this state was found in the data reported here nor in the recent studies mentioned above. A summary of levels up to an excitation energy of 912 keV is shown in table 7.5.1. The next three excited states at

Table 7.5.1
States of ^{109}Ag to 912 keV

Current Work	Ex (keV)			J^π
	B1 67	Fo 70	Gr 67	
0	0	0	0	$1/2^-$
311	311	311	311	$3/2^-$
415	415	415	415	$5/2^-$
702	704 (728)	702	701	$3/2^-$
863	863	863	863	$5/2^-$
912	915	912	912	$(5/2^-, 7/2^-)$

1091, 1259 and 1324 keV are in good agreement with the level scheme given by Ford et al. [Fo 70]. Black and Gruhle [B1 67] confirm the existence of the states at 1092 and 1322 keV but did not observe a state at 1259 keV. Above the 1324 keV state, a total of 12 possible levels has been deduced from our data. Of these, however, the level at 1.591 MeV is very tentative since evidence for it is based on one angle of observation. Of these twelve states it is likely that four have already been reported by Ford et al. [Fo 70] at 1.51, 1.61, 2.15 and 2.23 MeV. These twelve states are shown in table 7.5.2. In summary, the study of the reaction $^{109}\text{Ag}(p,p')^{109}\text{Ag}^*$ has contributed knowledge of as many as 8 new excited states of ^{109}Ag

Table 7.5.2
States of ^{109}Ag Above 912 keV

Ex (keV)			J^π [Fo 70]
Current Work	B1 67	Fo 70	
1091	1092	1091	$(7/2^-)$
1259		~ 1260	$(1/2^-)$
1324	1322	1324	
1498			
1524		~ 1510	$(9/2^-)$
(1591)			
1609		~ 1610	
~ 1640			
1843			
1895			
1960			
2078			
~ 2140		~ 2150	$(7/2^+)$
2214			
2251		~ 2230	$(5/2^+)$

above 1.324 MeV and has supported the observation of four higher states in ^{109}Ag made by Ford et al. [Fo 70].

7.6 INTERPRETATION OF ^{103}Rh DATA

7.6.1 Positive Parity States

The low-lying positive parity states in ^{103}Rh are at excitation energies of 40 keV, 93 keV, 538 keV, 650 keV and possibly 798 keV. The ground state of ^{103}Rh ($J^\pi = 1/2^-$) has the odd-proton configuration $(1g_{9/2})^{-4} (2p_{1/2})^{-1}$. These low-lying positive parity states can be expected to be formed by different coupling in the configuration $(g_{9/2})^{-5}$. The measured lifetime of the 538 keV state, [$\tau = (5.6 \pm 1.8) \times 10^{-11}$ sec], however, is suggested

by Rama Rao et al. [Ra 68] to be inconsistent with the assumption of either pure shell model configurations or mixing of different configurations. They consider that in order to explain their observed E2 enhancement (86 ± 29) for the γ -decay of the 538 keV state to the 40 keV state, the 538 keV state should include some collective excitation. The enhancement calculated assumed pure E2 nature for the 498 keV transition. Thus any conclusion depends critically upon a measurement of the E2/M1 mixing ratio for the transition.

7.6.2 Negative Parity States

General rules for weak coupling have been derived by De Shalit [Sh 61], Lawson and Uretzky [La 57] and Kisslinger and Sorensen [Ki 63]. For the case of odd-proton vibrational core nuclei with no permanent deformation, the weak coupling model contains the five features outlined in section 5.1. Since ^{103}Rh has a ground state spin and parity given by $J^\pi = 1/2^- (p_{1/2})$, and if the weak coupling model is applicable, then for each state of the even-even core, there should be a multiplet of states in ^{103}Rh consisting of two members each. At low excitation energy the level structure would thus be expected to be simple. Thus since we have two close states at 295 and 356 keV in ^{103}Rh we could reasonably expect a weak coupling between the odd particle (or particle hole) and the even-even core [Sh 61, Al 56]. The nucleus should then show core-excitation spectra. Figure 7.6.1 shows the energy levels of ^{103}Rh , excited by Coulomb excitation, compared to the doubly even nuclei ^{102}Ru and ^{104}Pd [Mc 68a]. Table 7.6.1 shows the $B(E2)_\downarrow$ values for the first excited 2^+ states of the doubly even nuclei [St 65] and the $B(E2)_\downarrow$ values for the 295 and 356 keV states of ^{103}Rh . From the weak coupling model the first two nega-

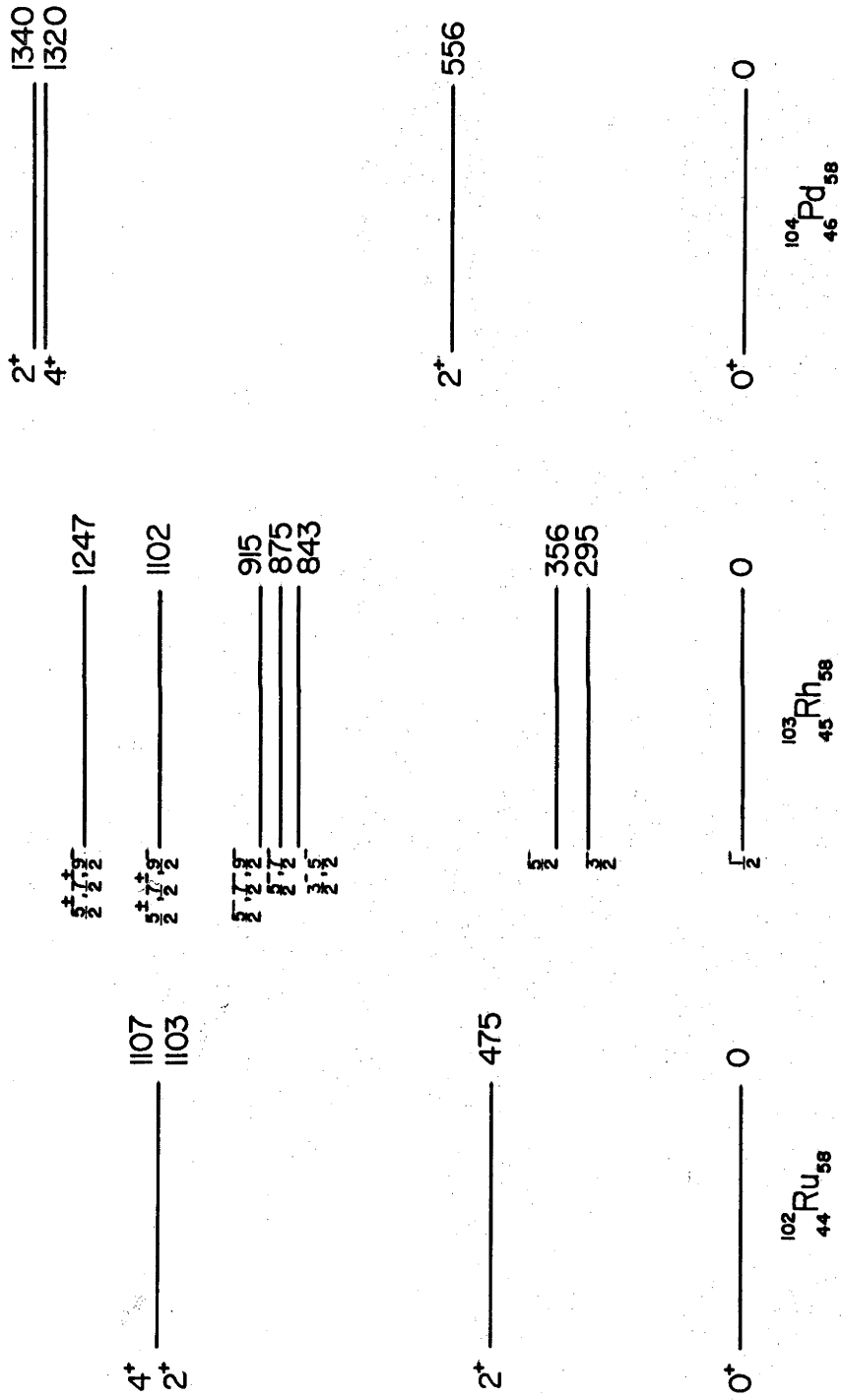


Figure 7.6.1: Energy levels of ^{103}Rh compared to those of the doubly even nuclei ^{102}Ru and ^{104}Pd .

tive parity states of ^{103}Rh are expected to have $J^\pi = 3/2^-$ and $5/2^-$ which is in accord with experimental observation. Also, as can be seen from table 7.6.1 there is very good agreement in $B(E2)_{\downarrow}$ values between those for the 295 and 356 keV states of ^{103}Rh and those for the first $J^\pi = 2^+$ states of ^{104}Ru and ^{104}Pd . The $B(E2)$ values are, moreover, enhanced over the single particle values by a factor of approximately 40 which is typical for collective vibrational states. The centre of gravity, however, of these two states in ^{103}Rh is lower than the excitation energy of either of the first 2^+ states in the neighbouring nuclei. A similar situation was found for the ^{107}Ag and ^{109}Ag isotopes [Bl 67 and section 7.7 of this thesis].

Table 7.6.1

Comparison between $B(E2)_{\downarrow}$ Values for
 ^{103}Rh and for Neighbouring Nuclei

	$^{102}_{44}\text{Ru}$	$^{103}_{45}\text{Rh}$		$^{104}_{46}\text{Pd}$
Energy (keV)	475	295	356	556
$B(E2)$ ($e^2 \cdot 10^{-49} \text{ cm}^{-4}$)	1.52 ± 0.1	1.05 ± 0.1	1.26 ± 0.1	1.10 ± 0.1

Further evidence for the proposition that the two low-lying states are built upon the lowest 2^+ states of the neighbouring even-even nuclei can be derived from the cross sections for excitation of the states by the (p,p') reaction. If the (p,p') reaction is assumed to be a direct reaction then the cross section [St 65] for the process is proportional to β_2^p . Thus the ratio of cross sections for excitation of the 295 and 356 keV states should be proportional to $2J + 1$ if the states belong to the same ($J_c = 2$)

multiplet. An experimental value of 1.42 for this ratio compares favourably with the expected theoretical value of 1.5 [B1 69].

The higher excitation negative-parity states observed in the (p,p') reaction and Coulomb excitation γ -decay preferentially through the 295 - 356 keV one-phonon doublet rather than to the ground state (section 5.1). This agrees with the predictions of the weak coupling model. The model predicts that, at approximately twice the energy of the 295 - 356 keV doublet, there should be four states formed by the coupling of the odd proton to the two-phonon core states with $J^\pi = 2^+$ and 4^+ . It is to be noted here that the 0^+ member of the vibrational triplet does not appear to be in the same energy region, although the 2^+ and 4^+ members are nearly degenerate. Only the 843 keV state shows a weak ground state transition. Since the 877 and 915 keV states do not show a ground state transition in the Coulomb excitation studies, population must occur by double Coulomb excitation. The relatively high intensity of the γ -ray transitions between these three states at 843, 875 and 915 keV and the 295 - 356 keV doublet indicates that the B(E2) values for these transitions must be strongly enhanced over single particle values.

The J^π values for the two-phonon states expected in ^{103}Rh must be $J^\pi = 3/2^-, 5/2^-$ ($J_c = 2^+$) and $J^\pi = 7/2^-, 9/2^-$ ($J_c = 4^+$). Restrictions placed on the J^π values are consistent with these values. If it is assumed that the 843, 875 and 915 keV states are members of the predicted quartet, then the fourth member could be the suspected 798 keV state. The Coulomb excitation data show that the state does not decay to either the ground state decay or to the 356 keV state. However, a 503 keV γ -ray transition to the 295 keV state is possible but would be masked in both the singles and coin-

vidence data by the very intense 511 keV annihilation γ -rays.

7.7 INTERPRETATION OF ^{107}Ag AND ^{109}Ag DATA

The cases of ^{107}Ag and ^{109}Ag were examined by de-Shalit [Sh 61]. These nuclei have ground state J^π values of $1/2^-$ and, as was outlined in the previous section, a doublet consisting of a $3/2^-$ and $5/2^-$ state is expected at low excitation. These conditions are illustrated well in figure 16 of the paper by Black and Gruhle [Bl 67] which is reproduced as figure 7.7.1 but it has been updated by inclusion of the data of Ford et al. [Fo 70] and the data reported herein. The doublet centres of gravity are at ~ 383 keV for ^{107}Ag and ~ 373 keV for ^{109}Ag . These compare reasonably well with the 2^+ excitations in ^{109}Pd at 512 keV, in ^{108}Cd at 633 keV, in ^{108}Pd at 434 keV and in ^{110}Cd at 658 keV. Again, as was reported by de-Shalit [Sh 61] the E2 transition probabilities for the γ -decay of these states' γ -decay to ground fall within the range of values obtained for the neighbouring even-even nuclei, as predicted by the weak-coupling model (section 5.1).

The data on ^{107}Ag and ^{109}Ag reported herein also support well the contention of Ford et al. [Fo 70] that the nature of the states around 1 MeV, which could arise from coupling to the two-quadrupole triplet states, is still uncertain. Coupling a $2p_{1/2}$ particle to spins of 0^+ , 2^+ and 4^+ should give five states. However, in the data reported herein as many as 11 states have been observed in the region. Possible configurations for a number of these states are discussed both by Black and Gruhle [Bl 67] and Ford et al. [Fo 70] but no consistent interpretation of the additional states can be given.

From the work reported in this thesis and the increased

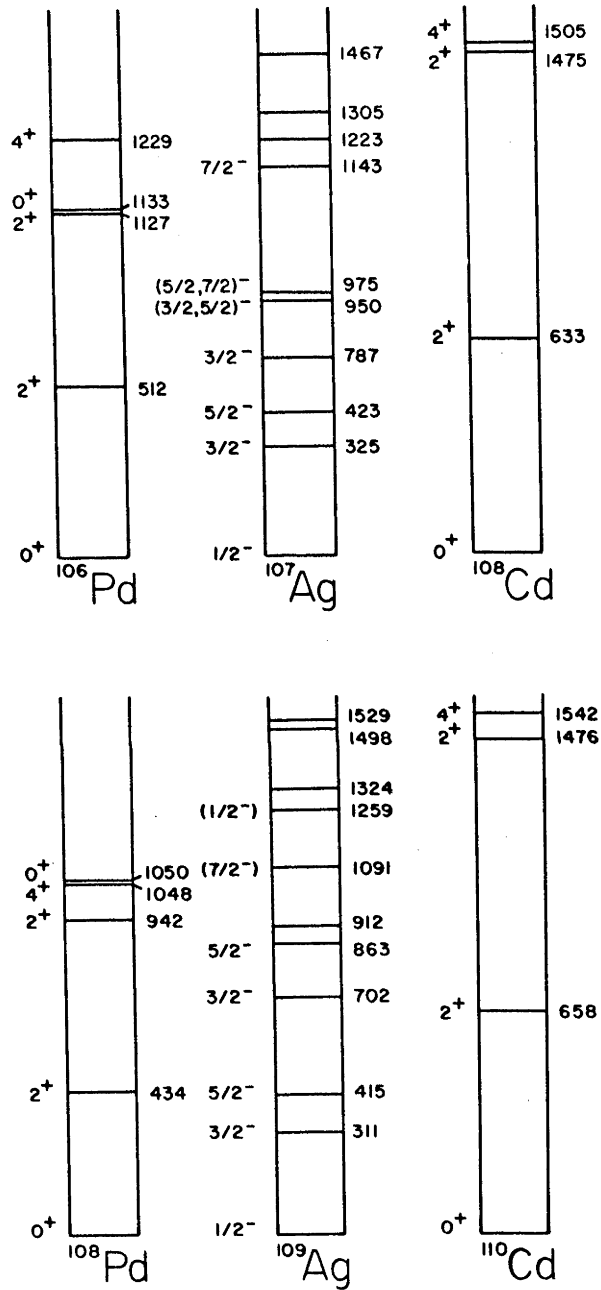


Figure 7.7.1: Comparison of levels in ^{106}Pd - ^{107}Ag - ^{108}Cd and ^{108}Pd - ^{109}Ag - ^{110}Cd ; (updated from figure 16 of the paper by Black and Gruhle [B1 67]).

number of studies on odd mass nuclei in the mass 100 region it has been possible to make the evaluation [Fo 70] that the weak-coupling model involving a single odd-particle in a single orbital could be too simple. This conclusion can only be arrived at after systematic studies of the low-lying states of a large number of odd-mass nuclei. Experimental work performed over the last ten years has led to the discovery of many more excited states in these nuclei up to around 2 MeV excitation. This represents a larger base of information than that present when the model was originally proposed besides providing a more detailed knowledge of higher excited states. The fact that the model applies well to the one-phonon doublets in ^{107}Ag and ^{109}Ag , for example, is again borne out well with new measurements of the $B(E2)\downarrow$ values for the first 2^+ excited states of ^{108}Cd and ^{110}Cd by Milner et al. [Mi 69]. These values, as shown in table 7.7.1 compare well with those quoted by Black and Gruhle [B1 67].

Table 7.7.1

$B(E2)\downarrow$ Values for ^{107}Ag and ^{109}Ag
Compared to ^{108}Cd and ^{110}Cd

Nucleus	Transition i (keV) \rightarrow f	$B(E2)\downarrow$ ($e^2 \cdot 10^{-49} \text{ cm}^4$)	Reference
^{107}Ag	325 \rightarrow g.s.	1.095 ± 0.075	B1 67
	423 \rightarrow g.s.	0.94 ± 0.08	B1 67
^{108}Cd	633.2 \rightarrow g.s.	0.884 ± 0.035	Mi 69
^{109}Ag	311 \rightarrow g.s.	1.25 ± 0.09	B1 67
	415 \rightarrow g.s.	1.21 ± 0.10	B1 67
^{110}Cd	657.7 \rightarrow g.s.	0.934 ± 0.037	Mi 69

Although, then, the weak coupling model appears to behave well for low excitation energies (in particular for the one-phonon states) in order to use it to explain the data obtained in these odd-mass nuclei at higher excitations additional refinements, as suggested by Ford et al. [Fo 70] seem to be needed. The possibility that the odd-mass isotopes of silver, as well as ^{103}Rh , are not non-deformed but do have static deformations and so a rotational structure, has been considered by Schick and Talbert [Sc 69]. These authors offer the suggestion that the odd-parity excited levels of the odd-mass silver isotopes may constitute at $K = 1/2$ rotational band according to the Nilsson model for deformed nuclei. However, as they point out, even though it is possible to explain some measurements on these odd-mass isotopes in this manner, e.g. the $B(E2)$ values for Coulomb excitation of the first $3/2^-$ and $5/2^-$ levels [Bl 67], a more thorough examination of these ideas depends upon more definite knowledge of spins and transition multipolarities over a wider range of odd-mass nuclei. Such systematic studies, as has already been stated, led to the proposition of the weak-coupling model and further such studies are needed if refinements to it are to be made.

REFERENCES

- Ad 67 E.G. Adelberger and A.B. McDonald, Phys. Lett. 24B (1967) 270, and erratum, Phys. Lett. 24B (1967) 618.
- Ad 69 E.G. Adelberger, A.B. McDonald and C. Barnes, Nucl. Phys. A124 (1969) 49.
- Ad 70 E.G. Adelberger, A.V. Nero and A.B. McDonald, to be published.
- Aj 68 F. Ajzenberg-Selove and T. Lauritsen, Nucl. Phys. A114 (1968) 1.
- Al 56 K. Alder, A. Bohr, T. Huus, B. Mottelson and A. Winther, Rev. Mod. Phys. 28 (1956) 432.
- Al 65 D.G. Alkhozov et al., Bull. Acad. Sci. USSR (Phys. Ser.) 28 (1965) 1559.
- Al 66 K. Alder and A. Winther, Coulomb Excitation, A Collection of Reprints with an Introductory Review, Academic Press, 1966.
- An 62 J.D. Anderson, C. Wong and J.W. McClure, Phys. Rev. 126 (1962) 2170.
- Ba 66 F.C. Barger, Nucl. Phys. 83 (1966) 418.
- Ba 69 F.C. Barker and N. Kumar, Phys. Lett. 30B (1969) 103.
- Ba 70 C.A. Barnes, D.C. Hensley and P.H. Nettles, private communication.
- Bi 65 L.C. Biedenharn and P.J. Brussard, Coulomb Excitation (Clarendon Press, Oxford, 1965).
- Bl 67 J.L. Black and W. Gruhle, Nucl. Phys. A93 (1967) 1.
- Bl 67a R. Bloch, R.E. Pixley and P. Tricol, Phys. Lett. 25B (1967) 215.
- Bl 69 J.L. Black, W.J. Caelli and R.B. Watson, Nucl. Phys. A125 (1969) 545.
- Bl 70 J.L. Black, W.J. Caelli and R.B. Watson, Phys. Rev. Lett. 25 (1970) 877.
- Bo 65 W. Booth and I.S. Grant, Nucl. Phys. 63 (1965) 481.
- Br 56 C.P. Browne and W.W. Buechner, Rev. Sci. Inst. 27 (1956) 899.
- Br 62 H.W. Brandhorst and J.W. Cobble, Phys. Rev. 125 (1962) 1323.

- Bu 63 W.E. Burcham, Nuclear Physics - An Introduction (Longmans, London, 1963), pg. 432.
- Ca 69 W.J. Caelli, D.F. Hebbard, W.J. Lamberth and T.R. Ophel, Proceedings of Fourth Australian Computer Conference, 1969, pg. 557.
- Ce 64 J. Cerny, R. Pehl and G. Garvey, Phys. Lett. 12 (1964) 234.
- Ce 66 J. Cerny, S. Cosper, G. Butler, R. Pehl, F. Goulding, D. Landis and C. Détraz, Phys. Rev. Lett. 16 (1966) 469.
- Ce 68 J. Cerny, Ann. Rev. Nucl. Sci. 18 (1968) 27.
- Ch 32 J. Chadwick, Proc. Roy. Soc. A136 (1932) 692.
- Cl 67 G.J. Clark, D.J. Sullivan and P.B. Treacy, Nucl. Phys. A98 (1967) 473.
- Co 58 B.L. Cohen and A.G. Rubin, Phys. Rev. 111 (1958) 1568.
- Co 61 B.L. Cohen and R.E. Price, Phys. Rev. 123 (1961) 283.
- Co 69 W.R. Coker and C.F. Moore, Physics Today 22 (1969) 53.
- Da 68 J.P. Davidson, Collective Models of the Nucleus (Academic Press, 1968).
- De 64 S. De Benedetti, Nuclear Interactions (Wiley, New York, 1964).
- Ed 61 W. Edwards and F. Boehm, Phys. Rev. 121 (1961) 1499.
- Fo 48 W. Fowler, C. Lauritsen and T. Lauritsen, Rev. Mod. Phys. 20 (1948) 236.
- Fo 64 J.D. Fox, C.F. Moore and D. Robson, Phys. Rev. Lett. 12 (1964) 198.
- Fo 67 J.L.C. Ford, C. Wong, T. Tamura, R.L. Robinson and P.H. Stelson, Phys. Rev. 158 (1967) 1194.
- Fo 70 J.L.C. Ford, R.L. Robinson, P.H. Stelson, T. Tamura and C. Wong, Nucl. Phys. A142 (1970) 525.
- Ga 59 E.L. Garwin, Phys. Rev. 114 (1959) 143.
- Ga 64 G.T. Garvey, J. Cerny and R.H. Pehl, Phys. Rev. Lett. 12 (1964) 726.
- Ga 68 G.T. Garvey and J. Cerny, quoted in J. Cerny, UCRL Report 18106 (1968) and Ann. Rev. Nucl. Sci. 18 (1968) 27.
- Ga 69a G.T. Garvey, in Proceedings of the Second Conference on Isospin in Nuclear Physics, 1969, edited by J. Anderson, S. Bloom, J. Cerny and W. True (Academic Press, New York, 1969).
- Ga 69b G.T. Garvey, Ann. Rev. Nucl. Sci. 19 (1969) 433.

- Gr 68 G. Graeffe and G.E. Gordon, Nucl. Phys. A107 (1968) 67.
- Ha 68 W.D. Harrison, A.R. Barnett, C. Bergman and D. Weisser, Bull. Am. Phys. Soc. 13 (1968) 1387.
- Ha 68a R.S. Hager and E.C. Seltzer, Nuclear Data 4A (1968) 1.
- Ha 69 S.S. Hanna, in Proceedings of the Second Conference on Isospin in Nuclear Physics, 1969, edited by J. Anderson, S. Bloom, J. Cerny and W. True (Academic Press, New York, 1969).
- Ha 70a S.S. Hanna, in Isospin in Nuclear Physics, edited by D.H. Wilkinson (North Holland, Amsterdam, 1970).
- Ha 70b J.C. Hardy, H. Brunnader and J. Cerny, Phys. Rev. C. 1 (1970) 561.
- He 68 D. Heikkinen, H. Kuan, K. Snover, F. Riess and S. Hanna, Bull. Am. Phys. Soc. 13 (1968) 884.
- Ja 69 J. Jänecke, Nucl. Phys. A128 (1969) 632.
- Ja 70 J. Jänecke, in Isospin in Nuclear Physics, edited by D.H. Wilkinson (North Holland, Amsterdam, 1970).
- Jo 70 H.P. Jolly and L.B. Hubbard, Phys. Rev. C. 1 (1970) 1979.
- Ki 63 L.S. Kisslinger and R.A. Sorensen, Rev. Mod. Phys. 35 (1963) 853.
- Ki 66 F. Kingston, R. Griffiths, A. Johnston, W. Gibson and E. McClatchie, Phys. Lett. 22 (1966) 458.
- Kn 52 A.W. Knudsen, Phys. Rev. 86 (1952) 571.
- Ko 64 S. Kopta, H. Niewodniczanski and B. Pudlowska, Acta. Phys. Polon. 26 (1964) 1133.
- Ku 67 H. Kuan, D. Heikkinen, K. Snover, F. Riess and S. Hanna, Phys. Lett. 25B (1967) 217.
- Ku 68 H. Kuan, F. Riess, K. Snover, D. Heikkinen, D. Healey and S. Hanna, Bull. Am. Phys. Soc. 13 (1968) 884.
- La 57 R.D. Lawson and J.L. Uretzky, Phys. Rev. 108 (1957) 1300.
- La 62 A.M. Lane and J.M. Soper, Nucl. Phys. 35 (1962) 676.
- La 62a N.L. Lark, P.F.A. Goudsmit, J.F.W. Jansen, J.E.J. Oberski and A.H. Wapstra, Nucl. Phys. 35 (1962) 582.
- La 66 T. Lauritsen and F. Ajzenberg-Selove, Nucl. Phys. 78 (1966) 1.
- Le 66 H.P. Leenhouts and P.M. Endt, Physica 32 (1966) 322.
- Le 67 H.P. Leenhouts, Physica 35 (1967) 290.

- Le 68 G. Lentz and D. Bernard, Bull. Am. Phys. Soc. 13 (1968) 673.
- Le 69 G. Lentz, M. Elton and D. Wilkins, Bull. Am. Phys. Soc. 14 (1969) 548.
- Ma 68 J.C. Manthuruthil, H.J. Hennecke and C.R. Cothorn, Phys. Rev. 165 (1968) 1363.
- Mc 58 F.K. McGowan and P.H. Stelson, Phys. Rev. 109 (1958) 901.
- Mc 67 R. McGrath, S. Cospers and J. Cerny, Phys. Rev. Lett. 18 (1967) 243.
- Mc 68 R. McGrath, J. Hardy and J. Cerny, Phys. Lett. 27B (1968) 443.
- Mc 68a F.K. McGowan, R.L. Robinson, P.H. Stelson and W.T. Milner, Nucl. Phys. A113 (1968) 529.
- Mc 69 R.L. McGrath, in Proceedings of the Second Conference on Isospin in Nuclear Physics, 1969, edited by J. Anderson, S. Bloom, J. Cerny and W. True (Academic Press, New York, 1969).
- Mc 70 R.L. McGrath, J. Cerny, J.C. Hardy, G. Goth and A. Arima, Phys. Rev. C. 1 (1970) 184.
- Mi 69 W.T. Milner, F.K. McGowan, P.H. Stelson, R.L. Robinson and R.O. Sayer, Nucl. Phys. A129 (1969) 687.
- Mu 65 A. Mukerji, D.N. McNelis and J.W. Kane, Jr., Nucl. Phys. 67 (1965) 466.
- Ne 69 J.O. Newton, Progress in Nuclear Physics, Vol. III, edited by D.M. Brink and J.H. Mulvey, pg. 53.
- No 63 L.C. Northcliffe, Ann. Rev. Nucl. Sci. 13 (1963) 67.
- Po 66 V.R. Potnis, E.B. Nieschmidt, C.E. Mandeville, L.D. Ellsworth and G.P. Agin, Phys. Rev. 146 (1966) 883.
- Po 70 D.L. Powell, Ph.D. Thesis, Australian National University, Canberra, Australia, 1970.
- Ra 55 B. de Raad et al., Physica 20 (1955) 1278.
- Ra 68 M.T. Rama Rao, V.V. Ramamurty and V. Lakshminarayana, Phys. Rev. 168 (1968) 1406.
- Ri 67 F. Riess, W.J. O'Connell, D.W. Heikkinen, H.M. Kuan and S.S. Hanna, Phys. Rev. Lett. 19 (1967) 217.
- Ro 58 M.E. Rose, Internal Conversion Coefficients (North Holland Publ. Co., Amsterdam, 1958).
- Ro 66 R.L. Robinson, J.L.C. Ford and P.H. Stelson, Bull. Am. Phys. Soc. 11 (1966) 119.

- Ro 66a D. Robson, *Ann. Rev. Nucl. Sci.* 16 (1966) 119.
- Ro 69 R.L. Robinson, F.K. McGowan, P.H. Stelson, W.T. Milner and R.O. Sayer, *Nucl. Phys.* A123 (1969) 193.
- Sa 55 B. Saraf, *Phys. Rev.* 97 (1955) 715.
- Sa 70 R.O. Sayer, J.K. Temperley and D. Eccleshall, *Bull. Am. Phys. Soc.* 15 (1970) 100, and private communication.
- Sc 66 E. Scarr, M.Sc. Thesis, Australian National University, Canberra, Australia, 1966.
- Sc 69 W.C. Schick, Jr. and W.L. Talbert, Jr., *Nucl. Phys.* A128 (1969) 353.
- Sh 61 A. de-Shalit, *Phys. Rev.* 122 (1961) 1530.
- Sn 69a K.A. Snover, Ph.D. Thesis, Stanford University, Stanford, California, 1969.
- Sn 69b K.A. Snover, D. Heikkinen, F. Riess, H. Kuan and S. Hanna, *Phys. Rev. Lett.* 22 (1969) 239.
- St 59 J.W. Starner, *Bull. Am. Phys. Soc.* 4 (1959) 99.
- St 65 P.H. Stelson and L. Grodzins, *Nuclear Data* 1A (1965) 21.
- Te 70 G.M. Temmer, in *Isospin in Nuclear Physics*, edited by D.H. Wilkinson (North Holland, Amsterdam, 1970).
- Th 67 B.V. Thosar, R.P. Sharma, K.G. Prasad and V.R. Pandharipande, *Proc. Int. Conf. on Nuclear Structure, Japan, 1967*, pg. 108.
- Th 69 T. Thwaites, P. Kupferman and S. Slack, *Bull. Am. Phys. Soc.* 14 (1969) 566.
- Wa 70 E.K. Warburton and J. Weneser, in *Isospin in Nuclear Physics*, edited by D.H. Wilkinson (North Holland, Amsterdam, 1970).
- Wi 37 E.P. Wigner, *Phys. Rev.* 51 (1937) 106.
- Wi 70 D.H. Wilkinson, in *Isospin in Nuclear Physics*, edited by D.H. Wilkinson (North Holland, Amsterdam, 1970).

Page	Line	
4	2 f.b.	"dependent" to "independent"
5	bottom	add after "summarises this" , " ; (Ψ is the resulting wave function);"
5	10 f.t.	change "operator, i.e. t_3 ," to "operator, i.e. T_3 ,"
6	top	change " $\Psi_0(T)$ " to " $\Psi(T)$ "
7	7 f.t.	change "(14)" to " (13) "
8	6 f.b.	change "have an equivalent Q" to "have a Q"
12	6 f.b.	add after "radiative capture reactions, " , " for the population of $T = 1$ and higher states,"
16	Table 1.4.1	add to caption "Excitation energies are given in MeV."
23	9 f.b.	change "a uninformed" to "an uninformed"
24	12 f.t.	change "Particle proton" to "Partial proton"
	13 f.t.	add after "given." , "in Temmer's table."
Fig. 2.5.2.,	caption	add after " $T = 2$ state." , "Excitation energies are in MeV. J^π and T values are given to the right of each state."
28	2 f.t.	change " $E_p = 2.675$ MeV" to " $E_p = 3.675$ MeV "
30	10 f.b.	change "1.033 MeV" to "10.33 MeV"
Fig. 2.5.6,	caption	add after "and ^{40}Ca ." , "All excitation energies are in MeV. J^π and T values are given to the right of each state. Energies of $T = 1$ states are given in fig. 2.5.2. "
36	19 f.t.	change " $^{24}\text{Mg} (p,t) ^{24}\text{Mg}$ " to " $^{26}\text{Mg} (p,t) ^{24}\text{Mg}$ "
Fig. 3.3.2,3.3.3		add to x and y axes, "CHANNEL" and "COUNTS PER CHANNEL" respectively.

<u>Page</u>	<u>Line</u>	
Fig. 3.3.4,	caption	change "Abbreviation are as" to "Abbreviations are as"
Fig. 3.3.5,	caption	add to caption after "2.5 ± 1 keV.", "Full lines are added to guide the eye."
Fig. 3.3.6,	caption	add after "in each case.", "Full lines are added to guide the eye."
57	6 f.t.	change " ¹² Ne." to " ¹² Be."
Fig. 4.1.1,	caption	add after "for ¹² C.", "Excitation energies are in MeV."
Fig. 4.3.1,	4.3.2,	add to x and y axes, "CHANNEL" and
	4.3.3	"COUNTS PER CHANNEL"
60	top	change "4.3.1" to "4.3.4"
60	12 f.b.	change "could be affected" to "could be successfully effected"
60	4 f.b.	change "small $\Gamma_{\gamma 1}/\Gamma$ " to " $\Gamma_{\gamma 1}$ "
60	2 f.b.	change "5 ± 8%" to "5 ^{+8%} / _{-5%} "
63	7 f.t.	change "= 1/3000," to "= 1/5000,"
65	13 f.b.	change "the fact that" to "the prediction that"
Fig. 5.3.1,	5.3.2,	add to x-axis label, "IN M.M."
	5.4.1,	
	5.4.2	
75	9 f.t.	change "Coulomb excitation cross section" to "Coulomb excitation yield"
76	15 f.t.	change "40 cm ³ " to "20 cm ³ "
Fig. 6.2.1		add to x and y axes, "CHANNEL" and "COUNTS PER CHANNEL"
Fig. 6.3.3		add to vertical axis scale "x 10 ⁵ "
79	10 f.t.	change "spectra were accumulated" to "spectra was accumulated"
Fig. 7.1.1		add to the top of each list of excitation energies, "E _x (MeV)"

<u>Page</u>	<u>Line</u>	
Fig. 7.1.1		place parentheses around the 1650 state, i.e. (1650)
89	8 f.t.	change "10 larger than" to "10 lower than"
89	last	change "show that" to "shows that"
90	caption	change "for State in" to "for States in"
93	12 f.t.	change "and 880 keV" to "an 880 keV"
94	13 f.b.	change "were then taken at 950 keV" to "were then assigned excitations of 950 keV"
Fig. 7.5.3., caption		add after "(Gr 68).", "All excitation energies are in keV."
97	Table 7.5.1	in heading to table under " J^π " add "Fo 70, Gr 67"
98	6 f.b.	add after "650 keV", "(see sect. 7.4)"
100	3 f.b.	change "proportional to β_2^P ." to "proportional to $(\beta_2^P)^2$, the square of the partial quadrupole deformation parameter for the state populated."
102	15 f.t.	change "of these states' γ -decay to ground" to "of these states to ground"